Integrated Tool Development for Used Fuel Disposition Natural System Evaluation – Phase I Report

Fuel Cycle Research & Development

Prepared for
U.S. Department of Energy
Used Fuel Disposition
Yifeng Wang & Teklu Hadgu
Sandia National Laboratories
Scott Painter, Dylan R. Harp & Shaoping Chu
Los Alamos National Laboratory
Thomas Wolery
Lawrence Livermore National Laboratory
Jim Houseworth
Lawrence Berkeley National Laboratory
September 28, 2012
FCRD-UFD-2012-000229
SAND2012-7073P

FCT Quality Assurance Program Document

Appendix E
FCT Document Cover Sheet

Name/Title of Deliverable/Milestone	Integrated Tool Development got Natural System Evaluation – Phase I Report /M2FT-12SN0807081
Work Package Title and Number	UFD Natural Evaluation & Tool Development
Work Package WBS Number	FT-12SN080708
Responsible Work Package Manager	Yifeng Wang (Name/Signature)

Date Submitted 8/24/2012

Quality Rigor Level for Deliverable/Milestone	☒ QRL-3	☐ QRL-2	☐ QRL-1 ☐ Nuclear Data	☐ N/A*

This deliverable was prepared in accordance with Sandia National Laboratories
(Participant/National Laboratory Name)

QA program which meets the requirements of
☒ DOE Order 414.1 ☐ NQA-1-2000

This Deliverable was subjected to:

☐ Technical Review

Technical Review (TR)

Review Documentation Provided

☐ Signed TR Report or,
☐ Signed TR Concurrence Sheet or,
☒ Signature of TR Reviewer(s) below

Name and Signature of Reviewers

Andy Miller Andrew W Miller 8-24-12

☐ Peer Review

Peer Review (PR)

Review Documentation Provided

☐ Signed PR Report or,
☐ Signed PR Concurrence Sheet or,
☐ Signature of PR Reviewer(s) below

*Note: In some cases there may be a milestone where an item is being fabricated, maintenance is being performed on a facility, or a document is being issued through a formal document control process where it specifically calls out a formal review of the document. In these cases, documentation (e.g., inspection report, maintenance request, work planning package documentation or the documented review of the issued document through the document control process) of the completion of the activity along with the Document Cover Sheet is sufficient to demonstrate achieving the milestone. QRL for such milestones may be also be marked N/A in the work package provided the work package clearly specifies the requirement to use the Document Cover Sheet and provide supporting documentation.

Executive Summary

The natural barrier system (NBS) is an integral part of a geologic nuclear waste repository. From a generally accepted multiple barrier concept, each barrier is supposed to be utilized for its safety function independently to its optimal extent. In this sense the NBS needs to be evaluated and necessary research conducted to ensure its optimal safety function. As one of its main objectives, the natural system evaluation and tool development package will ensure that sufficient research will be conducted to fully exploit the credits that can be taken for the NBS.

The work documented in this report is aimed to develop an integrated modeling framework that can be used for systematically analyzing the performance of a natural barrier system and identifying key factors that control the performance of the system. This framework is designed as an integrated tool for prioritization and programmatic decisions of UFDC natural system R&D activities, and it includes three key components: (1) detailed process models (with appropriate levels of fidelity) for flow field and radionuclide transport, (2) a probabilistic performance assessment capability, and (3) an associated technical database supporting model calculations. The integrated tool development for natural system evaluation adopts a phased approach. This report documents the results of phase I activities, which are focused on identifying relevant tools for subsystem analyses and performing preliminary demonstrations. Major FY12 accomplishments are summarized as follows:

- Two separate modeling frameworks were explored using different combinations of process simulators and performance assessment drivers: (1) PFLOTRAN + PEST and (2) FEHM + DAKOTA. Their preliminary application to flow and radionuclide transport in fractured granite and dolomite media was demonstrated using Monte-Carlo simulations. The potential application of a "plug-and-play" concept, common data format, and high performance computing techniques were explored.
- Calibration-constrained uncertainty analyses were performed for a flow field in a hypothetical fractured granite medium using PFLOTRAN and PEST.
- The modeling frameworks were demonstrated to be able to incorporate or use real field data (transmissivity fields), the dual-porosity capability of transport code (FEHM), the high performance parallel computing capability of PA driver (DAKOTA), and the embedded LHS sampling and statistical analysis techniques (DAKOTA).
- A comprehensive review of thermodynamic data relevant to nuclear waste disposal was performed, and the related data gaps were identified, especially for layered aluminosilicates.
- A comprehensive literature survey and data compilation were performed for modeling the near-field thermal-hydrological-mechanical-chemical evolution of a clay repository and for modeling flow and radionuclide transport in a fractured granite medium. These data will be used to develop an appropriate data model for UFDC data management.

Future work will include:

- Move the integrated tool development from phase I into phase II by merging the existing two separate modeling frameworks into a single integrated framework.
- Develop the capability to incorporate an advanced flow-transport model for fractured geologic media, such as a discrete fracture network (DFN) flow model, into the framework.
- Continue to explore and demonstrate the capability of model parameter estimation and uncertainty analyses using the established framework.
- Continue data collection and synthesis to establish a comprehensive technical database for natural system evaluation.

Table of Contents

1.0 Development of Integrated Tools for UFD Natural System Evaluation: An Introduction

1.1 Objectives

The natural barrier system is an integral part of a geologic nuclear waste repository. Spatially, it extends from a so-called disturbed rock zone, created by mechanical, thermal and chemical perturbations due to underground excavation or waste emplacement, to the surrounding geologic media, and continues all the way to a specified repository boundary. The work package of natural system evaluation and tool development supports the following Used Fuel Disposition Campaign (UFDC) objectives (Nutt, 2011):

1. Develop a fundamental understanding of disposal system performance in a range of environments for potential wastes that could arise from future nuclear fuel cycle alternatives through theory, simulation, testing, and experimentation.
2. Develop a computational modeling capability for the performance of storage and disposal options for a range of fuel cycle alternatives, evolving from generic models to more robust models of performance assessment.

From a well-accepted multiple barrier concept for waste repository safety, each barrier is to be independently utilized for its safety function to its optimal extent. In this sense the natural barrier needs to be evaluated and necessary research conducted to ensure its optimal safety function. From a repository design point of view, an appropriate balance must be maintained between the natural barrier system (NBS) and the engineered barrier system (EBS) in the contribution to the total system performance. In practice, there is a risk to place too much reliance on the engineered barrier while not fully taking credits for the natural system. Such practice often results in an overly conservative, very expensive EBS design. Thus, as one of its main objectives, the natural system evaluation and tool development package will ensure that sufficient research will be conducted to fully exploit the credits that can be taken for the NBS.

In FY11, a detailed research plan was developed for the NBS evaluation and tool development (Wang, 2011). In that plan, a total of 27 key research topics were identified. The effort on the integrated tool development for natural system evaluation tends to address the following three topics:

- Topic #S2. Disposal concept development: As explicitly identified in the UFDC Research & Development (R&D) roadmap (Nutt, 2011), there is a need for developing a range of generic disposal system design concepts. This research topic will support the overall UFDC effort on the development of disposal system design concepts by cataloging possible combinations and geometries of both host rock and far-field media (e.g., mineral and chemical compositions, physical dimensions, hydrologic properties). The topic will include the definition a generic set of key parameters (e.g., water chemistry) for other UFDC activities.

- Topic #S3. Disposal system modeling: Disposal system modeling is crucial for the whole life cycle of repository development. Such modeling tools will be essential for management decisions on project priority and resource allocation. This research will serve two purposes: (1) supporting the development of the total system performance assessment as well as the development of higher-fidelity performance assessment models, and (2) developing a comprehensive subsystem model for natural system performance evaluation. This subsystem model will be used for integration and prioritization of relevant natural system evaluation activities.

- Topic #S4. Development of a centralized technical database for natural system evaluation: Given the quantity of data already accumulated through various repository programs and also the data to be collected from the UFDC R&D activities, it is essential for future repository development to archive and categorize these data in an appropriate manner so that they can be easily accessible to UFDC participants and have appropriate quality assurance enforced. The data to be collected will include thermodynamic data for radionuclide speciation and sorption, groundwater chemistry, hydraulic and mechanical property data, mineralogical and compositional data of representative host and far-field media, spatial distributions of potential host formations, etc.

It is envisioned that the tools developed in this effort will be used to systematically analyze the performance of a NBS and identify key controlling factors through sensitivity analyses and then be used as an integration tool for prioritization and programmatic decisions of NBS-related R&D activities.

1.2 Technical Approach

The integrated tool development for NBS evaluation follows a probabilistic approach, similar to the one developed for a total system performance assessment (TSPA) (Helton et al., 1999). This effort focuses on the development a modeling framework that will include three key components: (1) detailed process models (with appropriate levels of fidelity) for flow field and radionuclide transport calculations, (2) probabilistic performance assessment capabilities, and (3) an associated technical database supporting model analyses (Figure 1-1). In this framework, one or more detailed process models may be linked and wrapped by a probabilistic performance assessment driver (PPAD). The PPAD then drives probabilistic performance assessment calculations by sampling uncertain model input parameters and invoking Monte-Carlo simulations using the linked process model(s). It is important for the modeling framework to be flexible enough to accommodate various alternative models. This can be done through a plug-and-play technique.

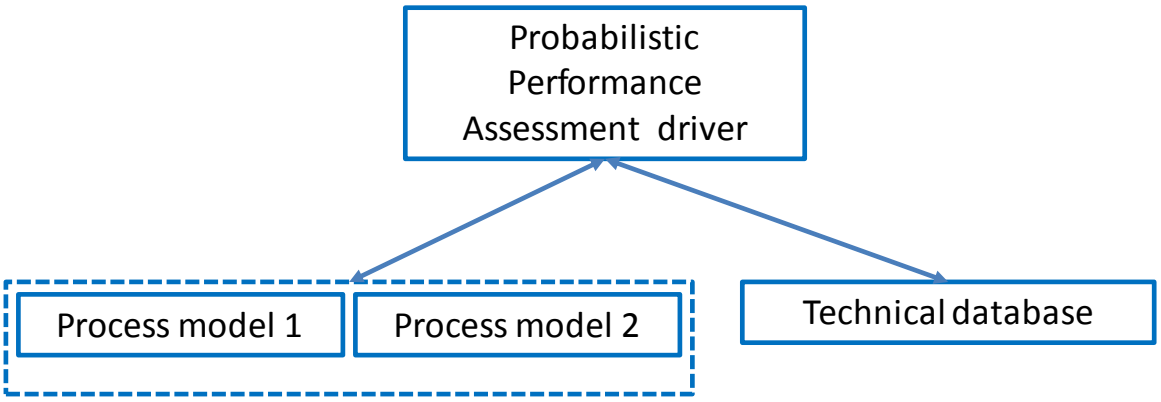

Figure 1-1. Integrated modeling framework for UFDC Natural Barrier System Evaluation

Given typical dimensions of the NBS and the level of process model details that may be needed for a meaningful subsystem evaluation, a probabilistic performance assessment of a NBS may be computationally intensive. To facilitate these calculations, we need to leverage recently developed high performance computing techniques. Specifically, we need to explore the parallelization of process-level codes and the parallel work assignment of sequential codes. The latter is important, because many legacy codes for flow and transport in a far field of a repository are not parallelized.

The integrated tool development adopts a phased approach. In phase I, relevant tools will be identified and preliminary demonstration will be performed. In phase II, the tools identified in phase I will be aggregated into a single coherent framework and its function as an integrated tool will be preliminarily demonstrated. In phase III, the established framework will be ready to support a comprehensive analysis of a NBS. This report documents the work completed for phase I in FY12.

As mentioned above, the methodology adopted for this effort may resemble, in many aspects, to that used for a TSPA. However, there are two significant distinctions between them in terms of the level of model fidelity and the use of process models. First of all, our effort here focuses on the performance evaluation of a NBS, not on a total disposal system. For this purpose, the process models to be used for this effort for natural system flow and transport calculations are much more detailed than those used for a TSPA calculation, and at the same time, for simplicity, only a stylized source term is used to represent radionuclide release from a EBS to its surrounding NBS. Second, the NBS tool development pays specific attention to the parameter estimation and uncertainty quantification using inverse process models. Despite these distinctions, we are fully aware that the two efforts – the integrated tool development for NBS and the tool development for TSPA – share much common ground and they will be closely coordinated. It is our intention that the tools developed for the NBS can eventually be transferred for TSPA uses as they become matured.

1.3 Structure of This Report

- Section 1.0 describes the concept and the objective of the integrated tool development for natural system evaluation. (Contributor: Y. Wang, SNL)
- Section 2.0 describes the development of an integrated process modeling framework for natural system evaluation using an optimization code (PEST) and a parallelized reactive transport code (PFLOTRAN). The framework is then applied to a granite repository environment. This section also discusses calibration-constrained uncertainty analyses using null-space Monte Carlo simulations. (Contributors: Scott Painter and Dylan R. Harp, LANL)
- Section 3.0 describes the development of an integrated process modeling framework using an optimization code (DAKOTA) and a sequential flow-transport code (FEHM) and the application of this framework to radionuclide transport in a fractured dolomite formation. (contributor: T. Hadgu, SNL)
- Section 4.0 provides a comprehensive review of thermodynamic data that are needed for performance assessments of high level nuclear waste disposal. (contributor: Thomas Wolery, LLNL)
- Section 5.0 documents key technical data needed for NBS evaluation for both granite and clay repositories. (contributors: Jim Houseworth, LBNL and Shaoping Chu, LANL)
- Section 6.0 provides the summary of the FY12 work and the future direction.

1.4 References

Helton, J. C., Anderson, D. R., Jow, H.-N., Marietta, M. G., and Basabilvazo G., 1999, Performance assessment in support of the 1996 compliance certification application for the Waste Isolation Pilot Plant, Risk Analysis, 19(5), 959-986.

Nutt M. (2011) *Used Fuel Disposition Campaign Disposal Research and Development Roadmap*, FCR&D-USED-2011-000065, Rev 0.

Wang, Y. (2011) Integrated Plan for Used Fuel Disposition (UFD) Data Management. U.S. Department of Energy Used Fuel Disposition Campaign. FCRD-USED-2011-000386.

2.0 Development of an Integrated Process Modeling Framework for Performance Assessments of Natural Barrier Systems

2.1 Introduction

As mentioned in Section 1.0, a subsystem analysis of a natural barrier system (NBS) resembles, in many aspects, a total system performance assessment of a repository. The term *performance assessment* (PA) has historically been connected with risk assessments of nuclear reactors and geologic disposal of radioactive waste. The term has been used synonymously with *probabilistic risk assessment* in the United States (60 FR 42622). An early definition of a PA in the context of radioactive waste disposal is provided by the Nuclear Energy Agency of the European Organisation for Economic Co-Operation and Development (OECD/NEA) (Nuclear Energy Agency, 1990) as:

> *an analysis to predict the performance of a system or subsystem, followed by a comparison of the results of such analysis with appropriate standards and criteria.*

Ewing *et al.* (1999) describe a PA as:

> *Performance Assessment (PA) is the use of mathematical models to simulate the long-term behavior of engineered and geologic barriers in a nuclear waste repository; methods of uncertainty analysis are used to assess effects of parametric and conceptual uncertainties associated with the model system upon the uncertainty in outcomes of the simulation.*

Campbell & Cranwell (1988) state that a PA includes:

> *(i) identification and evaluation of the likelihood of all significant processes and events that could affect a repository, (ii) examination of the effects of these processes and events on the performance of a repository, and (iii) estimation of the releases of radionuclides, including the associated uncertainties, caused by these processes and events.*

Gallegos & Bonano (1993) identify a key ingredient of a PA as:

> *the attempt to estimate the effect on risk from (1) the expected temporal evolution of the environment and the system, and (2) a range of plausible, yet less likely, futures.*

From these definitions and experience several key ingredients can be identified: (1) the focus is on radionuclide releases and comparisons with appropriate standards; (2) the scope of the analyses may vary from total system to subsystem (i.e. geologic barriers); and (3) methods of uncertainty analysis are used to assess uncertainty in outcomes. It is noted that, in practice, PA studies typically make use of lower fidelity models that are simplifications or "abstractions" of more complex and computationally demanding process models. Moreover, methods to incorporate available measurements on the present state of a natural barrier system (e.g. hydraulic head) are rarely considered formally in the uncertainty analysis.

This section explores the use of an integrated framework that couples multiple process models for a performance assessment of the NBS of a generic granitic repository. Specifically, a flexible design for an integrated assessment framework is proposed and demonstrated. In addition, opportunities to exploit parallel computing resources in the subsystem assessment are identified and explored. Techniques to make use of existing calibration data in uncertainty assessments are also demonstrated.

2.2 Design Considerations for a Next-Generation PA framework

The following design principles are proposed for the next generation assessment framework:

1. Provide a flexible and extensible framework where alternative, existing process models and uncertainty analysis approaches can be interchanged in a "plug and play" type structure;
2. Use a common data format for efficient data storage, processing, and organization;
3. Incorporate parallel and concurrent simulations (HPC) wherever possible;
4. Use calibration-constrained uncertainty analyses wherever possible;
5. Use sampling-based uncertainty analysis wherever calibration-constrained uncertainty analysis is not possible;
6. Use PA-tailored radionuclide transport algorithms.

Principles 1 and 2 facilitate the use and exploration of various simulators and analyses within a given NBS subsystem assessment. A *common data format* discussed in principle 2 ensures that principle 1 is possible. Of course, the realization of principle 1 will require more than a common data format alone. The inclusion of complex physics-based models and uncertainty analyses should not be precluded from an assessment solely on the basis of computational constraints. In situations where complex models and analyses are appropriate and justified, an assessment should make use of these models. Principle 3 attempts to ensure that computational constraints do not limit the complexity of models and analyses by suggesting that parallel simulators and concurrent model evaluation be used whenever necessary. Assessments should utilize available data to constrain uncertainty (principle 4). In an actual application, it is likely that sparse hydraulic head measurements will be available from site characterization activities. These head measurements are typically not sufficient to fully specify the groundwater velocity but they do provide important constraints on the present day flow field. Sparse measurements on groundwater age or other groundwater chemistry information provide similar partial constraints. Methods for producing multiple realizations of the permeability field that are consistent with partial constraints – calibration-constrained uncertainty analysis – are needed for this step. Principle 5 suggests that in cases where data are not available for calibration-constrained uncertainty analysis, sampling based uncertainty analyses should be used. The current availability of radionuclide transport algorithms specifically designed to work in an assessment framework should be used whenever possible (principle 6).

2.2.1 Uncertainty and sensitivity analysis

Uncertainty and sensitivity analysis techniques are integral components of a PA. In their most basic form, such analyses involve modifying one parameter or a set of assumptions at a time and evaluating the response of the model (*ceteris paribus* approach). Some other more formal approaches are discussed below.

Differential analysis is a surrogate-based approach using a truncated Taylor series as an approximation of the model. Once established, uncertainty and sensitivity of the Taylor series is evaluated. Differential analysis provides a local analysis of sensitivities around a base case. While the development of the Taylor series can be challenging and computationally intensive, once it is developed, the uncertainty and sensitivity analyses are efficient. The validity of these analyses depends on how well the Taylor series approximates the model, which will not typically be known at this stage of the analysis (Helton, 1993).

Response surface methodologies include approaches that develop surrogate models to approximate the original model using experimental design approaches (e.g. factorial, fractional factorial, central composite, etc.) to sample the parameter space. The order of the surrogate model and the inclusion of

cross-products depend on the experimental design and information available to the modeler about the model structure (Helton, 1993). In experimental design, samples are chosen to expose sensitivities between inputs and outputs, and are not intended for a probabilistic analysis. Similar to differential analysis, the quality of analyses using response surface methodologies depends on the ability of the surrogate model to approximate the original model.

The Morris method (Morris, 1991), based on statistical one-at-a-time approaches, ensures that the parameter space sampling includes pairs of samples where only one input is varied. At the minimum, this is ensured for each input. Higher levels of analysis can be performed including multiple instances where a single input is varied. In this way, it is ensured that elementary effects (i.e. single input sensitivities on the outputs) are exposed without interaction from other inputs. An attraction of the approach is the lack of assumptions regarding the sparsity of important inputs, monotonicity of input effects on outputs, and adequacy of surrogate-based approximations to the model.

The Fourier Amplitude Sensitivity Test (FAST) transforms the multidimensional integral over all inputs defining the expected value of the output to a one-dimensional integral. A Fourier series representation of this integral exposes the fractional contributions of individual inputs to the variance in the outputs. Advantages to the FAST approach are that the full range of the inputs is evaluated, the analysis is performed directly on the model (i.e. a surrogate model is not used), and the original model does not need to be modified to use the FAST approach. Downsides to the FAST approach are that it is complicated, difficult to explain, not widely known or used, may require a large number of model evaluations, the cumulative distribution function (CDF) of the output is not produced, and input correlations cannot be included (Helton, 1993).

Monte Carlo (MC) analysis involves post-processing of a propagation of probabilistically selected input samples to model outputs. Sampling scheme variants include random sampling, importance sampling, and Latin hypercube sampling (LHS). As mentioned above, LHS has been used predominantly in radioactive waste repository PA's (Iman *et al.*, 1978). LHS is a stratified sampling scheme ensuring that the full range of each input is efficiently sampled. The estimated expected value is unbiased for LHS, while the estimated variance is known to contain a bias. Empirical research indicates that this bias is small (Helton, 1993). Post-processing of MC results include estimation of output distribution functions. These are unbiased for random sampling and LHS. Various approaches are available for sensitivity analysis using MC samples. Perhaps the simplest is multi-regression, successively fitting the most important input to the remaining variance in output with each iteration. Difficulties in this approach due to nonlinearities can be alleviated using rank transformation of the data, thereby extracting information concerning the monotonic relationships between inputs and outputs. Sensitivities are exposed through regression coefficients. Techniques to recognize over-fitting have been developed including evaluation of the predicted error sum of squares.

Although not historically utilized in performance assessments, calibration-constrained uncertainty analysis approaches provide a means to use existing measurements from the field to reduce uncertainty. It is often the case that data are available to calibrate the groundwater flow field in the form of pressure heads obtained from monitoring wells, and that these are the only site-specific observations available. For instance, observations of radionuclide transport at the site are not likely to be available. This provides the ability to constrain the set of possible flow fields to the historical record. Such information can be utilized as a set point for further uncertainty analyses associated with the potential future flow fields.

The calibration-constrained uncertainty analysis of the flow field can be performed as a separate step in the assessment, and the results provided where they are needed (e.g. dissolved oxygen transport and radionuclide transport submodels). Many approaches are available to provide a calibration-constrained

uncertainty analysis, including Markov Chain Monte Carlo (MCMC) (Higdon, 1998; Vrugt *et al.*, 2009) and Null-Space Monte Carlo (NSMC) (Tonkin and Doherty, 2009). Once the results are obtained as a set of possible flow fields or a statistical representation of flow fields, these can be used as inputs to the other submodels. If observations of major ion concentrations are available, a calibration constrained uncertainty analysis of the ambient chemistry can also be performed.

The results of a calibration constrained uncertainty analysis of the flow field described above will produce a set of potential flow fields or a statistical characterization of potential flow fields. A sampling analysis (e.g. post-processing an MC sampling or LHS, as described above) of the remaining submodels based on the potential flow fields provides a probabilistic uncertainty analysis of the radionuclide concentration at the ground surface. Similarly, the results of a calibration constrained uncertainty analysis of the ambient chemistry can be used in sampling-based analyses to propagate the ambient chemistry uncertainty through subsequent submodels.

2.2.2 File formats

The submodels to include in a particular assessment will be site or design-specific and are likely to be modified throughout the assessment process. Therefore, a framework intended to facilitate the development of a system or subsystem PA must provide a means to add, remove, and substitute process kernels (i.e. computational simulators). We propose the use of a common data structure to facilitate the passing of array-oriented simulator input and output between submodels. Many libraries and toolkits currently exist for this purpose, and provide machine independent formats that are self-describing through the use of metadata. The Common Data Format (CDF) was developed by NASA for the manipulation of multi-dimensional data sets. One of the major drawbacks to CDF is that a large part of its programming interface is obsolete (Heijmans, 2001). The Hierarchical Data Format (HDF) provides a library to store and organize large amounts of numerical data. The HDF5 format has been created to improve the older HDF format, HDF4. The format is efficient, allowing quicker data access than from Structured Query Language (SQL) databases. While one of the advantages of HDF is the ability for applications to create files with any structure they want, this is also a drawback, as creating import modules to account for all the possible file structures would be difficult (Heijmans, 2001). The Network Common Data Form (NetCDF), originally designed on CDF, also provides a common data structure that has been widely used to store scientific data. The latest version of NetCDF, version 4, is based on HDF5. NetCDF is considered a less powerful alternative to HDF5 that is easier to use (Heijmans, 2001). The CFD General Notation System (CGNS, where CFD stands for computational fluid dynamics) has become a popular format for storing CFD data. CGNS originally used the Advanced Data Format (ADF) as a database manager, but has recently extended the format to optionally use HDF5 for this purpose. The eXtensible Model Data Format (XMDF) is another format that utilizes HDF5. The use of Extensible Markup Language (XML) allows data to be formatted so that both humans and computers can read it. However, large data sets become unwieldy in XML compared to binary formats. Most of the formats described above have officially supported APIs in C/C++, Fortran, and Java. While not officially supported, many also have third-party bindings available for Perl, Python, MATLAB, Mathematica, etc.

Based on its increasing use in the computational sciences, efficient binary format, flexible structure, and Python bindings, HDF5 has been selected for the current research. HDF5 files are organized into a hierarchical structure of *groups* and *datasets*. *Groups* can contain other *groups* (*subgroups*) and *datasets*. *Datasets* are multidimensional arrays of data elements. This hierarchical structure is analogous to a UNIX filesystem, where *groups* are similar to directories and *datasets* are similar to files. Also similar to a UNIX filesystem, a HDF5 file can mount another HDF5 file. In this way, a "master" HDF5 file can be used to organize a PA by mounting other HDF5 files containing components of the PA. It is also possible to mount a single instance of static data (e.g. coordinates) which are common to multiple submodels of

the PA. The h5py Python interface (Collette, 2008) is a near-complete wrapping of the HDF5 C API, providing high-level functionality to read, create, and modify HDF5 files.
In order to create a framework in which alternative models and analyses can be easily exchanged, a common storage and organization scheme must be implemented. We are proposing to use the HDF5 file format for this purpose. The h5py python module (Collette, 2008) is used to manipulate the HDF5 files. Python is used to create a master HDF5 file. Within the master file, a *model group* is created for each scenario that will be evaluated within the PA. Within each *model group*, subgroups and datasets can be created and populated with data from the cascade of simulations that comprise the PA model. If a simulator outputs in HDF5 format, these files can be mounted as subgroups within the *model groups*. Results from one simulator can be used to populate input files for the next submodel using python. This results in a highly structured and organized assessment framework where alternative models and analyses can be interchanged.

Depending on the process kernels used, the *model groups* may contain the following datasets:

- velocities
- pressures
- temperatures
- ion concentrations
- radionuclide flux at EBS
- radionuclide flux at ground surface

Each of these groups will contain *datasets* structured to account for the spatial dimensions (e.g. *x*,*y*,*z*).

2.3 Concept for a Generic Granitic Repository and Associated Assessment Framework

A hypothetical repository situated in fractured granite is considered. Details of the EBS system are not relevant here, although the KBS-3 concept with bentonite buffers surrounding waste packages may be used to fix the concept. Based on existing understanding of flow and transport in fractured rock, the groundwater flow field is assumed to be only partially constrained by site characterization data. Moreover, the highly channelized nature of flow in fractured rock is assumed to lead to discrete transport pathways that link locations of failed waste packages to the biosphere.

Six major process groups linked sequentially can be identified (Figure 2-1). In an assessment framework, a *process kernel* may be associated with each group of processes. The term *process kernel* (PK) is used there to refer to process modeling software that represents a small number of relatively tightly coupled processes. Each PK is part of a model chain, and loosely coupled with upstream and downstream PKs in the model chain. In the proposed framework, PK1 represents groundwater flow fields. In PK2, evolution of the groundwater chemistry upstream of the engineered barrier system is simulated. If the groundwater flow system is adequately represented as steady over the time frame of interest and if thermal perturbations of the flow and chemical system are modest, then this step is not necessary because measured groundwater chemistry may be used in place of simulated chemistry for downstream models. However, if transient flow or thermal perturbations are to be modeled then simulation of chemistry in future climates may be needed. PK3 simulates thermal conditions. PK4 involves degradation of engineered barriers, release of radionuclides from the waste form, and transport of radionuclides through the engineered barrier system (EBS). This step is beyond the scope of this report, but is mentioned here because it couples to the geosphere through the effect of groundwater chemistry on EBS degradation, the

thermal conditions in the EBS and in the near field, and the release of radionuclides. PK5 represents carrier-plume reactive transport, the evolution of groundwater chemistry downstream of a failed waste package taking into account the effects of EBS degradation products and thermal perturbations. PK6 is radionuclide transport, possibly taking into account the effect of major ion chemistry calculated from PK5. The separation of radionuclide transport (PK6) from major ion chemistry (PK5) is consistent with the expected low concentrations of radionuclides in the geosphere such that radionuclides do not significantly influence the overall solution chemistry. It is important to note, however, that one-way coupling is represented. Thus, the concentration of complexing agents as calculated by PK5 may influence equilibrium distribution coefficients, the so-called "smart K_d" approach. If surface complexation models are used to calculate radionuclide immobilization, the parameters appearing in those models may be calculated from the output of PK5. This separation into two process kernels is computationally expedient given that the application requires dozens of radionuclides to be represented.

The structure of the framework shown in Figure 2-1 has two prominent features. The first structural feature is that the six PKs are arranged into two loops. In the first loop, ambient groundwater flow and chemistry PKs are called in a calibration constrained uncertainty loop. This analysis will produce alternative flow fields that are all consistent with the available constraints on hydraulic head, groundwater age, etc. In the second loop, unconstrained (sampling based) uncertainty analysis is used to drive the remaining model chain in a more traditional assessment mode. The second structural feature is that the PKs are not passing data directly among themselves. Instead, each is reading from and writing to a common data layer, which as discussed in Section 2.2.2, is implemented as a hierarchical HDF5 file system. This feature is essential to the plug and play nature of the framework, as it allows process kernels to be replaced without initiating a cascading set of changes the PKs upstream and downstream in the workflow.

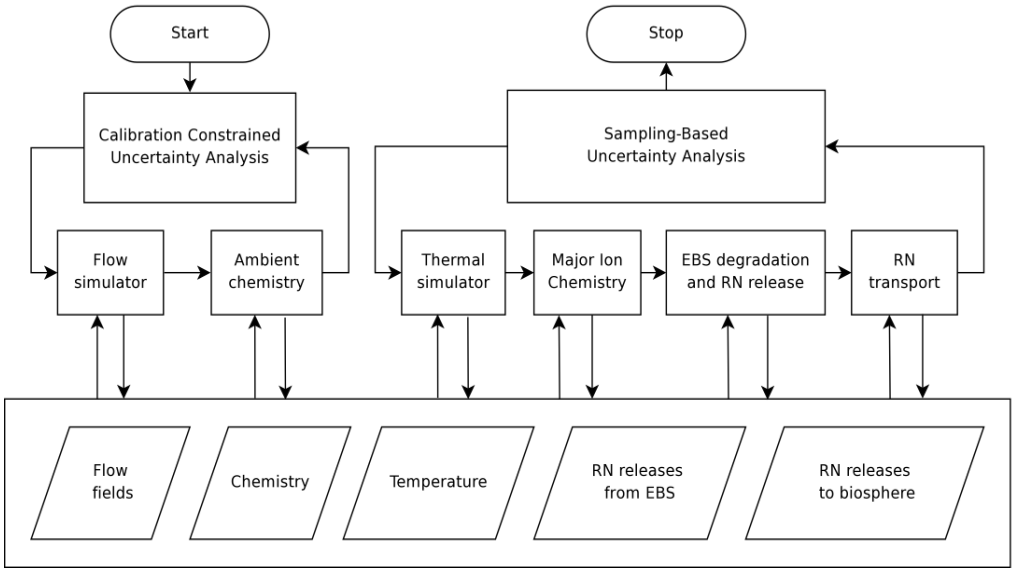

Figure 2-1. Schematic of a proposed assessment framework

2.4 Tool Demonstration

2.4.1 Synthetic example

A 2D model (vertical plane) is utilized to demonstrate the assessment framework. A diagram of the conceptual model is provided in Figure 2-2. The model domain is saturated with no flow boundaries along the sides and bottom. A constant flow boundary of 0.063m^3/s is applied to the top left side of the model domain and a constant head boundary of zero is applied to the top right side of the model domain. A uniform porosity of 0.05 is assumed. The permeability of the "true" model domain is a geostatistical realization of a spherical variogram with a scale of 1.0 and range of 200 m. The geostatistical realization is conditioned at 32 locations with random permeability values uniformly distributed from 1×10^{-14} to 1×10^{-16} m^2 and 9 locations with permeability values of 1×10^{-19} m^2 positioned along the vertical center of the model extending from near the top of the model domain to a depth of around 200 m. The 32 locations with random permeabilities are used as geostatistical pilot points. The locations of the conditioning points are presented in Figure 2-3. The "true" permeability field is presented in Figure 2-4. A vertical line of low permeability conditioning points along x=400 m creates a vertical barrier to flow extending from the top to a little below the center of the model domain. A flow field is thereby induced from the left side of the top of the model domain through the bottom of the model domain and exiting at the right side of the top boundary. The magnitude of the 'true' steady-state groundwater velocities are presented in Figure 2-5. It is assumed that steady state hydraulic head observations are available from 20 locations indicated in Figure 2-6. It is assumed that a nuclear waste repository is under consideration near x=400 m and z=50 m.

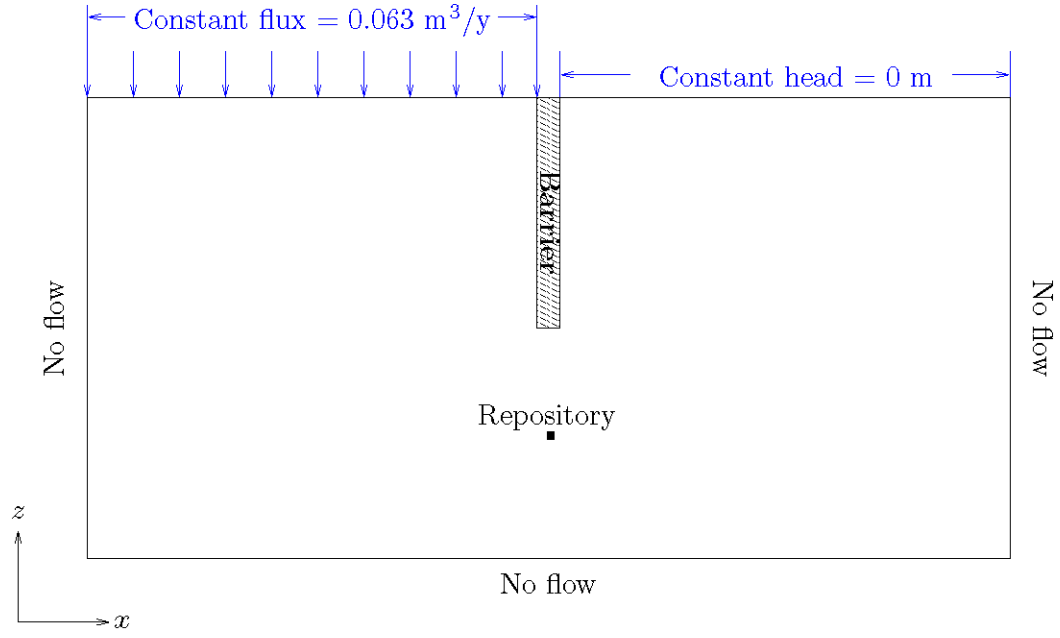

Figure 2-2. Conceptual model of a generic granitic repository

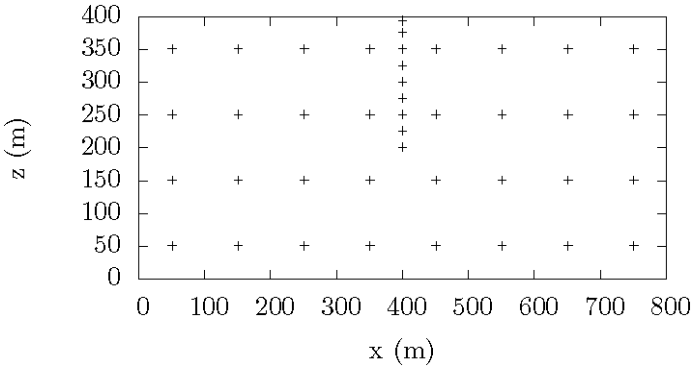

Figure 2-3. Location of pilot points within model domain

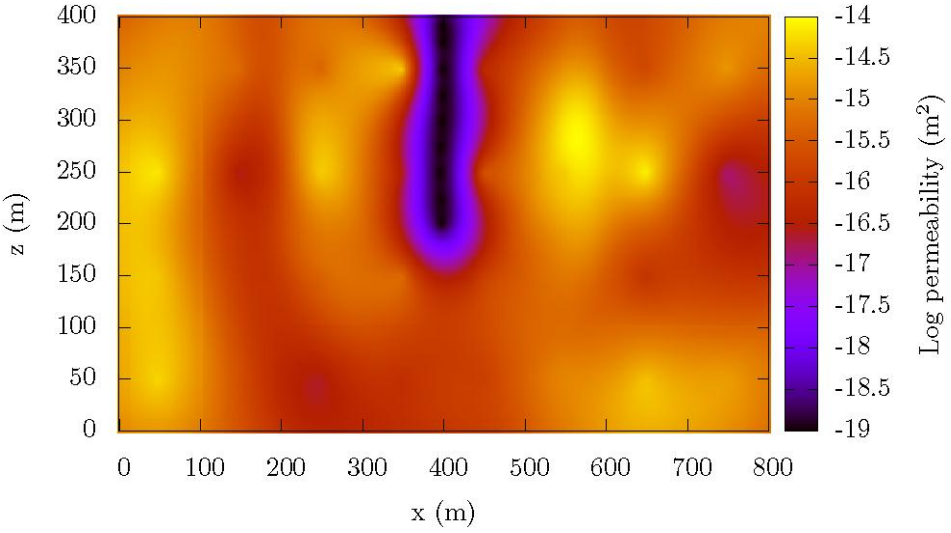

Figure 2-4. Permeability for the "true" aquifer

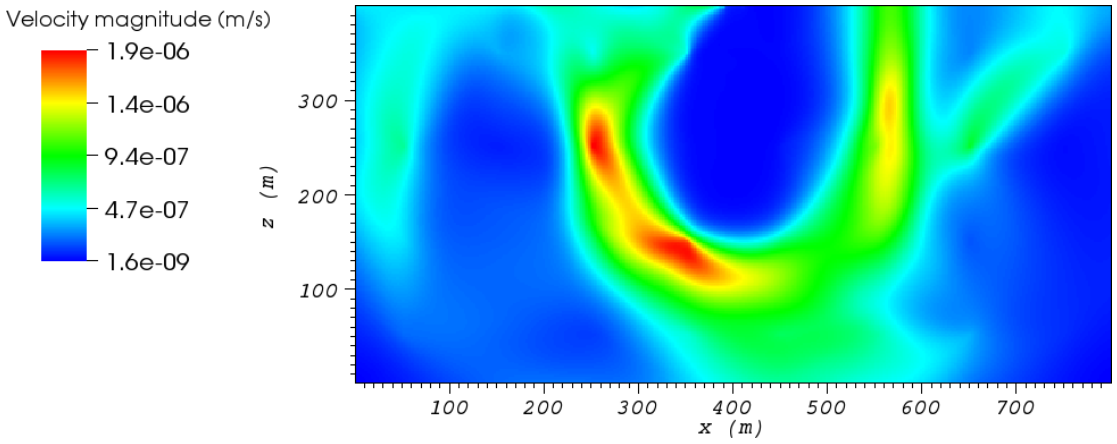

Figure 2-5. Magnitude of groundwater velocities for the "true" aquifer where flow is from the left side of the top of the model, through the bottom of the model, and out the right side of the top of the model

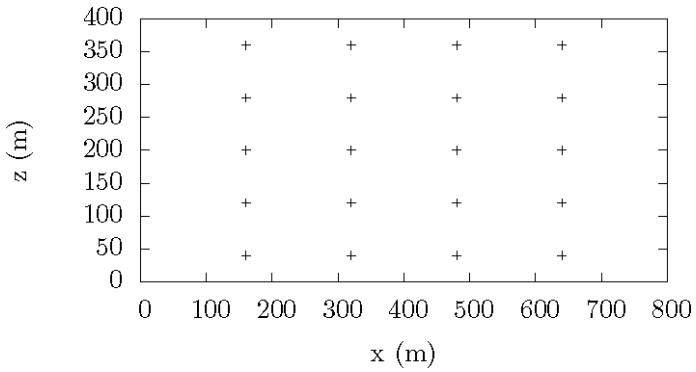

Figure 2-6. Location of steady state hydraulic head observations

2.4.2 Workflow

While we are describing a general framework for PA, we have selected specific physics simulators and uncertainty analysis methodologies for demonstration purposes. The intention is that the appropriate simulator or uncertainty analysis methodology can be substituted into the framework described here for a given PA in a "plug-and-play" type approach. The selections made here will be appropriate in some cases

and inappropriate in others. Their use facilitates the demonstration of the framework but does not imply that the framework is "hard-coded" to these selections.

Development of flow model: This step involves selecting a simulator and implementation of the conceptual model. In this example, this step is idealized by using the boundary and initial conditions of the "true" model. In reality, this step will require careful consideration of the available information about the natural system. PFloTran (Lichtner et al., 2009) is selected as the groundwater flow model in this example. PFloTran is a parallel flow and transport simulator using the PETSc library for parallelization. PFloTran includes adaptive mesh refinement (AMR) and strong capabilities for the reaction of solutes. The model uses an orthogonal grid with a uniform 2 m spacing. The boundary conditions discussed above are implemented in the simulator. The geostatistical program gstat (Pebesma & Wesseling, 1998) is used to krig the permeability field using the pilot points and variogram model discussed above.

Generation of a set of potential velocity fields: NSMC Tonkin & Doherty (2009) is used to obtain a set of velocity fields constrained to available head observations from the field given uncertainty in the permeability field. NSMC provides an approximation of model uncertainty in a computationally efficient manner using subspace techniques to reduce the dimensionality of the parameter space. NSMC involves the following steps:

1. Obtain a calibrated model (use SVD if the number of parameters is large)
2. Compute sensitivities of calibrated model
3. Based on sensitivities from the calibrated model, determine the calibration space and null-space of the parameter space
4. Generate samples in the null space constrained to the calibrated parameter combinations in the calibration space
5. Recalibrate samples using PEST's SVD-Assist with sensitivities from step 2

The calibration attempts to reduce the model residuals by modifying the permeability values of the pilot points as

$$\min_{\Theta} \Phi(\Theta) = \sum_{i=1}^{N} r_i^2 \qquad (2\text{-}1)$$

where $\Phi(\Theta)$ is the objective function, Θ is a vector containing the model parameters (i.e. permeabilities at the pilot points), N is the number of measurements, and r_i is the *i*-th model residual defined as $y_i - \hat{y}_i$, where y_i and $\hat{y}_i$ are the *i*-th head measurement and associated simulated value from the PFloTran model, respectively.

Computing flow paths from velocity fields: An ordinary differential equation (ODE) solver using an adaptive quadrature algorithm (Jones et al., 2001; Piessens et al., 1983) written specifically for this research was used to calculate the flow paths from the repository to the surface. The ODE solver solves the equation

$$\frac{d\boldsymbol{x}_p}{dt} = \boldsymbol{v}\left(\boldsymbol{x}_p, t\right) \qquad \boldsymbol{x}_p(0) = \boldsymbol{x}_{p0} \qquad (2\text{-}2)$$

where $\boldsymbol{x}_p(t)$ is the location for the particle, t is time, and $\boldsymbol{v}(\boldsymbol{x}, t)$ is a vector function defining the velocities in the field determined by linearly interpolating the velocity fields generated by PFloTran.

Thermal effects from heat-generating waste on velocities are not considered in this example demonstration. In practice, thermal effects will typically need to be considered.

Determination of radionuclide release due to EBS degradation: A complete model of EBS degradation is outside of the scope of this report. Therefore, it is assumed that a constant 1 mol/y release of Np237 occurs for a duration of 1 year (from t=0 to t=1 year).

Computing radionuclide breakthrough curves: Breakthrough curves are computed by sampling the computed flow paths and retention properties. Sampling of flow paths is performed within the computer code Migration Analysis of Radionuclides in the Far Field (MARFA; Painter & Mancillas (2010)), which models the transport of radionuclides along the computed flow paths using the released radionuclides as the source. The radionuclide source of each flow path is weighted by its likelihood using a generalized likelihood (Beven & Binley, 1992) as

$$L=(\Phi^2)^{-N} \tag{2-3}$$

where N is a user-specified parameter controlling the manner in which likelihoods are distributed across flow paths. If N=0, every flow path will have equal likelihood, while $N\rightarrow\infty$ will apply non-zero likelihood only to the flow path with the smallest Φ (i.e. best fit). The source for each flow path is calculated as

$$S_{0,i} = S_0 \frac{L_i}{\sum_{j=1}^{n} L_j} \tag{2-4}$$

where *i* is a flow path index, S_0 is the total source of radionuclides released from the EBS in mol/y and *n* is the number of flow paths. Retention properties are sampled by LHS and used in independent runs of MARFA.

MARFA is a particle-based Monte Carlo approach using non-interacting particles to represent packets of radionuclide mass. MARFA produces particle arrival times at the surface, which can be used to calculate cumulative mass discharge at the surface at a given time. MARFA models the transport of particles through each segment utilizing the non-retarded (water) residence time τ and the transport resistance parameter β. The particle arrival time t_{ar} probability density can be defined as

$$f_{ar}(t_{ar}) = \int_0^\infty \int_0^\infty f_{ret}\left(t_{ar} - t_{in} - \tau \,|\, \tau\bar{\beta}/\bar{\tau}\right) f_\tau(\tau) f_{in}(t_{in}) d\tau\, dt_{in} \tag{2-5}$$

where $f_{in}(t_{in})$ is the start time probability distribution (normalized source history), $f_\tau(\tau)$ is the non-retarded residence time probability density, τ and β are properties of the pathway segment representing values of τ and β neglecting longitudinal dispersion. Using equation (2-5), the cumulative tracer breakthrough curve can be defined as

$$R_{out}(t) = S_0 \int_0^\infty H(t - t_{ar}) f_{ar}(t_{ar}) dt_{ar} \tag{2-6}$$

where H[−] is the Heaviside function. Equation (2-6) can be approximated by the Monte Carlo estimate

$$\hat{R}_{out}(t) = \frac{S_0}{N_{part}} \sum_i H\left(t - t_{ar,i}\right) \tag{2-7}$$

where N_{part} is the number particles released. MARFA computes the cumulative breakthrough curve by:

(1) Sample a random start time t_{in} from the normalized source $f_{in}\left(t_{in}\right)$;

(2) Sample a τ value based on longitudinal dispersion. The appropriate distribution has density $\bar{\tau}\, f_\tau(\tau) = \sqrt{\frac{\eta}{4\pi}}(\tau')^{-3/2} \exp\left(-\frac{\eta}{4}\frac{(1-\tau')^2}{\tau'}\right)$ where $\tau' = \frac{\tau}{\bar{\tau}}$, $\eta = \frac{\ell}{\alpha}$, ℓ is the length of the segment, and α is the dispersivity. An algorithm for sampling this is described in the appendix of Painter at al. [2008];

(3) Calculate a β value from $\beta = \tau\bar{\beta}/\bar{\tau}$. Note that this step properly accounts for the interaction between retention and longitudinal dispersion;

(4) Sample a retention time t_{ret} from $f_{ret}\left(t_{ret} \mid \beta\right)$. Retention time distributions for important retention models are compiled in Painter et al. (2008);

(5) Calculate the particle arrival time as $t_{ar} = t_{in} + \tau + t_{ret}$. This value represents one sample from the arrival time distribution;

(6) For a given time *t*, if $t_{ar} < t$ the particle contributes an amount S_0 / N_{part} to the cumulative mass discharge;

(7) Repeat from Step 1 a total of N_{part} times.

MARFA needs the following information to define a flow path: the beginning and ending coordinates of each segment and the values for τ and β for each segment calculated as

$$\tau(s) = \int_0^s \frac{ds'}{v(s')} \tag{2-8}$$

and

$$\beta(s) = \int_0^s \frac{ds'}{b(s')v(s')} \tag{2-9}$$

where *s* is the distance along a streamline segment, *b* is the fracture half-aperture, and *v*(*s*) is the speed at distance *s* along a streamline.

Rock properties required by MARFA for a limited diffusion retention model (other retention models are available in MARFA) are the matrix effective diffusion coefficient D_{eff} [L^2 T^{-1}], matrix retardation factor R_m [–], the size of matrix region accessible by diffusion Δ [L], sorption coefficient for equilibrium sorption on fracture surfaces k_a [L^{-1}], and the longitudinal dispersivity α [L]. The matrix retardation factor is defined as

$$R_m = 1 + \frac{\rho_b K_d}{\theta_m} \tag{2-10}$$

where ρ_m is the bulk density of the matrix [M L^{-3}], K_d is the equilibrium distribution coefficient [L^3 M^{-1}], and θ_m is the matrix porosity [–].

2.4.3 Storage and organization

The HDF5 file format is used to organize and store the subsystem assessment using Python scripts that utilize the h5py Python module (Collette, 2008). Data and results from each step are stored in the HDF5 file format and mounted within a master HDF5 file. Some submodels retrieve necessary information via the master file and subsequently mount their results within the master file. This not only organizes the assessment workflow but also facilitates its traceability. To illustrate the concept, the steps in our example are:

1. Perform NSMC to create velocity fields (*PFloTran* outputs results in HDF5 format);
2. Create master HDF5 file and mount each velocity field HDF5 file within its own 'model' group and add objective function attribute to each model group;
3. The ODE solver extracts each velocity field, computes the flow path, outputs flow path in HDF5 format and automatically mounts the flow path into its model group;
4. A Python script extracts the flow paths and creates *MARFA* input files;
5. A Python script creates HDF5 files from the *MARFA* output and mounts these in the master file.

In this way, the entire PA is organized and traceable within a single HDF5 file.

2.5 Example Assessment

The NSMC is performed using PEST (Doherty *et al.*, 1994). We assume that the 'true' hydraulic head measurements from the field are known to a resolution of 0.01 m. The 'true' head measurements are truncated to this resolution and utilized as the calibration targets. Random measurement noise has not been added to the calibration targets in this example. We assume that the 'true' permeabilities at the pilot points are not known, and an initial model calibration is performed with initial permeability values at the pilot points modified from the 'truth' and set as unknown model parameters.

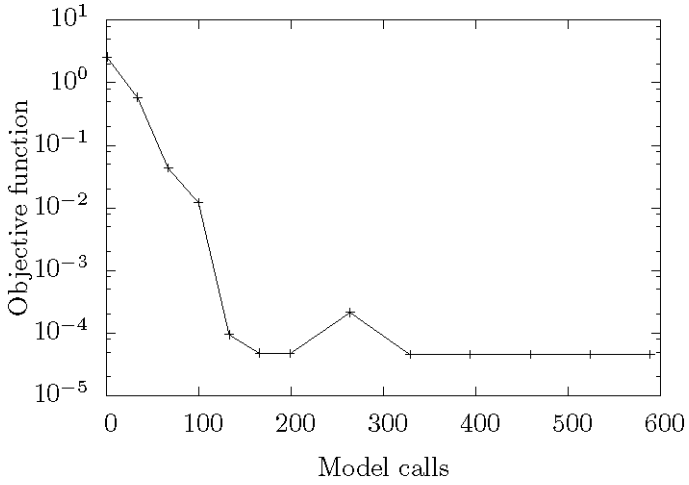

Figure 2-7. Objective function value (Eq. 2-1) during *PEST* calibration

Since the resolution of the measured hydraulic heads is limited to 0.01 m, the 'true' pilot points values are not likely to be identified. Therefore, our example is similar to reality where measurements are imprecise and the truth is not known. The 'model run' for the calibration involves kriging the permeability field using the 32 pilot point permeability values provided by *PEST* followed by a flow simulation performed by *PFloTran* using the kriged permeability field. This effectively calibrates the permeability field to the available head measurements. The *PFloTran* simulation is performed using 4 processors. The calibration is performed using *Parallel PEST* with singular value decomposition (SVD) running 3 model runs concurrently. Therefore the calibration is performed using 12 cpus. This parallelization can readily be scaled up to more cpus.

Figure 2-7 presents the progress of *PEST* in reducing the objective function during the calibration. The final objective function value is 4.6×10^{-5} m^2, which corresponds to an average model residual (discrepancy between observed and simulated head) of 3.3×10^{-4}m. Identification of the 'truth' is not possible (i.e. an objective function value of zero) because of the truncated resolution of the head measurements.

Using the parameter sensitivities of the calibrated model, a set of 100 calibration-constrained velocity fields is generated. This is accomplished using *PEST* by creating 100 parameter sets with values fixed in the calibration solution space (i.e. parameter combinations that influence the calibration), but with random values in the null space (i.e. parameter combinations that do not influence the calibration). If these parameter sets are no longer in calibration, calibration with SVD-Assist is performed with the existing calibrated parameter sensitivities to recalibrate parameters spanning the calibration solution space while retaining the random values in the null space. As this step uses existing sensitivities in a "superparameter" approach, this usually requires a small number of optimization iterations per recalibration.

A python code written for this research is used to parallelize the re-calibration step of the NSMC. In the example, 3 re-calibrations were performed concurrently resulting in the use of 12 cpus (*PFloTran* simulations used 4 cpus each). This parallelization scheme can scale to the number of cpus available. The result after the re-calibrations is a set of calibration-constrained velocity fields. Figure 2-8 presents histograms of the initial objective function values for the NSMC samples and their values after recalibration. The lower objective function values after recalibration are apparent. Other uncertainty analysis approaches could be interchanged for NSMC here, such as MCMC or postprocessing of MC and LHS sampling in order to obtain a set of calibrated velocity fields.

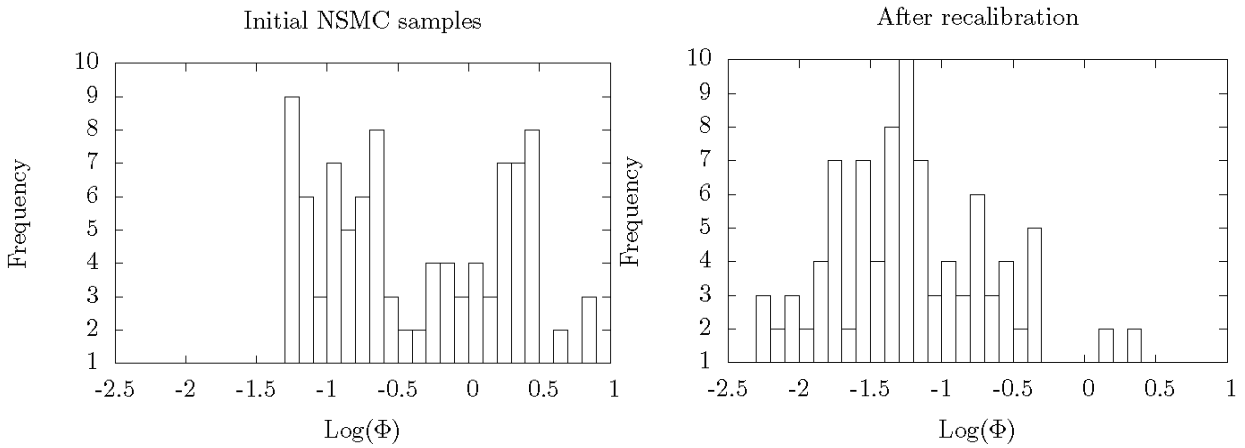

Figure 2-8. Histograms of log10 transformed objective function values for the 100 NSMC samples prior to recalibration and after recalibration

Once the NSMC is completed, a Python script is used to create a master HDF5 file, create *model groups* in this file, and mount the *PFloTran* HDF5 output files containing the calibration-constrained velocity field data. The fact that *PFloTran* outputs in HDF5 format is one advantage of its use as a simulator in this example.

The ODE solver described above extracts the velocity field data from the master file, calculates the flow paths, outputs the flow path data in HDF5 files and mounts these files within each *model group* of the master file. Figure 2-9 presents the computed flow paths superimposed on the 'true' permeability field. Note that the each flow path is generated from a different permeability field that is constrained to the head measurements, but is otherwise different. Since in our example we only know the head measurements, we must consider all the flow paths as possible in the PA. The ODE solver is a parallel code written using Parallel Python (Vanovschi, 2010) where the number of flow paths to calculate concurrently can be specified based on the available cpus. The use of Parallel Python allows this code to be easily scaled up to other systems with multiple processors or cores and clusters. The end result of running the ODE solver is an updated master file containing *flow path group* within each *model group*. It is important to remember that the objective function *attribute* assigned to each *model group* is also associated with each flow path.

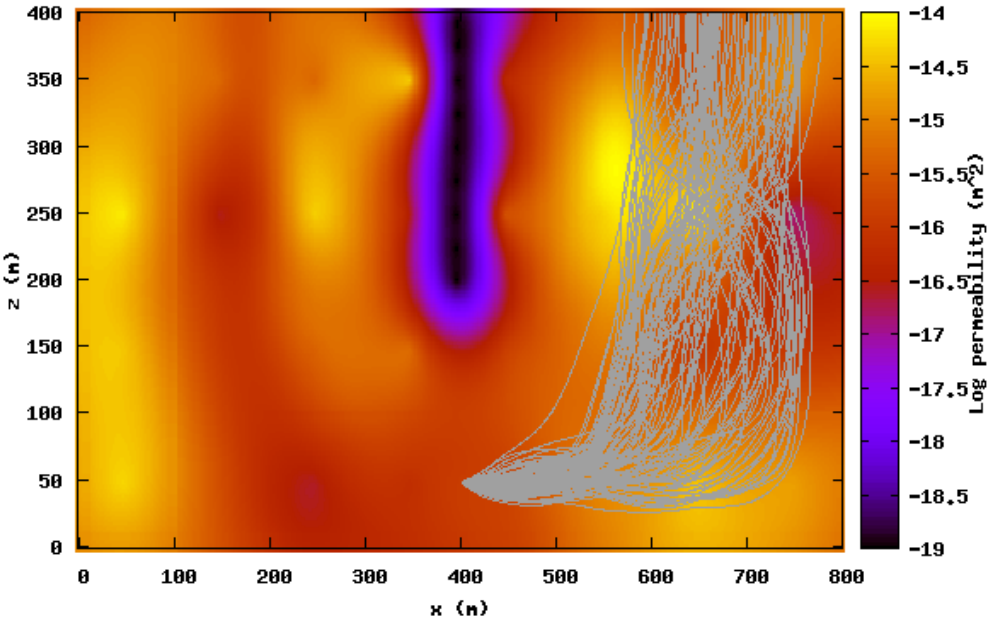

Figure 2-9. Calculated trajectories from the repository (x=400 m, y=50 m) to the ground surface (y=800 m) plotted over the 'true' permeability field. Each trajectory is consistent with the available hydraulic head measurements.

A Python script written for this research extracts the flow path information from the master file and generates *MARFA* input files. One input file contains beginning and ending coordinates and computed $\bar{\tau}$ (equation 8) and $\bar{\beta}$ (equation 9) values for approximately 1 m segments of the flow paths. The fracture half-aperture b required to compute β is set at 0.05 mm for all segments.

The other file contains radionuclide source information for each flow path weighted by their likelihood (refer to equation 3). It is assumed that 1.0 mol/y of ^{237}Np is released from the EBS for a 1 year duration. We consider the Neptunium series through ^{229}Th as ^{237}Np→^{233}Pa→^{233}U→^{229}Th. Given the relatively short half-life of ^{233}Pa, it is ignored in the decay chain. Therefore, we model the decay chain ^{237}Np→^{233}U→^{229}Th using decay constants of 3.2×10^{-7} y^{-1}, 4.4×10^{-6} y^{-1}, and 9.5×10^{-5} y^{-1}, respectively.

Tables 2-2-1 and 2-2-2 contain the fixed and LHS sampled limited diffusion retention model rock properties. The DAKOTA toolkit (Adams *et al.*, 2009) is used to generate 100 samples from the retention properties defined in Table 2-2 and execute the *MARFA* runs concurrently using a Python script to create

the *MARFA* input files using the sample properties. The Monte Carlo sampling was performed on 12 cpus.

Table 2-1. Fixed retention properties

Parameter	Value
R_m[kg/m^3]	2700
Δ [m]	2.0
k_a	0
α	0

Table 2-2. Sampled retention properties

Parameter	Distribution
Θ [–]	Uniform; min=1×10^{-3} max=2.5×10^{-3}
D_{eff} [m^2/y]	Lognormal; mean=2.0×10^{-14} std=1.6×10^{-14}
$K_{d,Np}$ [m^3/kg]	Lognormal; mean=5.2×10^{-2} std=1.8×10^{-1}
$K_{d,U}$ [m^2/kg]	Lognormal; mean=5.2×10^{-2} std=1.8×10^{-1}
$K_{d,Th}$ [m^2/kg]	Lognormal; mean=5.2×10^{-2} std=1.8×10^{-1}

Figures 2-10 to 2-13 presents correlation maps between sampled parameters and model outputs, where the rows are outputs defined as the cumulative breakthrough of radioactivity at the surface (z=400 m) in Bq at 1 million years for ^{237}Np (Cum$_{Np}$), ^{233}U (Cum$_{U}$), and ^{229}Th (Cum$_{Th}$), the maximum dose rate in Sv/y at the surface for ^{237}Np (Max$_{Np}$), ^{233}U (Max$_{U}$), and ^{229}Th (Max$_{Th}$), and the time when the maximum dose rate is achieved for ^{237}Np (Time$_{Np}$), ^{233}U (Time$_{U}$), and ^{229}Th (Time$_{Th}$). Figure 10 maps the simple Pearson's correlation coefficient, Figure 2-11 maps the partial Pearson's correlation coefficient (i.e. correlations with effects from other variables removed), Figure 2-12 maps the simple Spearman's rank correlation coefficient, and Figure 2-13 maps the partial Spearman's rank correlation coefficient. The sampled parameters are listed in Table 2-2-2 and defined above.

The similarities between the simple and partial correlation plots is apparent (compare Figure 2-10 with Figure 2-11 and Figure 2-12 with Figure 2-13). This is due to *DAKOTA*'s use of a restricted pairing method in its LHS algorithm that forces near-zero correlation between uncorrelated inputs (Adams *et al.*, 2009). Near-zero correlation are indicated by red cells, strong positive correlations by yellow cells, and strong negative correlations by black cells. As expected, correlations are primarily between sampled parameters and model outputs associated with the same radionuclide (e.g. Cum$_{Np}$ and $K_{d,Np}$). The

strength of many correlations increases from Pearson's to Spearman's rank correlations, indicating that nonlinearities exist in the correlations (this can also be due to differences in magnitudes between sampled parameters and model outputs, i.e. D_{eff} and model outputs have large differences in magnitude). There is also an increase in the strength of correlations between simple and partial Spearman's rank correlations, indicating that some of the sampled parameters are correlated. It can be concluded from the correlations that the matrix porosity θ is not strongly correlated with any of the model outputs.

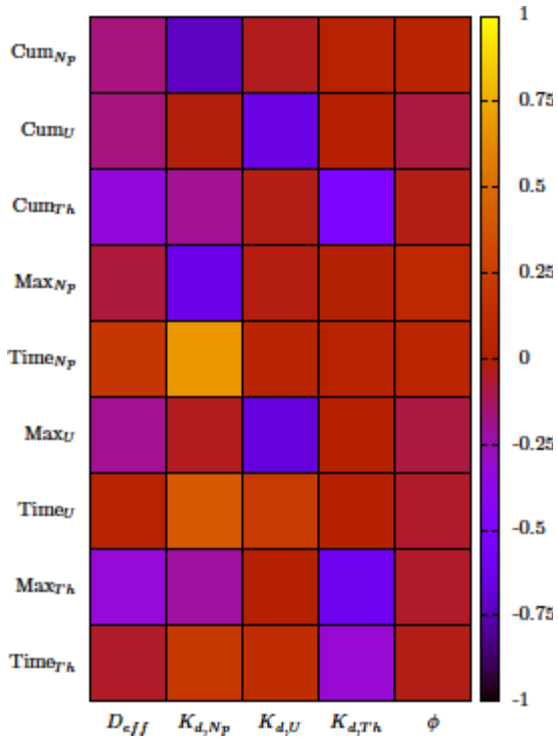

Figure 2-10. Simple Pearson's correlations between sampled parameters (columns) and model outputs (rows)

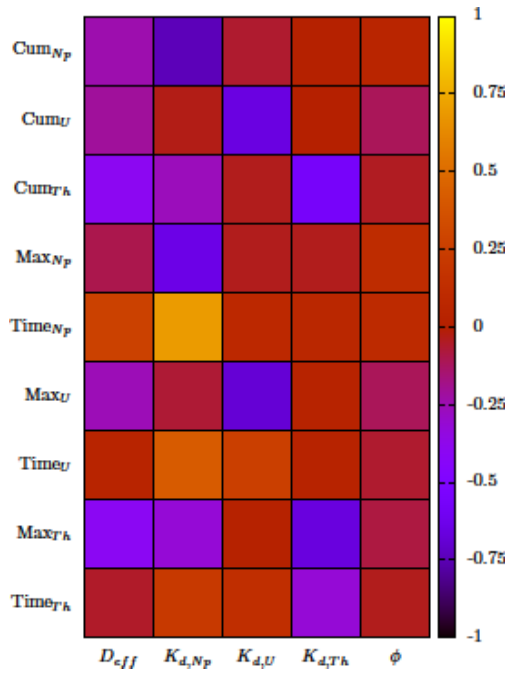

Figure 2-11. Partial Pearson's correlations between sampled parameters (columns) and model outputs (rows)

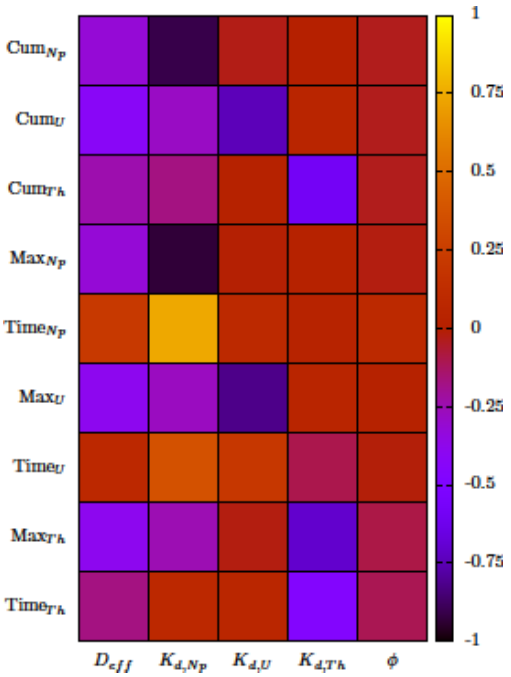

Figure 2-12. Spearman's Rank correlations between sampled parameters (columns) and model outputs (rows)

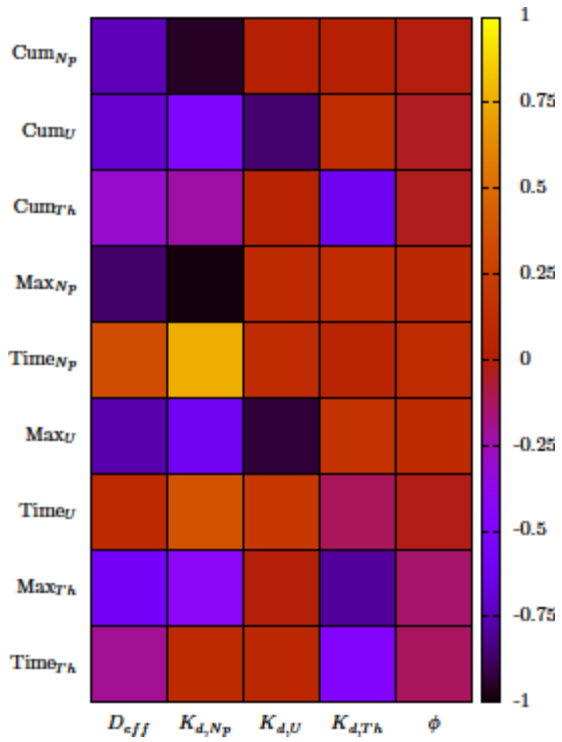

Figure 2-13. Partial Spearman's rank correlations between sampled parameters (columns) and model outputs (rows)

Model results are presented as histograms from the retention property samples of the cumulative radioactivity to reach the ground surface at 1 million years (Figure 2-14), the maximum dose rate at the ground surface (Figure 2-15), and the time of the maximum dose rate (Figure 2-16). In this example demonstration, it is apparent that the maximum radiation due to any single radionuclide is not over 6000 MBq at 1 million years, the maximum dose rate due to any single radionuclide is not over 0.9 μSv/y, and that the distributions of times to maximum dose rate is similar for all radionuclides, never exceeding 11 million years.

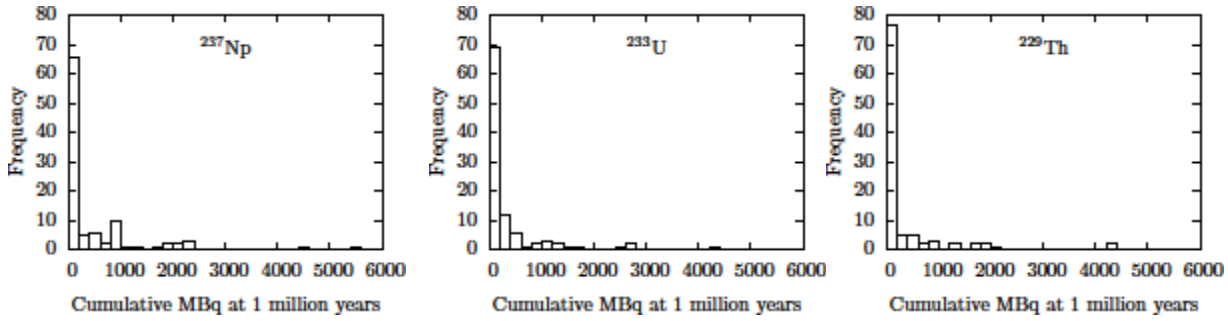

Figure 2-14. Cumulative breakthrough of radioactivity at the ground surface at 1 million years

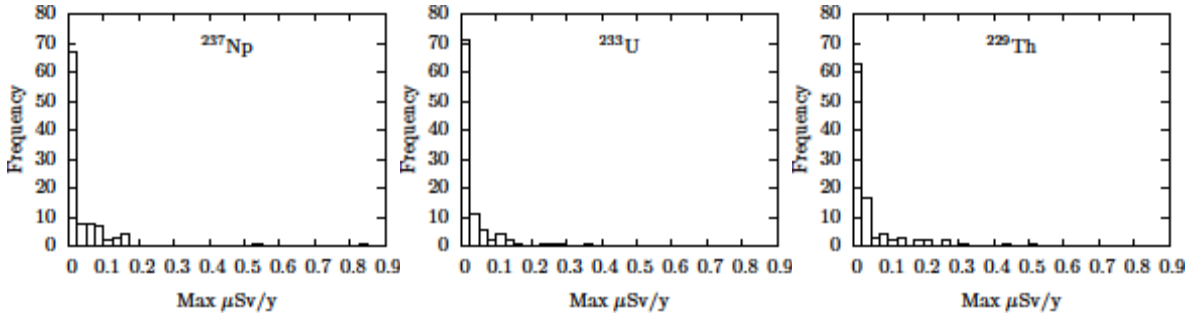

Figure 2-15. Maximum dose rate at the ground surface

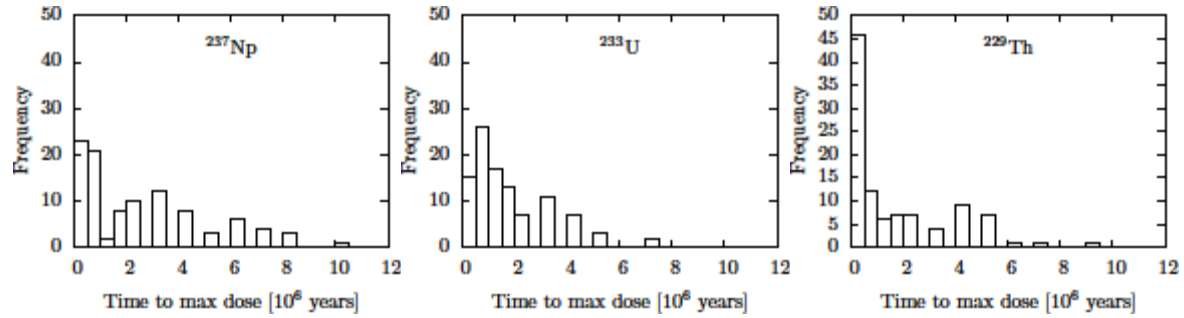

Figure 2-16. Time of maximum dose rate at the ground surface

2.6 Conclusions

The following design principles are proposed for a next-generation assessment framework:

1. Provide general framework where alternative process models and uncertainty analysis approaches can be interchanged in a "plug and play" type structure
2. Use common data format for efficient storage, processing, and organization
3. Incorporate parallel and concurrent simulations (HPC) wherever possible
4. Use calibration-constrained uncertainty analyses wherever possible
5. Use sampling-based uncertainty analysis wherever calibration-constrained uncertainty analysis is not possible
6. Use PA-tailored radionuclide transport algorithms

The framework shown in Figure 2-1 is a general framework that implements the six design principles. A synthetic example was used to demonstrate specific implementation of an assessment workflow that follows the proposed framework. This example demonstrates feasibility of such an approach using currently available modeling tools and taking advantage of HPC resources.

It is noted that the framework is extensible and that the addition of new process kernels is relatively straightforward. However, additional work is needed to develop the capability to incorporate discrete fracture network (DFN) flow models into the framework. A particularly appealing approach would be to

combine permeability fields upscaled from discrete fracture flow models and conditioned to available head measurements with stochastic transport downscaling algorithms (Painter and Cvetkovic, 2005) derived from DFNs.

2.7 References

Adams, B.M., Bohnhoff, W.J., Dalbey, K.R., Eddy, J.P., Eldred, M.S., Gay, D.M., Haskell, K., Hough, P.D., Swiler, L.P. (2009) *DAKOTA, a Multilevel Parellel Object-oriented Framework for Design Optimization, Parameter Estimation, Uncertainty Quantification, and Sensitivity Analysis: Version 5.0 User's Manual*. Sandia Technical Report SAND2010-2183, Sandia National Laboratory, Albuquerque, NM.

Baer, T. A., Price, L. L., Emery, J. N., Olague, N. E. (1994) *Second Performance Assessment Iteration of the Greater Confinement Disposal Facility at the Nevada Test Site*. Tech. rept. SAND93-0089. Sandia National Laboratories, Albuquerque, NM.

Beven, K., Binley, A. (1992) The future of distributed models: model calibration and uncertainty prediction. *Hydrological processes* **6**(3), pp. 279–298.

Campbell, J.E., Cranwell, R.M. (1988) Performance assessment of radioactive waste repositories. *Science*, **239**(18 March), pp. 1389–1392.

Collette, A. (2008) *H5PY for Python*. http://h5py.alfven.org/.

Doherty, J., Brebber, L., Whyte, P. (1994) Pest. *Watermark Computing, Corinda, Australia*.

Ewing, R.C., Tierney, M.S., Konikow, L.F., Rechard, R.P. (1999) Performance assessments of nuclear waste repositories: A dialogue on their value and limitations. *Risk Analysis* **19**(5), pp. 933–958.

Gallegos, D.P., Bonano, E.J. (1993) Consideration of uncertainty in the performance assessment of radioactive waste disposal from an international regulatory perspective. *Reliability Engineering & System Safety*, **42**(2-3), pp. 111–123.

Heijmans, J. (2001) *An introduction to distributed visualization*. Delft University of Technology, Delft.

Helton, J.C. (1993) Uncertainty and sensitivity analysis techniques for use in performance assessment for radioactive waste disposal. *Reliability Engineering & System Safety*, **42**(2-3), pp. 327–367.

Higdon, D. (1998) A process-convolution approach to modelling temperatures in the North Atlantic Ocean. *Environmental and Ecological Statistics*, **5**(2), pp. 173–190.

Iman, R.L., Helton, J.C., Campbell, J.E. (1978) *Risk Methodology for Geological Disposal of Radioactive Waste: Sensitivity Analysis Techniques*. Tech. rept. SAND78-0912, NUREG/CR-0390. Sandia National Laboratories, Albuquerque, NM.

Jones, E., Oliphant, T, Peterson, P. (2001) *SciPy: Open source scientific tools for Python*. http://www.scipy.org/.

Lichtner, P..(2009) PFLOTRAN project web site. *https://software. lanl. gov/pflotran*.

Morris, M.D. (1991) Factorial sampling plans for preliminary computational experiments. *Technometrics*, pp. 161–174.

Nuclear Energy Agency (1990) Disposal of High-Level Radioactive Wastes: Radiation Protection and Safety Criteria. In: NEA Workshop, Paris, 5-7 November 1990. NEA, Organisation for Economic Co-Operation and Development, Paris, 1991, Paris.

Painter, S., Mancillas, J. (2010) *MARFA Version 3.2.2 User's Manual: Migration Analysis of Radionuclides in the Far Field*. Svensk kärnbränslehantering (SKB), Stockholm Sweden.

Painter, S., Cvetkovic, V., Mancillas, J., Pensado, O. (2008) Time domain particle tracking methods for simulating transport with retention and first-order transformation. *Water resources research*, **44**(1), W01406.

Painter, S., Cvetkovic, V. (2005) Upscaling discrete fracture network simulations: An alternative to continuum transport models, Water Resour. Res., 41, W02002, doi:10.1029/2004WR003682.

Pebesma, E.J., Wesseling, C.G. (1998) Gstat: a program for geostatistical modelling, prediction and simulation. *Computers & Geosciences*, **24**(1), pp. 17–31.

Piessens, R., Doncker-Kapenga, D., Überhuber, C., Kahaner, D. (1983) *QUADPACK, A subroutine package for automatic integration*. Springer. ISBN: 3-540-12553-1.

Rechard, R. P. (1999) Historical Relationship Between Performance Assessment for Radioactive Waste Disposal and Other Types of Risk Assessment. *Risk Analysis*, **19**(5), pp. 763–807.

Tonkin, M., Doherty, J. (2009) Calibration-constrained Monte Carlo analysis of highly parameterized models using subspace techniques. *Water Resources Research*, **45**(12), W00B10.

Vanovschi, V. (2010) *Parallel Python Software*. http://www.parallelpython.com.

Vrugt, J.A., Ter Braak, CJF, Diks, CGH, Robinson, B.A., Hyman, J.M., Higdon, D. (2009) Accelerating Markov chain Monte Carlo simulation by differential evolution with self-adaptive randomized subspace sampling. *International Journal of Nonlinear Sciences and Numerical Simulation*, **10**(3), pp. 273–290.

3.0 Integrated Tool Development for Far-Field Radionuclide Transport in a Salt Repository

3.1 Introduction

In this section, we continue to explore the potential use of probabilistic risk assessment tools to evaluate the capability of a natural barrier system (NBS) and to identify key controlling factors of the system. The work presented here adopts part of the enhanced performance assessment system (EPAS) developed by Wang et al. (2010) for the evaluation of geologic storage of carbon dioxide. We here apply the EPAS to simulate groundwater flow and radionuclide transport in a dolomite formation – a representative far-field release pathway of a salt repository.

The flowchart of the EPAS methodology is shown in Figure 3-1. The forward model components represent the typical steps of a typical existing performance assessment (PA) methodology. According to the existing methodology, a PA starts with Feature, Event, and Process (FEP) evaluation, through which potentially important FEPs are identified for inclusion for further PA analysis. FEP evaluation also helps define performance scenarios of a system of interest by identifying major radionuclide release pathways. The next step of a PA analysis is to develop appropriate computational models for the selected FEPs and the defined performance scenarios and then to constrain model input parameters. The model input parameter values and their uncertainty distributions are constrained from field observations and laboratory experimental data. The whole cycle of a PA analysis is then completed by uncertainty quantification and sensitivity analysis, typically performed using multiple Monte-Carlo simulations. The whole PA process is generally iterative. The EPAS extends the existing PA methodology by adding the inverse model components, as shown in Figure 3.1. These inverse components provide necessary tools for optimization of long-term system performance, process optimization, as well as updating of parameter estimates as new data are obtained. To fulfill these new functionalities, a new PA system must have a built-in optimization capability. The EPAS includes a built-in optimization capability for model parameterization and monitoring system design.

The high-level EPAS architecture is shown in Figure 3-2. The system consists of three layers. The middle layer hosts detailed process models to capture all important physics involved in a high-level radioactive waste disposal. The bottom layer provides all necessary data to support process model runs. These two layers are then wrapped by a PA driver that is able to couple different process models, direct Monte-Carlo simulations, and assist PA analysis. In order for the PA system to be able to do inverse modeling, the PA driver must have a built-in optimization capability. For this work DAKOTA was chosen to be the PA driver. DAKOTA (Design Analysis Kit for Optimization and Terascale Applications) is a powerful and versatile software toolkit that provides a flexible and extensible interface between simulation codes and iterative analysis methods used in large-scale systems engineering optimization, uncertainty quantification, and sensitivity analysis (Eldred et al, 2002). A full set of PA calculations impose stringent requirements on process code performance. The process codes must be robust and fast enough to run multiple model simulations in a widely spanned model parameter space. For the work documented here, FEHM is used as the flow and transport reservoir simulator.

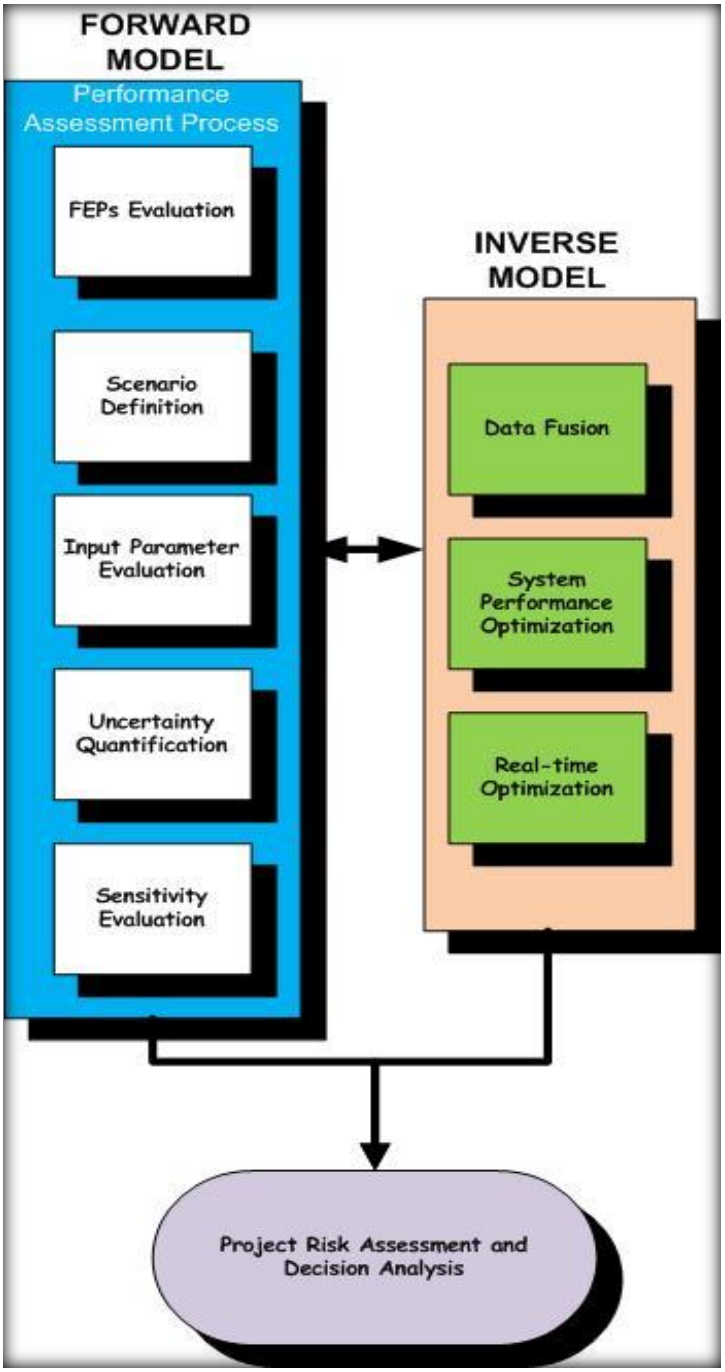

Figure 3-1. Flow chart of the Enhanced Performance Assessment System (EPAS)

The DAKOTA-FEHM coupling allows for concurrent execution of code runs in a parallel computation mode when multiple CPUs are available. This scalable code execution mode allows fully coupled multiphase FEHM simulations with various levels of complexity to be completed in a reasonable amount of time.

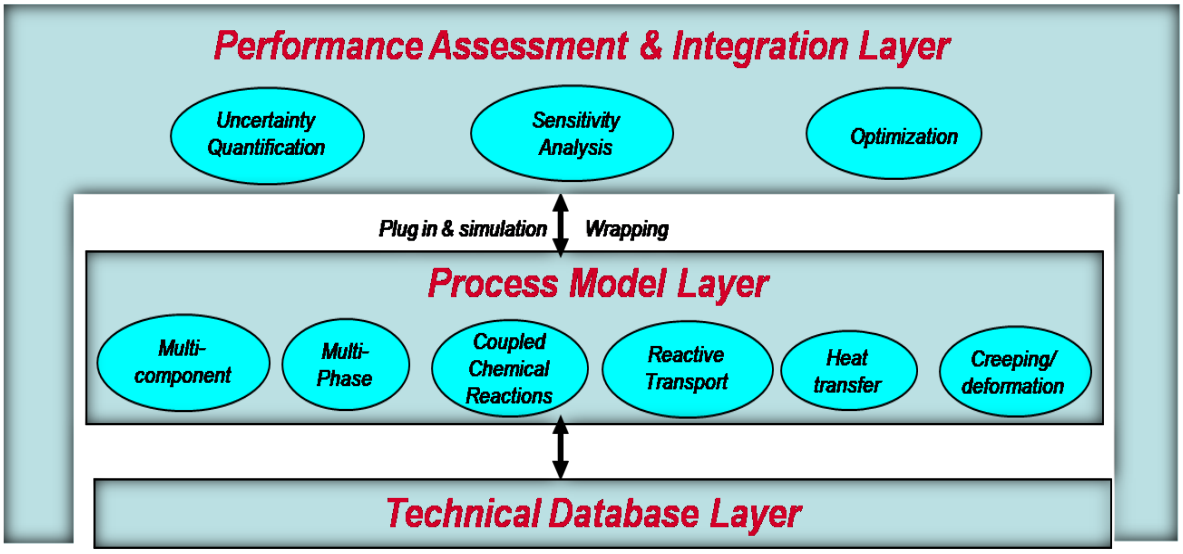

Figure 3-2. An example of total performance assessment system architecture

3.2 Generic Salt Repository and Model Setup

The conceptual model for radionuclide release and transport from a generic salt repository was developed using the literature data of existing salt repository sites including the Waste Isolation Pilot Plant (WIPP) site (Wang and Lee, 2010). Figure 1 shows a schematic for the conceptual model for radionuclide release and transport in a generic salt repository. Two scenarios are considered for repository radionuclide release and transport: the reference case, and the disturbed case. The reference case releases radionuclides by a sequence of typical processes that are expected to occur in a salt repository, and the disturbed case represents a non-typical process that provides a fast pathway for radionuclide to the far-field due to human intrusion. For the purpose of tool demonstrations, we here focus on the flow and radionuclide transport in the far field of a salt repository in a human intrusion scenario. As stated above, the integrated tool development for far-field radionuclide transport was developed by wrapping the flow and transport reservoir simulator (FEHM) with the uncertainty quantification and optimization code (DAKOTA).

3.2.1 Description of FEHM Reservoir Simulator

FEHM is a finite-element heat- and mass-transport numerical code that simulates nonisothermal, multiphase, multicomponent flow, and solute transport in porous media (Zyvoloski, 2007; Zyvoloski, et al. 1997). FEHM has been used to simulate groundwater and contaminant flow and transport in deep and

shallow, fractured and un-fractured porous media. For this study FEHM V. 2.24 has been used to model flow and transport in the far-field of a generic salt repository.

3.2.2 Description of DAKOTA

DAKOTA (Design Analysis Kit for Optimization and Terascale Applications) is a software toolkit that provides a flexible and extensible interface between simulation codes and iterative analysis methods used in large-scale systems engineering optimization, uncertainty quantification, and sensitivity analysis (Eldred et al, 2002). The DAKOTA toolkit can perform parameter optimization through the use of gradient and non-gradient-based methods. It can also be used to conduct sensitivity analysis with the purpose of investigating variability in response to variations in model parameters using sampling methods such as Latin Hypercube Sampling (LHS), among others. Further capabilities of the toolkit include uncertainty quantification with sampling, analytic reliability, and stochastic finite element methods; and parameter estimation with nonlinear least squares methods. These capabilities may be used on their own or as components within system models. By employing object oriented design to implement abstractions of the key components required for iterative systems analyses, the DAKOTA toolkit provides a flexible and extensible problem-solving environment for design and performance analysis of computational models on high performance computers. For this analysis, DAKOTA version 5.2 was utilized.

3.2.3 Wrapping FEHM with DAKOTA

Specific to this study, a DAKOTA based nondeterministic sampling algorithm is implemented for the new performance assessment framework. Figure 3-3 schematically depicts the overall scheme of how DAKOTA is coupled to FEHM. The overall sampling flow involves embedded FEHM functional evaluations within a DAKOTA run. First, a set of uncertain parameters with assigned probability distributions is specified in the DAKOTA input parameter file. A sample is drawn using Latin Hypercube sampling (LHS) internal to DAKOTA. The sample is processed by an input filter routine to transcribe each sample element, comprising a value for each uncertain parameter, into a formatted template file that is compatible with FEHM. After each sample element is executed, an output filter extracts the pertinent output values via an output filter routine and returns these to DAKOTA.

LHS can be described as a stratified sampling method where the range of each variable to be sampled is divided into intervals of equal probability and a value is randomly sampled from each interval (Adams et al., 2010). Sampled values are randomly paired for different variables to form sample elements. Overall, LHS needs fewer samples relative to other random sampling methods (e.g., Monte Carlo) to obtain statistically stable estimates of mean values and has become widely used in uncertainty analysis. DAKOTA summarizes the statistical spread of the output observations at the completion of each DAKOTA run.

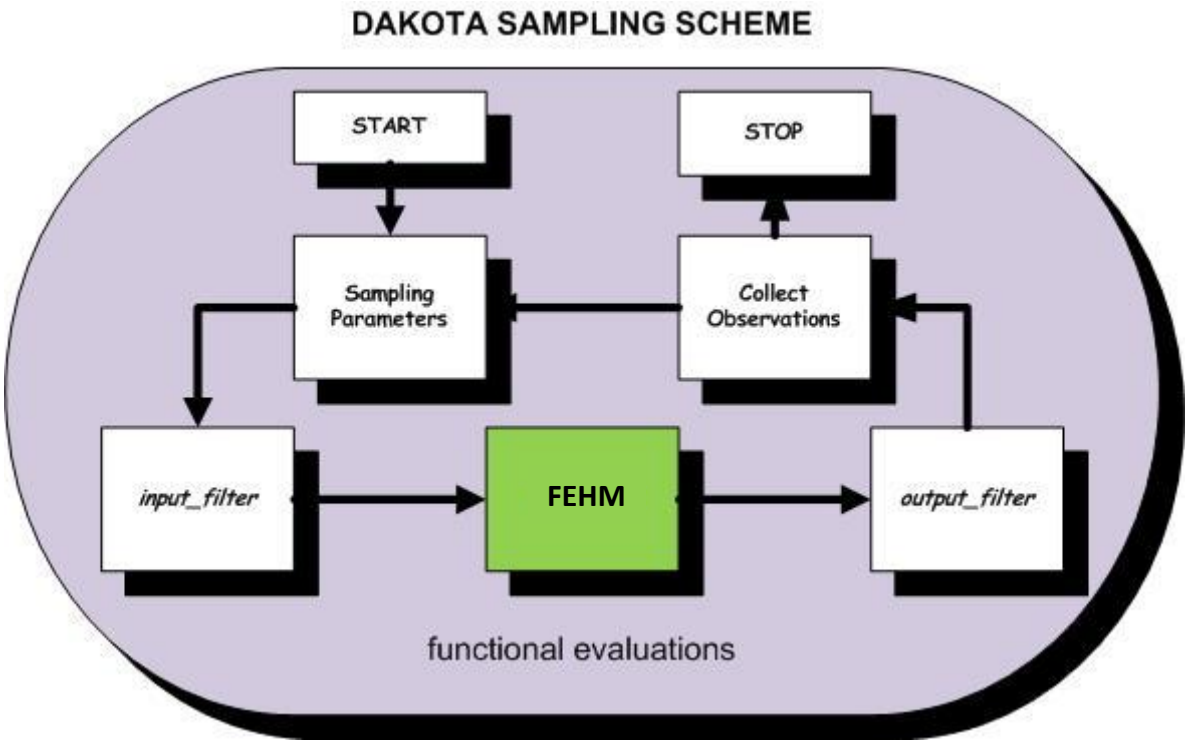

Figure 3-3. Schematic of DAKOTA-based PA framework

3.2.4 Parallel version of DAKOTA-FEHM

DAKOTA is designed to support large-scale simulations that can be computationally intensive. Different levels of parallelism are available for users to utilize in DAKOTA. For the new framework, a hybrid parallelism is assumed. Figure 3-4 shows how the flow of information works in a hybrid implementation. Extraction scripts embedded in the DAKOTA simulation script were also developed for the extraction of FEHM outputs in each code run.

Specification of asynchronous concurrency within DAKOTA provides a level of parallelism at the functional evaluation level. A number of concurrent serial FEHM jobs can be executed at any given time as long as the computational CPUs are available. This level of parallelism essentially shortens the overall calculation cycle. Such coupling can further be refined and expanded to run in parallel onhigh-performance computational clusters.

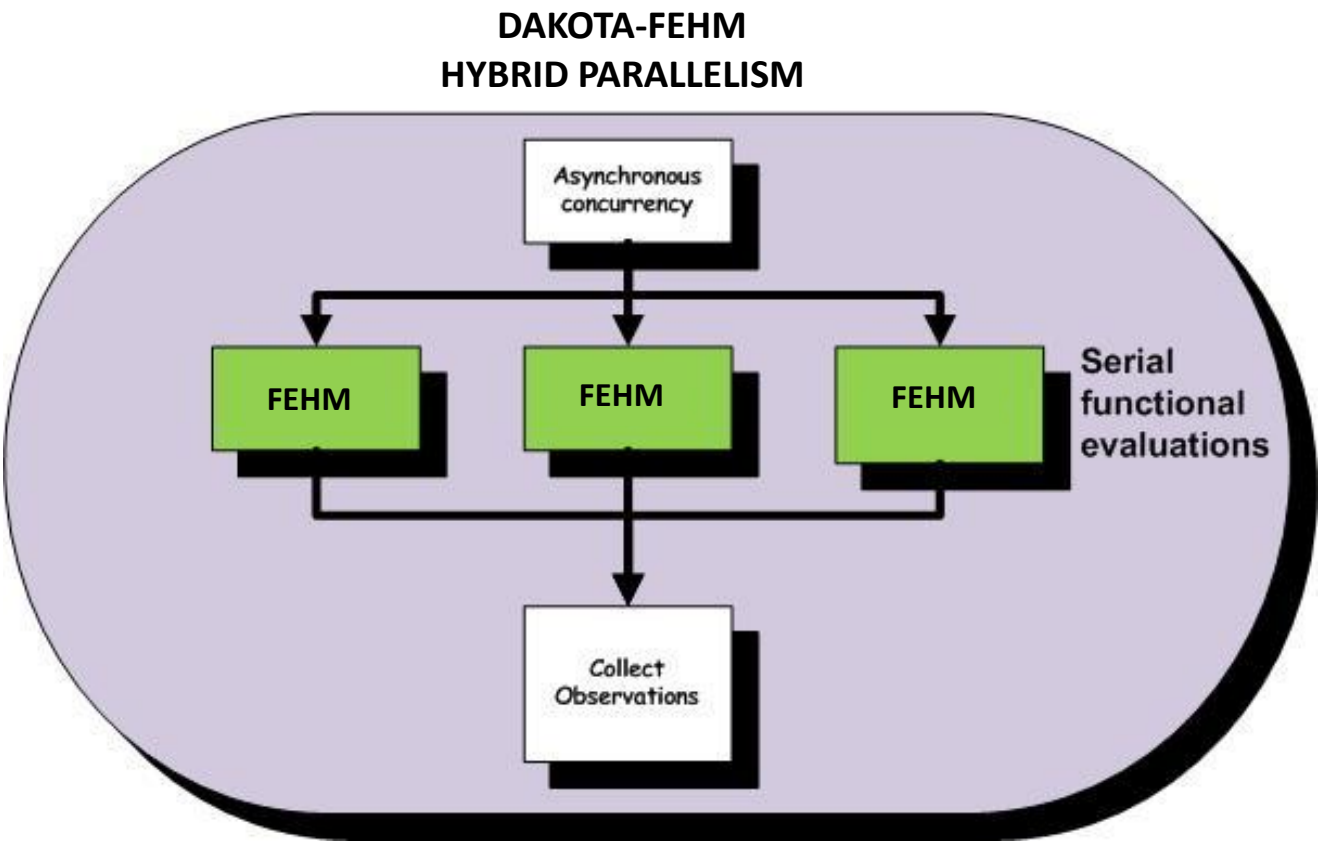

Figure 3-4. Schematic diagram hybrid parallelism used in this study

3.3 Tool Demonstration

For tool demonstration isothermal flow and transport dual porosity simulations in the Culebra Dolomite member of the WIPP repository were used as analog for radionuclide transport in the far-field of a generic high-level nuclear waste repository in bedded salt. The Culebra is a carbonate aquifer that is the most transmissive unit above the repository, and it is assumed to comprise primarily dolomite matrix. It is considered the most likely pathway for transport of radionuclides from the salt repository to the accessible environment, and thus represents the upper far field of the WIPP salt repository (Helton et al., 2000). Figure 3-5 shows the conceptual pathways for radionuclide transport from the WIPP repository for undisturbed and disturbed conditions. Transport to the Culebra could be upwards through the shaft seal system (undisturbed) or through a borehole that penetrates the waste disposal region and underlying pressurized brine pocket (disturbed). For this exercise the disturbed case scenario assumes radionuclide transport up through a borehole to the Culebra dolomite.

3.3.1 Flow simulations

Transport in the Culebra is a function of groundwater flow represented by transmissivity fields. For this analysis groundwater flow data were obtained from Kuhlman (2010). For brevity simplifications were made in the simulations wherever possible. This analysis did not consider the impacts of potential mining within WIPP the Land Withdrawal Boundary, and thus the original transmissivity fields from Hart et al. (2009) were used.

The Culebra Dolomite member is about 7.75 m thick fracture rock with heterogeneities in both horizontal and vertical directions. The Culebra has been modeled as a dual porosity system with groundwater flow represented by fracture porosity and diffusion represented by matrix porosity. For modeling purposes heterogeneities in the vertical direction have been ignored as the errors of doing so have been determined to be negligible (Corbet, 1995). In groundwater flow calculations, the full 7.75 m thickness of the Culebra was used, while for transport and particle tracking purposes the thickness is reduced to 4.0 m to focus all flow through the lower, more permeable portion of the Culebra (Holt, 1997). In flow simulations the Culebra was modeled as a single porosity system with a flow domain covering an area of 28.4 km (east-west) by 30.7 km (north-south). Transmissivity fields were obtained for the flow domain for grid blocks of 100 m x 100 m x 7.75 m size, for 600 realizations representing two mining scenarios, three replicates and 100 LHS samples (Kuhlman 2010). For transport calculations the domain used is a subregion of that used for the groundwater flow calculations, and covers an area of about 7.5 km by 5.4 km (Kuhlman, 2010).

For this exercise flow and transport in the transport domain has been modeled. The geometry of the simulation domain is 7500 m x 5400 m by 4 m thickness. The Cubit mesh generation tool (SNL 2011) was used to generate the mesh. The grid consists of a two-dimensional uniform mesh with 100 m x 100 m x 4 m grid blocks for a total of 4050 grid blocks (Figure 3-6). Permeability, horizontal anisotropy and head data (i.e. transmissivity fields) covering the transport domain were extracted from the larger groundwater flow domain presented by Hart et al. (2009). Perl scripts were used for extraction of data. For demonstration purposes only transmissivity fields for Realization 1 were used. Forward steady-state groundwater flow simulation was first done using permeability, horizontal anisotropy fields and head boundary conditions at the boundary of the transport domain. Figures 3-7 to 3-9 show the x-permeability field, the y-permeability field and steady state head data. Figure 3-10 shows the corresponding velocity directions.

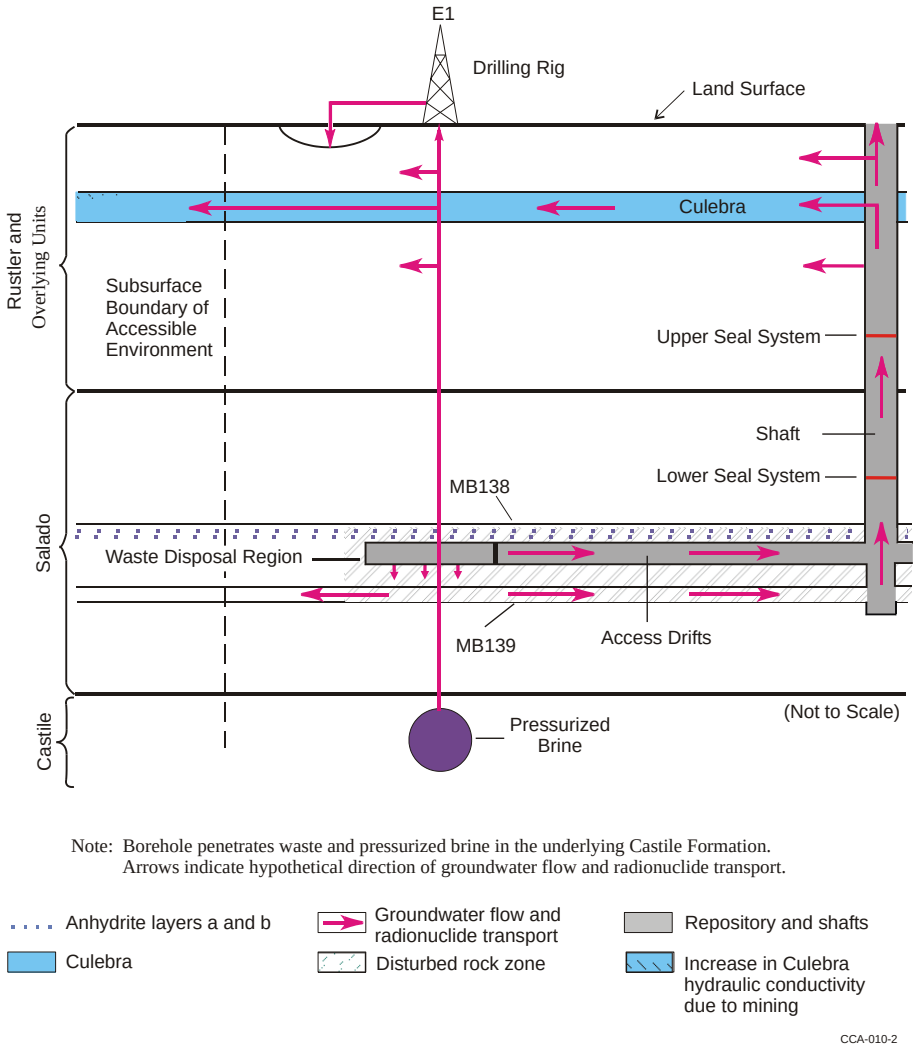

Figure 1-5. Conceptual radionuclide release pathways for a disturbed scenario of a generic salt repository (based on the WIPP repository)

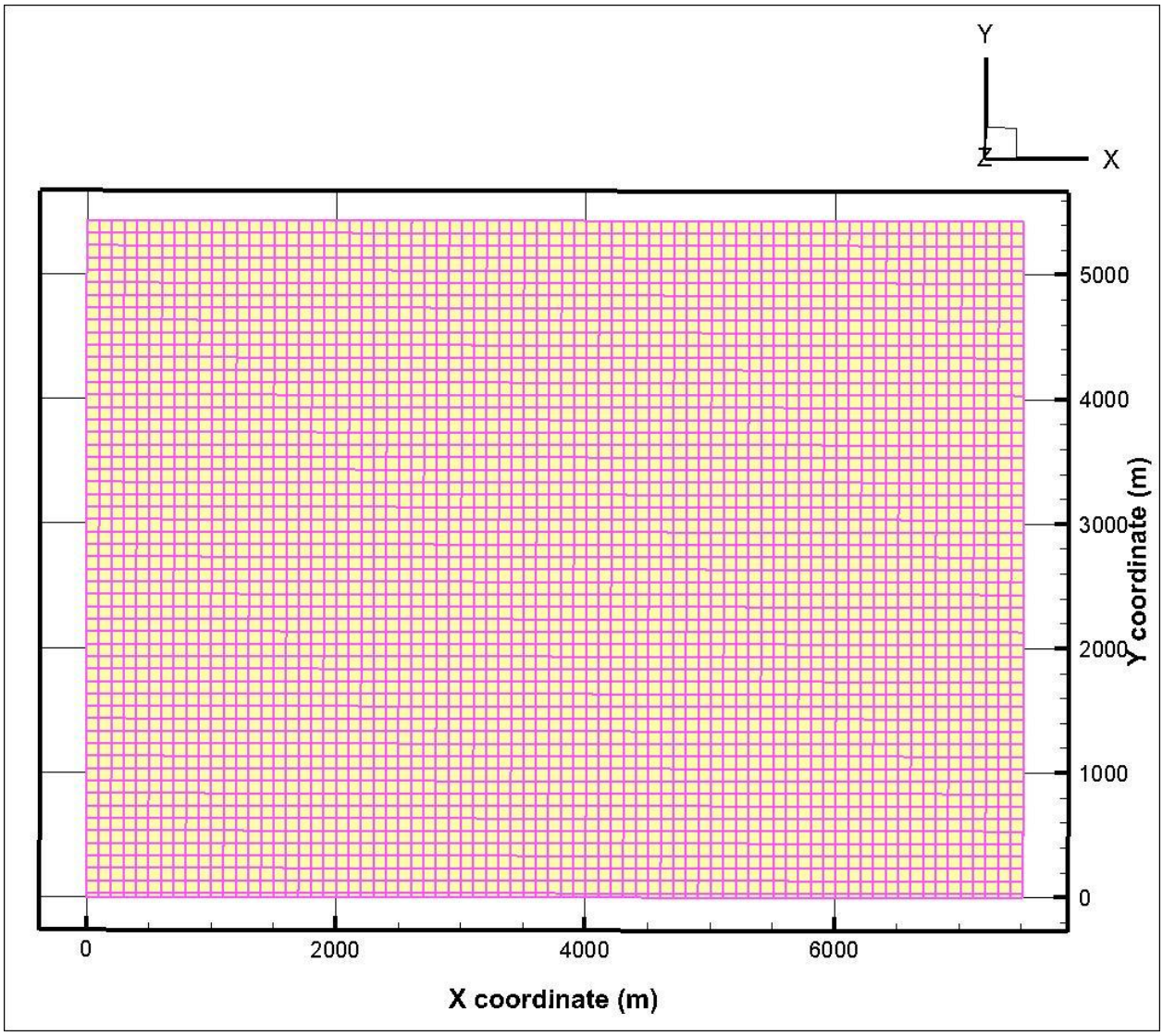

Figure 3-6. Mesh representing the transport domain for Culebra Dolomite transport simulations (100 m x 100 m x 4 m blocks used)

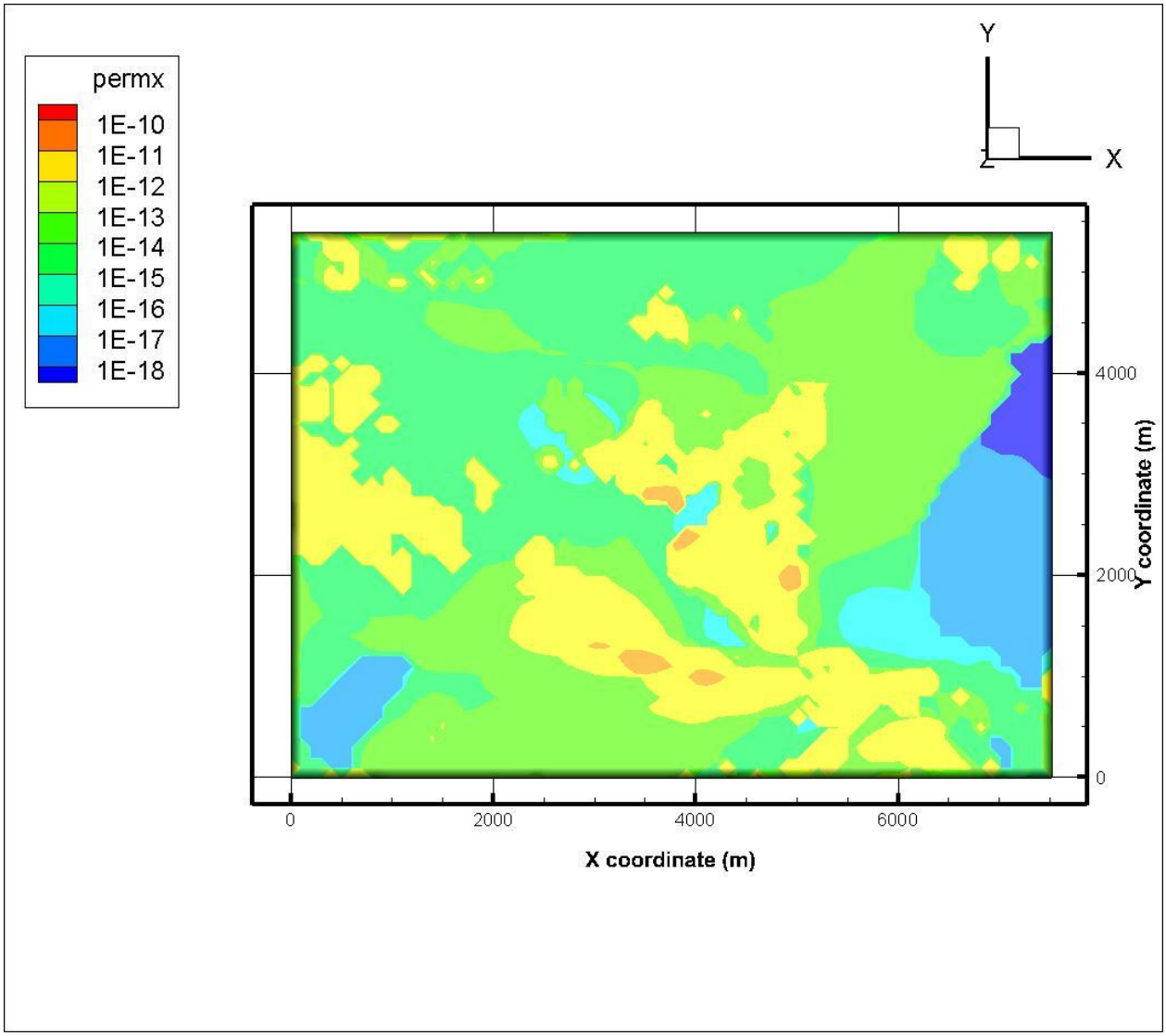

Figure 3-7. Permeability field in the x-direction applied to the transport domain (based on Realization 1 data)

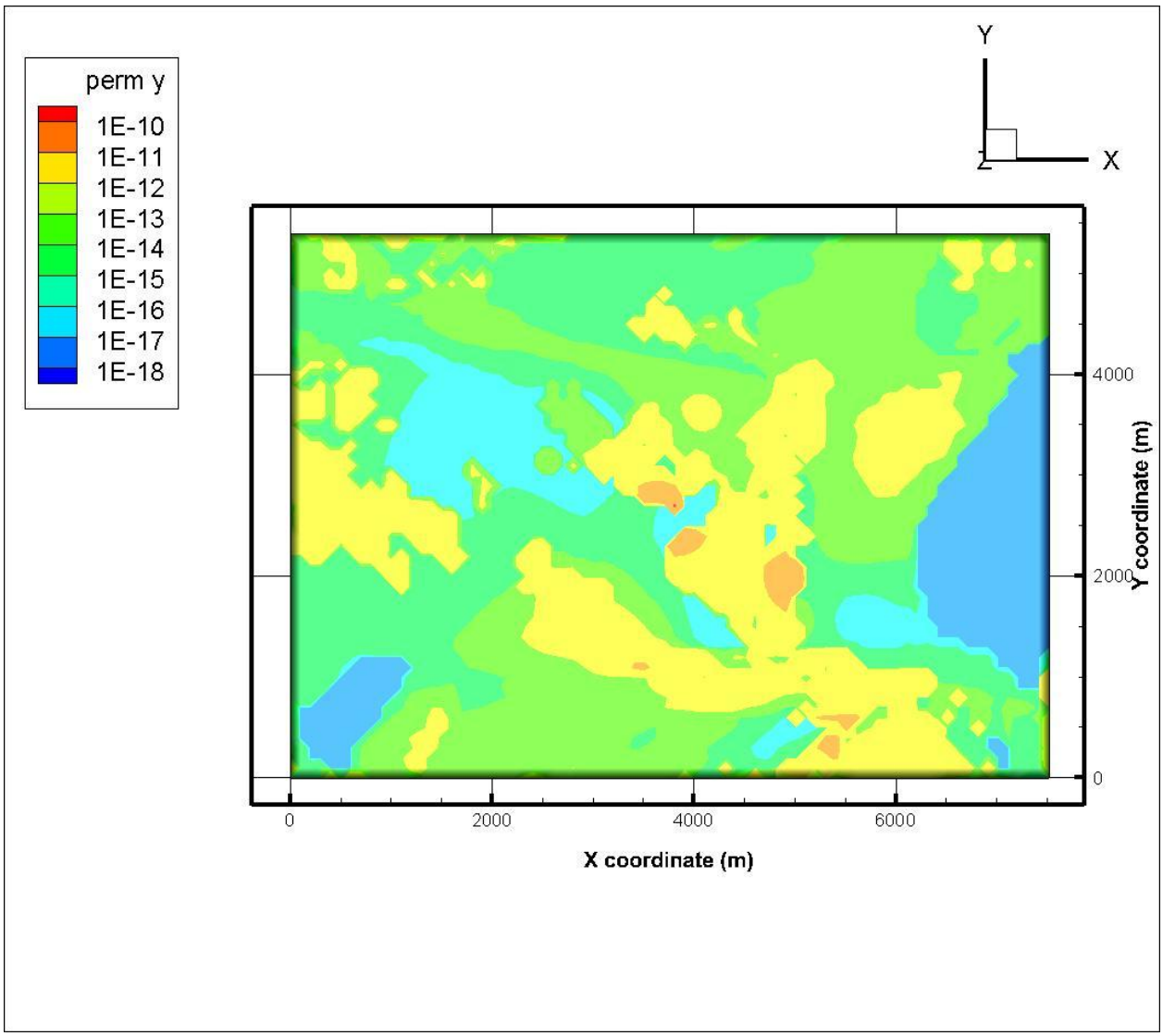

Figure 3-8. Permeability field in the y-direction applied to the transport domain (based on Realization 1 data)

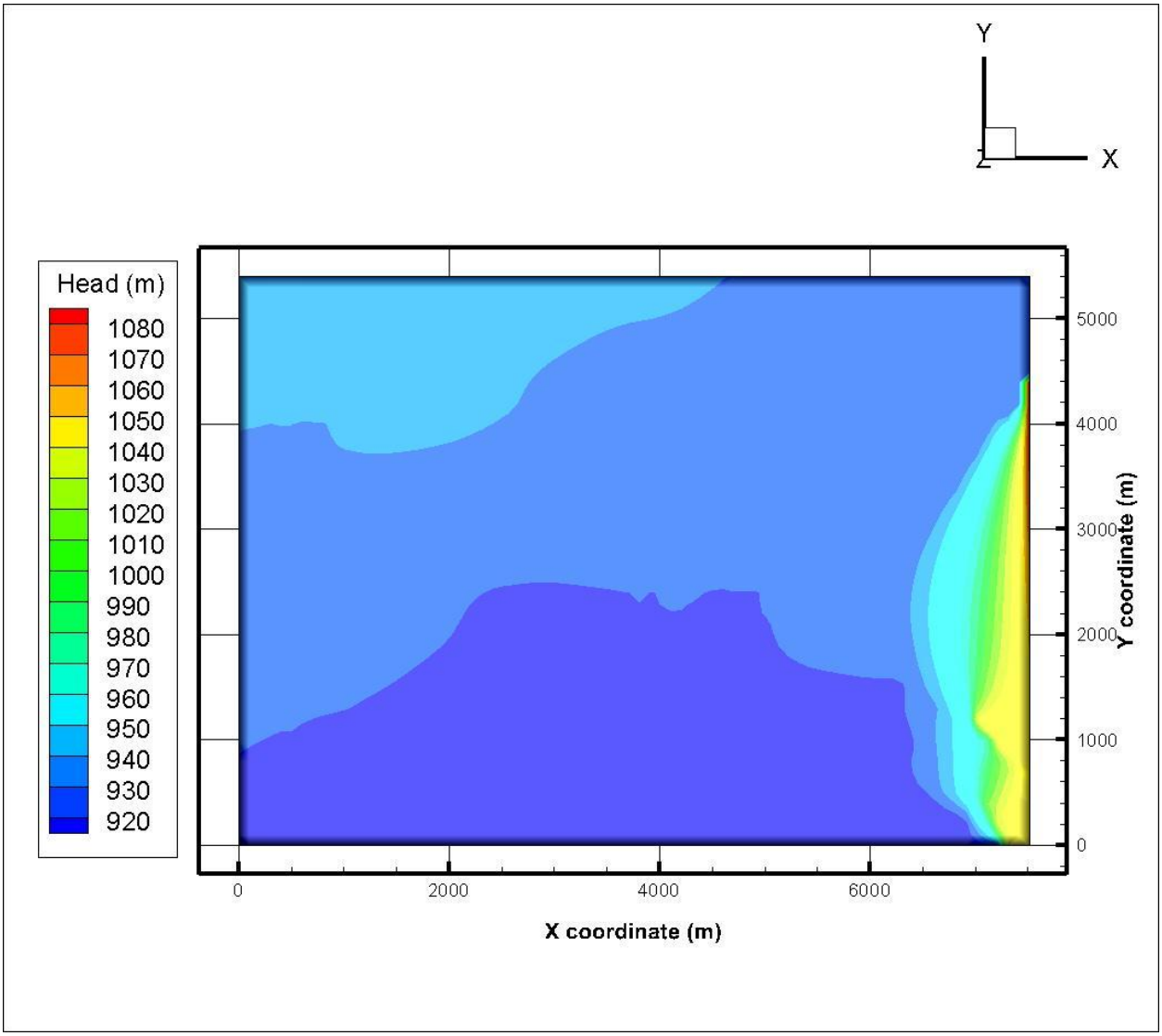

Figure 3-9. Steady-state head data (based on Realization 1 data)

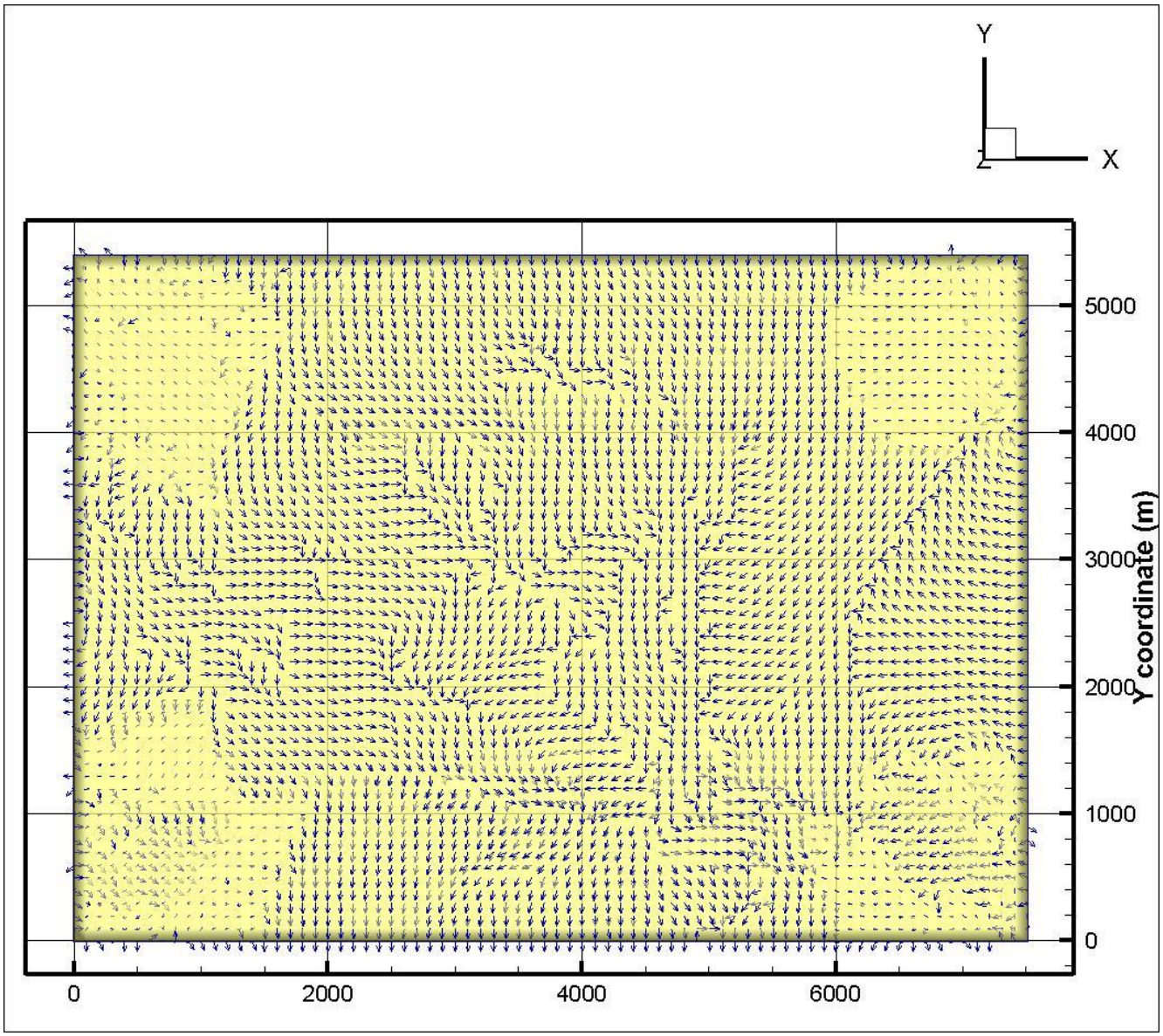

Figure 3-10. Steady-state flow velocity direction (based on Realization 1 data)

3.3.2 Deterministic transport simulations

FEHM-only transport runs were carried out to compute particle pathlines and a breakthrough curve. The results can be used to determine travel time and particle-tracking directions. Particle tracking was done using the steady-state flow field from a point in the Culebra transport domain above the center of the WIPP disposal panels to the transport domain boundary. The release point was taken to be at x = 3100m and y = 2000 m in the transport domain coordinates, approximately corresponding to the location of monitoring well C-2737, directly above the center of the WIPP waste panels (Kuhlman, 2010). The same grid was used for both flow and transport simulations (Figure 3-6). Parameter data used are shown in Table 3-1. For the deterministic simulations matrix porosity of 0.1, fracture porosity of 0.01, aperture of 0.01 m were used with no sorption. Two separate runs were made to generate the particle pathlines and the breakthrough curve. For the run to determine pathlines 100 particles were placed at the release point. For transport simulations the Streamline Particle Tracking (sptr) macro of FEHM was used. The particle transport macro represents advective as well as diffusive components. However, it does not include radionuclide decay and ingrowth. For these simulations FEHM was run to 100,000 years. Results of the first simulation run are shownin Figure 3-11, indicating mass travel directions. WIPP PA takes no credit for hydrodynamic dispersion in Culebra transport directions (Kuhlman, 2010). Both the deterministic and probabilistic simulations in this report also did not include dispersion (see Table 3-1). The general travel direction is to first move to the east and then south towards the southern boundary of the transport domain. Most of the mass exits near a relatively higher transmissivity area.

In the second FEHM run to obtain the breakthrough curve 1000 particles were placed at the release point. Figure 3-12 shows a breakthrough curve with cumulative relative mass at the transport domain boundary vs. time. As discussed above dispersion was not included in these runs. In addition, as mentioned above, the simulations do not include sorption or radionuclide decay. As a result the travel time towards the transport domain boundary is relatively fast.

In Figure 3-11 the mass transport covers a narrow area because hydrodynamic dispersion was not included. To illustrate the effect of dispersion on the travel path a FEHM run was made with dispersion included. For the exercise longitudinal dispersivity of 50 m, transverse horizontal dispersivity of 5.0 m, and traverse vertical dispersivity of 0.5 m were used. The results are shown in Figure 3-13, with the mass spread over a larger area.

Table 3-1. List of input parameters

Parameter	Distribution Type	Parameter Value and Description
Longitudinal dispersivity (m)	Constant	0
Tansverse horizontal dispersivity (m)	Constant	0
Transverse vertical dispersivity (m)	Constant	0
Matrix diffusion coefficient (m^2/s)	Constant	1.0E-11
Molecular diffusion coefficient (m^2/s)	Constant	2.2E-09
Material grain density (kg/m^3)	Constant	2820
Fracture porosity	Log-uniform	1.0E-04 (min); 1.0E-02 (max)
Matrix porosity	Uniform	1.0E-01 (min); 2.5E-01 (max)
Matrix half-block length (m)	Uniform	5.0E-02 (min); 5.0E-01 (max)
K_d for Radioelement (mL/g):		
I	Uniform	0.0 (min); 1.0 (max)
Pu(IV)	Log-uniform	0.5 (min); 1.0E+04 (max)
U(VI)	Log-uniform	3.0E-02 (min); 2.0E+01 (max)

NOTE: Data in this table are from Kuhlman (2010). The matrix porosity distribution was changed from cumulative to uniform, and the Kd data for I is from Miller and Wang 2012). Diffusion coefficients were set in this report.

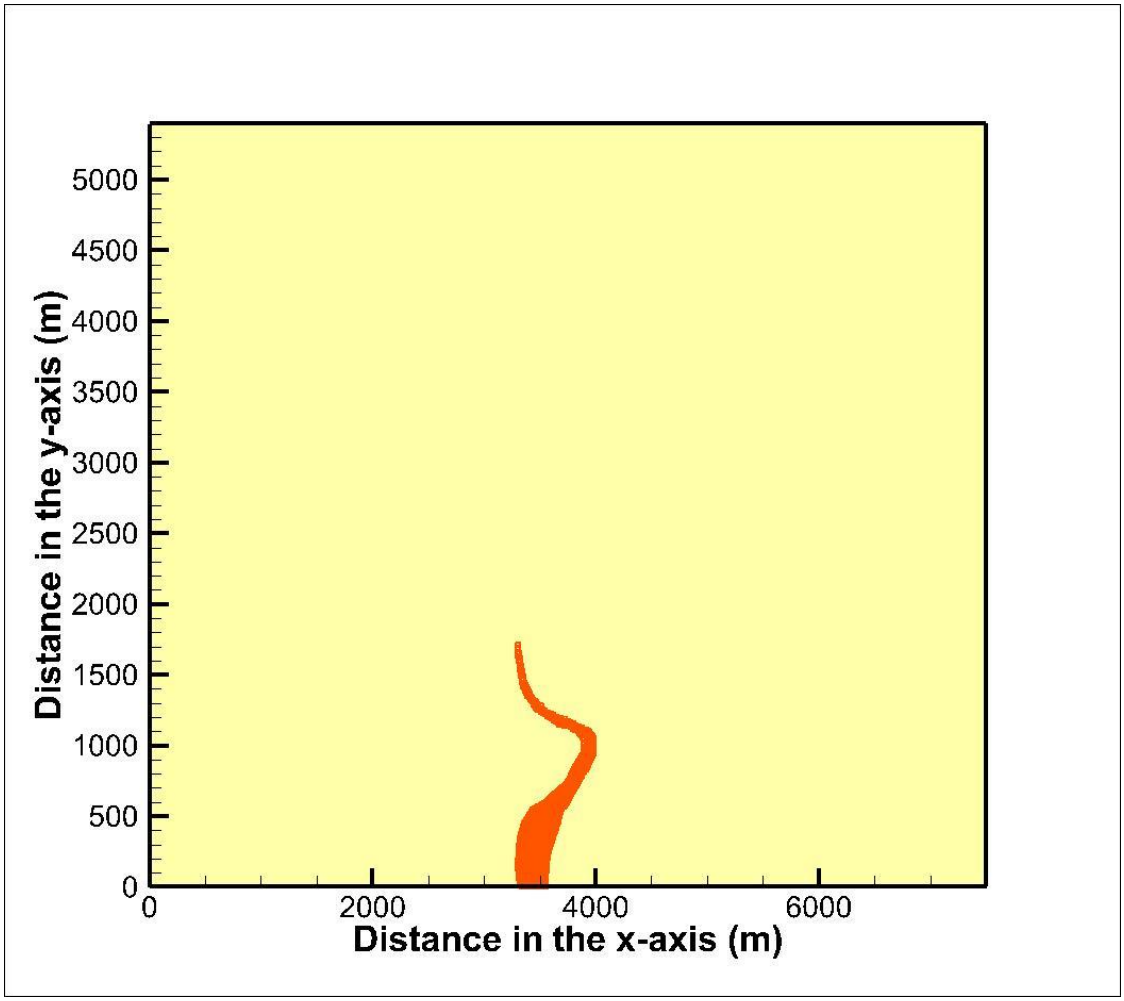

Figure 3-11. Particle pathlines in the transport domain for the deterministic case with no radionuclide sorption (100 particles placed at the source: x= 3297 m, y = 1715 m, z = -2 m)

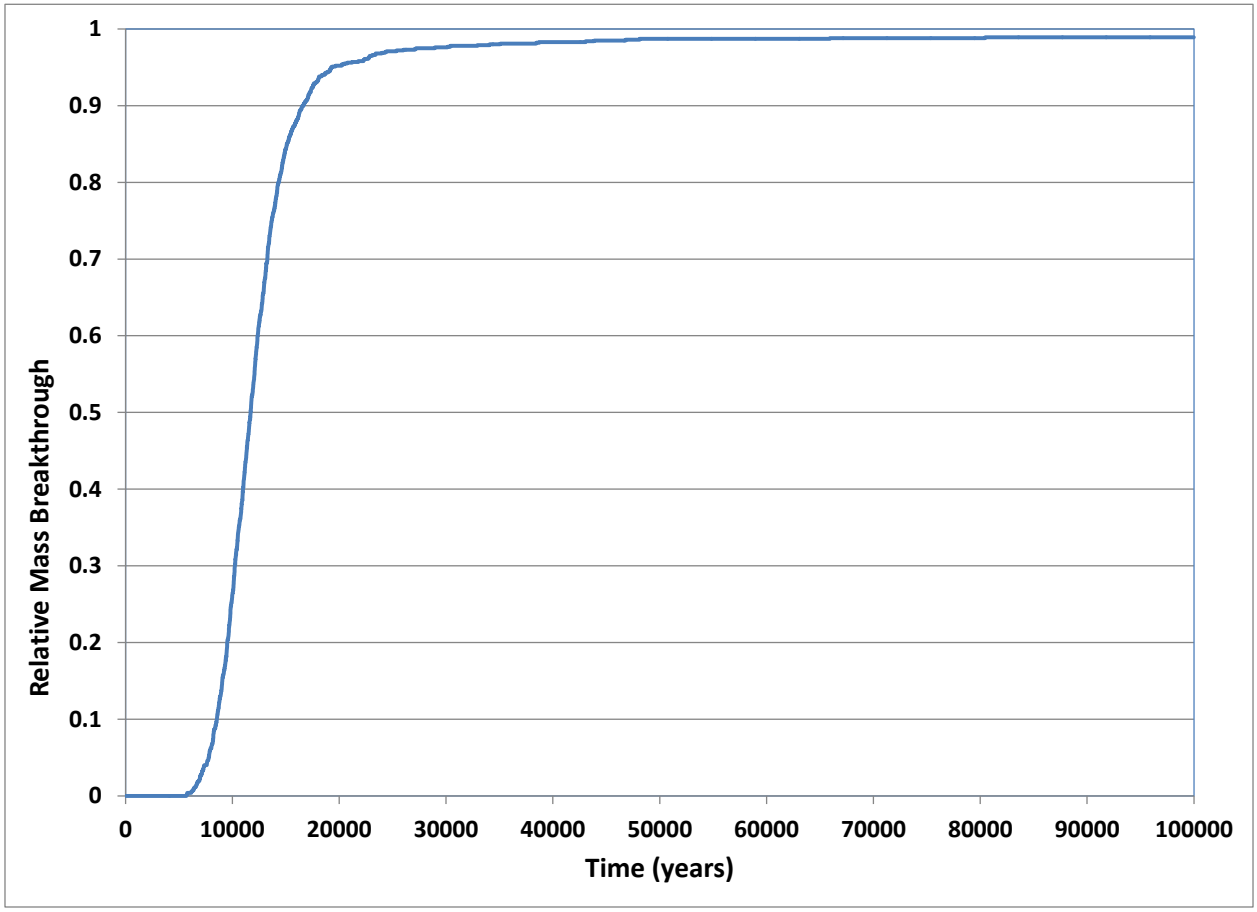

Figure 3-12. Cumulative relative mass breakthrough at the transport domain boundary for the deterministic case with no radionuclide sorption (1000 particles placed at the source: x= 3297 m, y = 1715 m, z = -2 m)

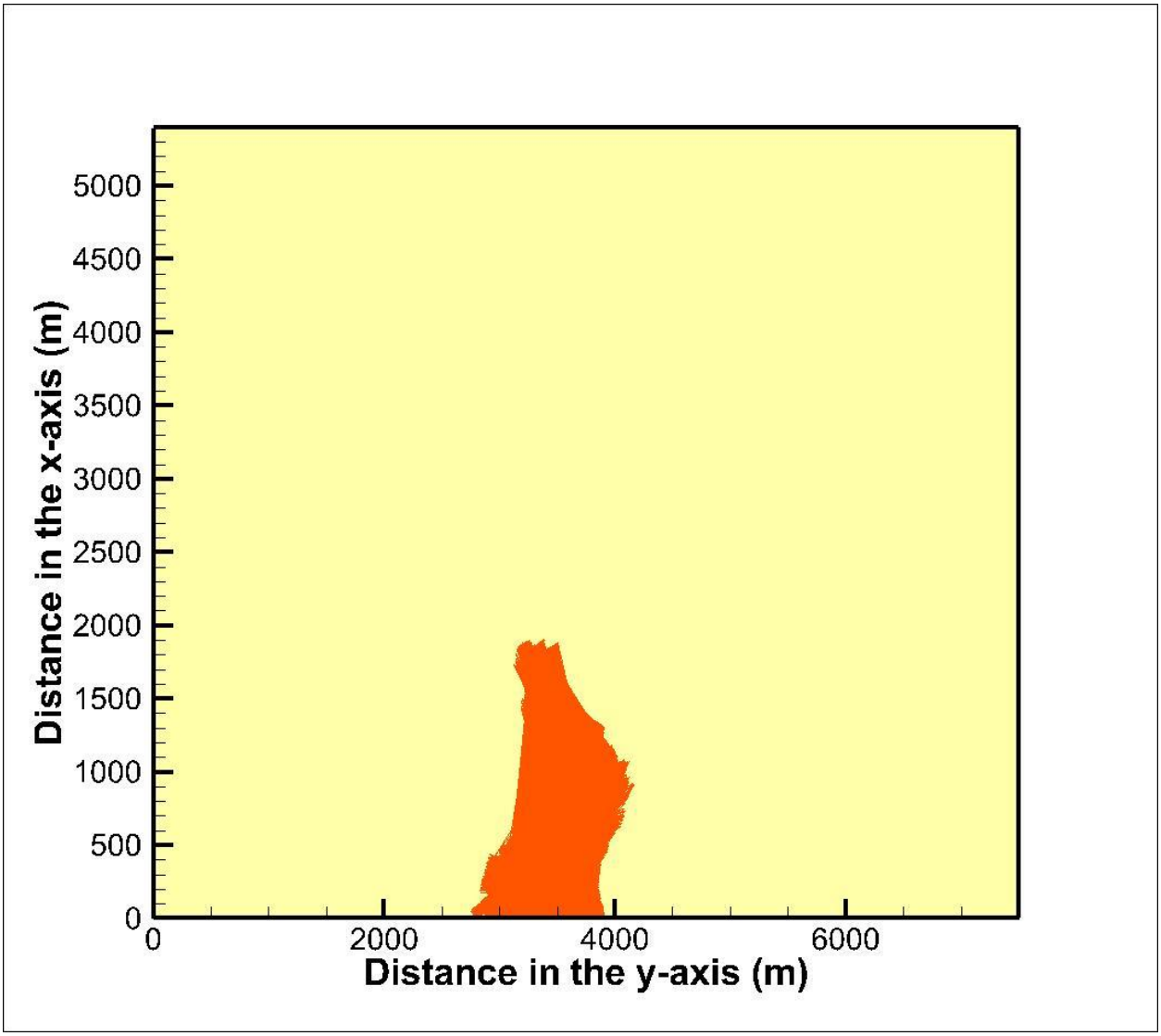

Figure 3-13. Particle pathlines in the transport domain for the deterministic case with no radionuclide sorption but with dispersion included (100 particles placed at the source: x= 3297 m, y = 1715 m, z = -2 m)

3.3.3 Probabilistic transport simulations

The coupled DAKOTA-FEHM codes were run to simulate radionuclide transport from the release point to the transport domain boundary. Three radionuclides, iodine (I^-), plutonium [Pu(IV)] and uranium [U(VI)] were selected for the tool demonstration simulations. Parameter data in Table 3-1 were used for the simulations. DAKOTA generated 100 samples of uncertain parameters and then direct FEHM runs. FEHM and DAKOTA results for each radionuclide are described below. The results include plots of cumulative relative mass at total time (i.e. the output) vs. each uncertain parameter, and tables of statistical data. The tables of statistical data include Moment-based statistics for the output, Simple

Correlation Matrix among all inputs (i.e. uncertain parameters) and the output, Partial Correlation Matrix between input and the output, Simple Rank Correlation Matrix among all inputs and the output and Partial Rank Correlation Matrix between input and the output.

The "sptr" macro of FEHM uses fracture aperture as an input. For the probabilistic transport simulations aperture was obtained using the uncertain parameters in Culebra Dolomite transport as shown below. The fracture aperture is defined in terms of advective porosity (fracture porosity) and matrix half-block length as (Kuhlman, 2010, equation 15):

$$b = \frac{B\varphi_f}{1-\varphi_f} \qquad (3\text{-}1)$$

where b = fracture aperture; φ_f = fracture porosity; B = matrix half-block length. Equation 3-1 was inserted in the DAKOTA template that prepares the FEHM input file for each realization.

3.3.3.1 Simulations of iodine transport

For iodine transport FEHM was run to 10^5 years. Figures 3-14 to 3-18 plots cumulative relative mass against the uncertain input parameters for iodine transport. Relative mass breakthrough curves for iodine transport are shown in Figure 3-14. The iodine mass reaches the transport domain boundary in only about one third of the 100 realizations within the selected simulation period. Figure 3-15 shows a plot of cumulative relative mass vs. iodine Kd. The plot shows a transition at Kd of about 0.3 mL/g where sorption effectively retards the advance of iodine mass to the boundary. Table 3-2 shows statistical output of DAKOTA. The simple correlation matrix among the response function (i.e. cumulative relative mass at total time) and Kd shows a value of -0.8024 indicating a strong inverse correlation, complementing the results shown in Figure 3-15. Figures 3-16 through 3-18 plot cumulative relative mass vs. matrix porosity, fracture porosity and matrix half-block length, respectively. These figures do not seem to show clearly defined relationships as was seen in the Kd plot (Figure 3-15). Table 3-2 shows a simple correlation matrix for the correlation between the cumulative relative mass (the response function) and the input parameters: -0.0224 (matrix porosity), 0.0997 (fracture porosity) and 0.0489 (matrix half-block length). The correlation values show much weaker relationships compared to Kd. Dakota provides provisions for further analysis of these correlations, which can be accomplished in future work.

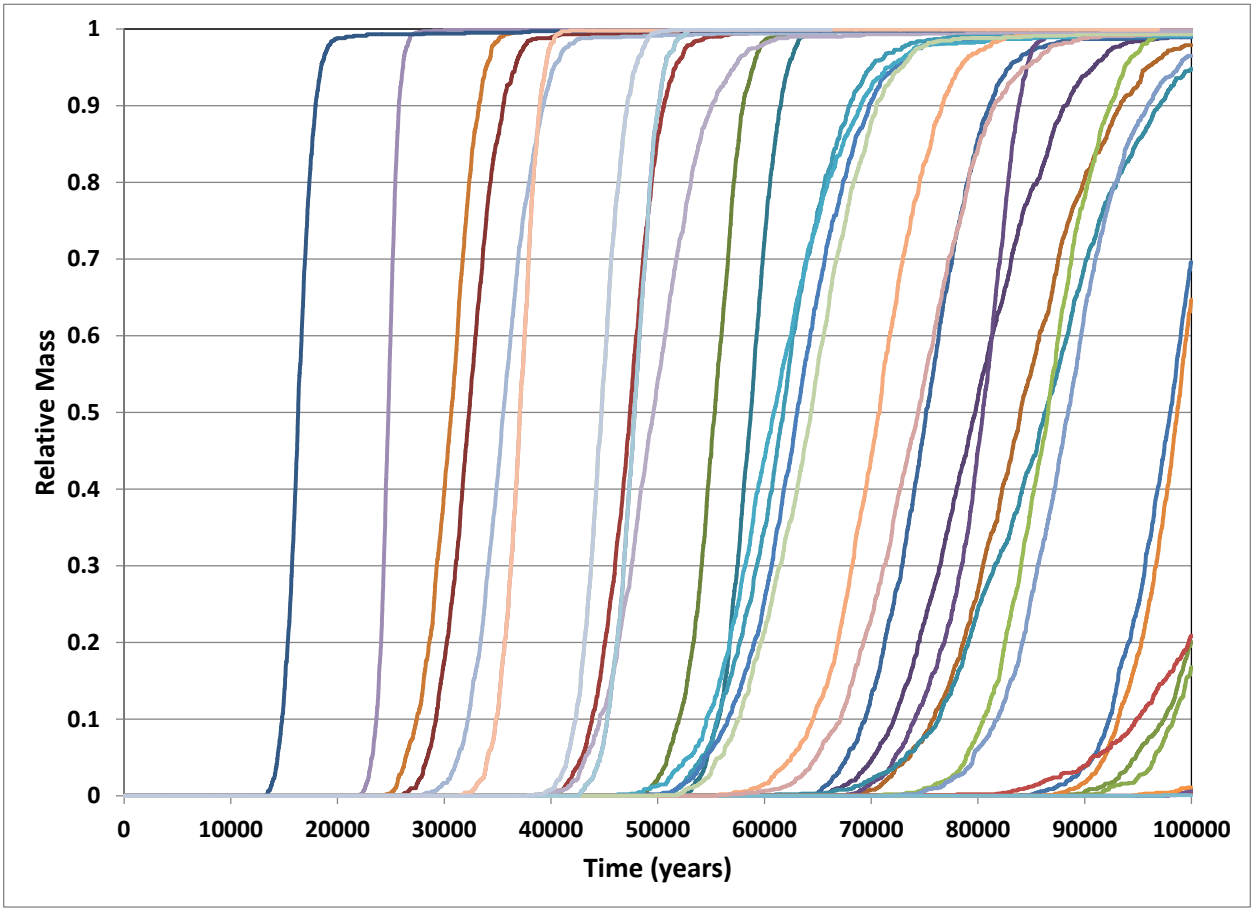

Figure 3-14. Iodine transport simulation: cumulative relative mass breakthrough at the transport domain boundary (1000 particles placed at the source: x= 3297 m, y = 1715 m, z = -2 m). Each breakthrough corresponds to one set of sampled values of uncertainty parameters.

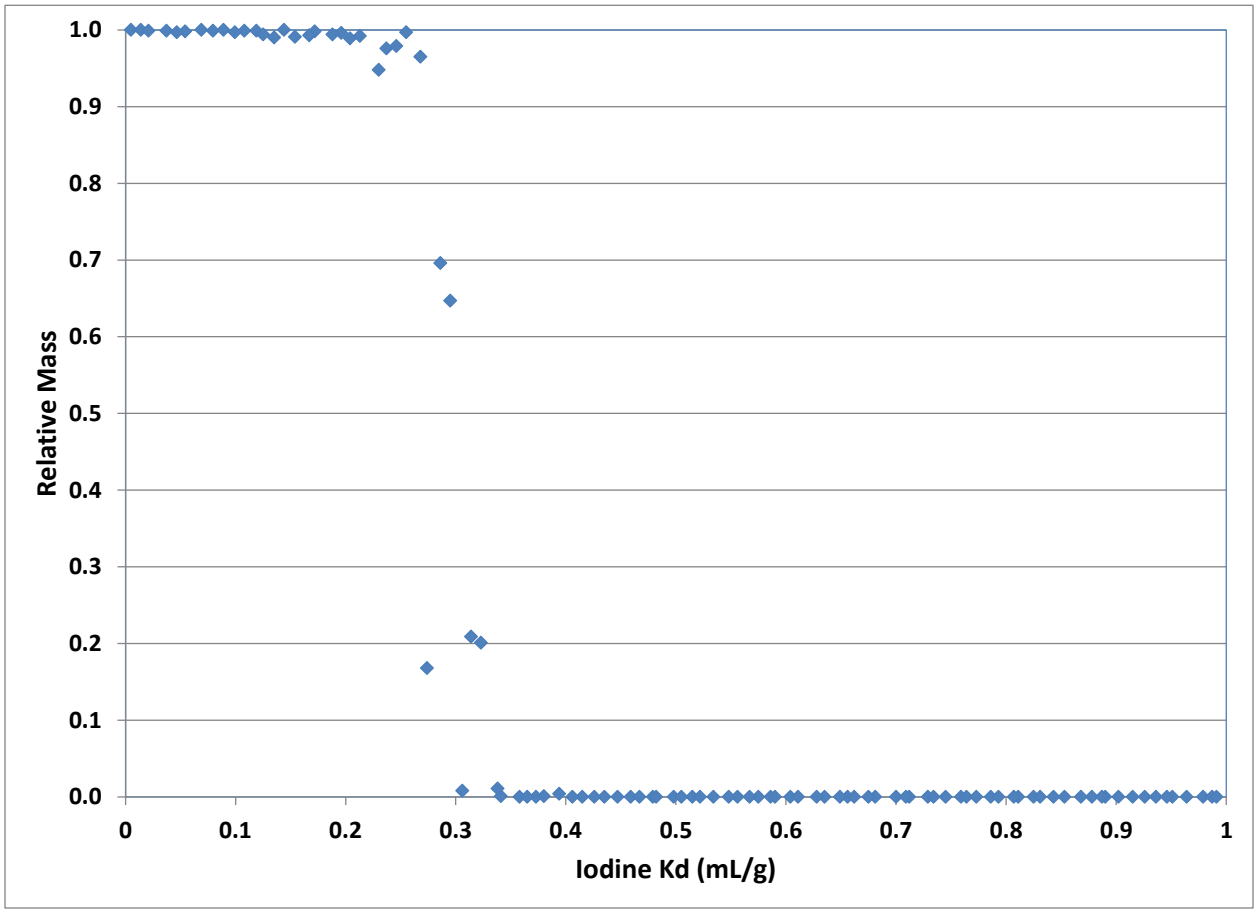

Figure 3-15. Iodine transport simulation: cumulative relative mass at boundary of transport domain at 10^5 years versus sorption (Kd) for the uncertain case (1000 particles placed at the source: x= 3297 m, y = 1715 m, z = -2 m)

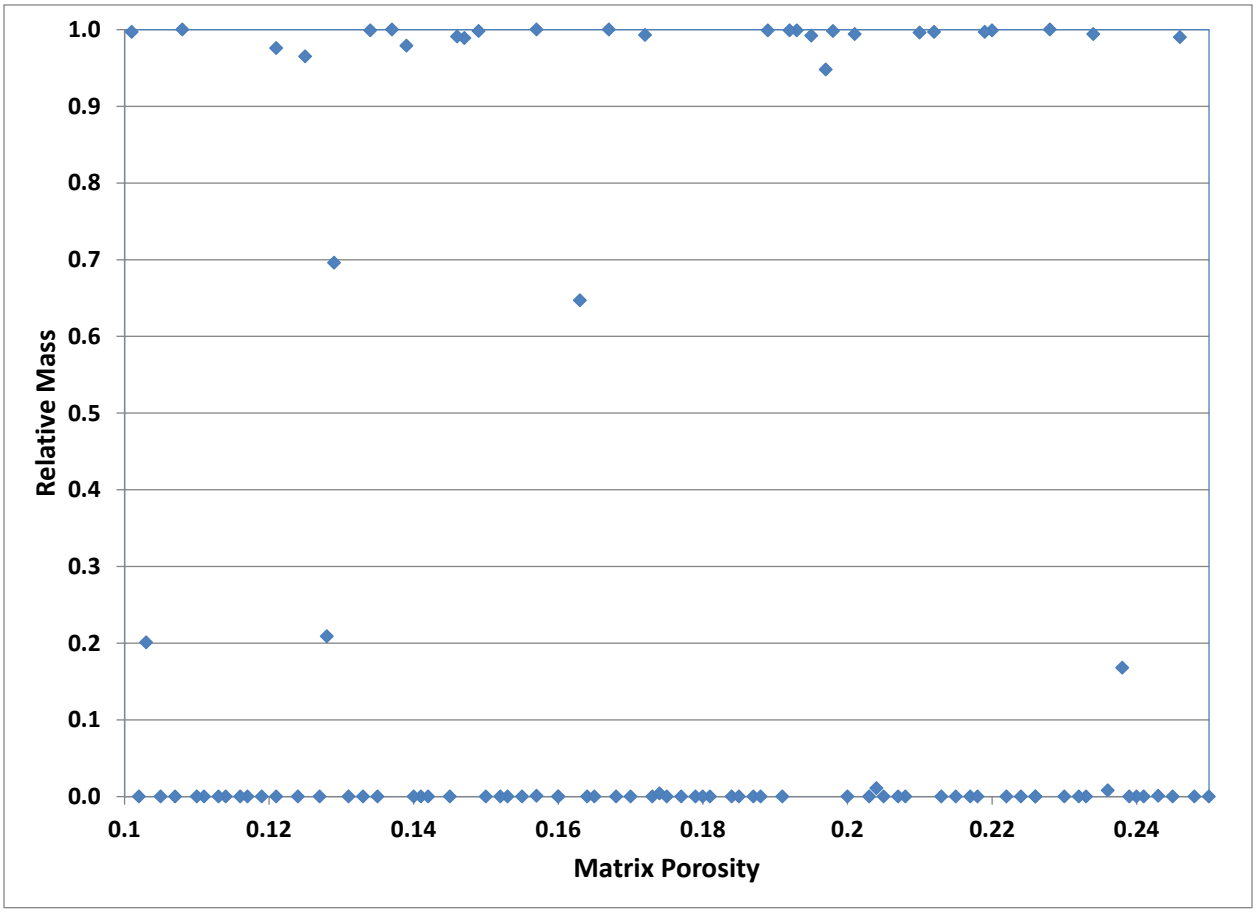

Figure 3-16. Iodine transport simulation: cumulative relative mass at boundary of transport domain at 10^5 years versus matrix porosity for the uncertain case (1000 particles placed at the source: x= 3297 m, y = 1715 m, z = -2 m). Lack of correlation between the two variables seems to indicate that radionuclide release at the boundary is insensitive to matrix porosity.

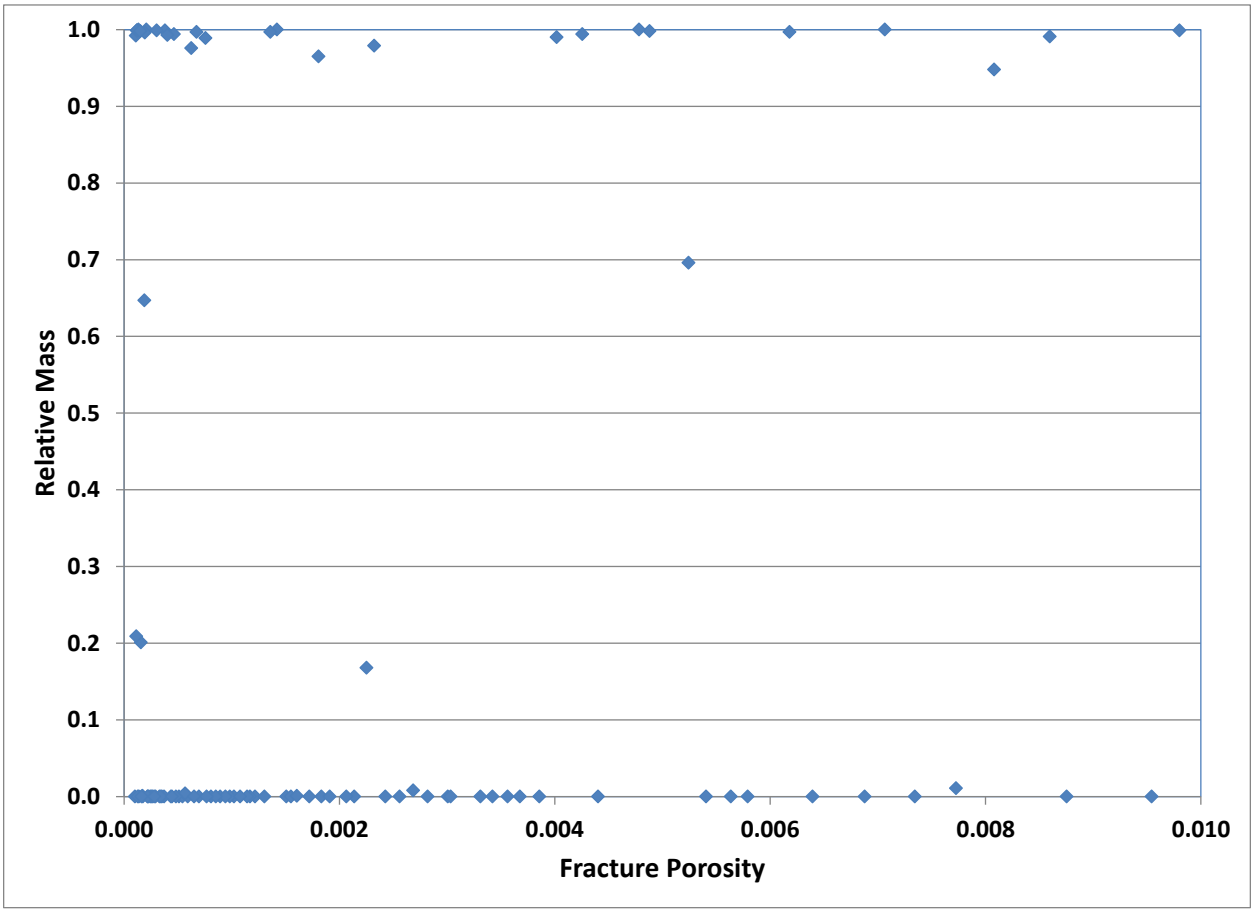

Figure 3-17. Iodine transport simulation: cumulative relative mass at boundary of transport domain at 10^5 years versus fracture porosity for the uncertain case (1000 particles placed at the source: x= 3297 m, y = 1715 m, z = -2 m). Lack of correlation between the two variables seems to indicate that radionuclide release at the boundary is insensitive to fracture porosity.

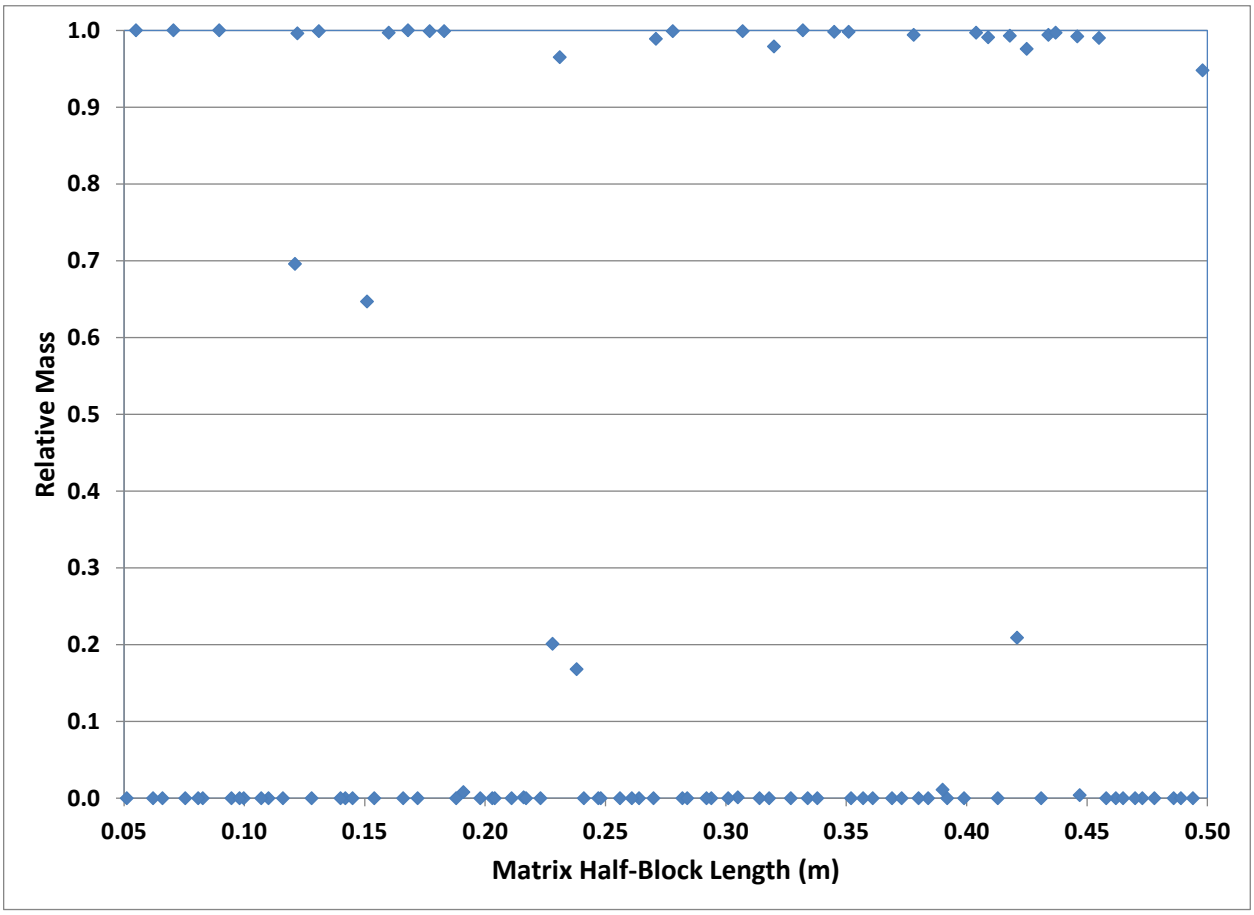

Figure 3-18. Iodine transport simulation: cumulative relative mass at boundary of transport domain at 10^5 years versus matrix half-block length for the uncertain case (1000 particles placed at the source: x= 3297 m, y = 1715 m, z = -2 m). Lack of correlation between the two variables seems to indicate that radionuclide release at the boundary is insensitive to matrix half-block length.

Table 3-2. DAKOTA Output of statistical data for iodine transport

Moment-based statistics for each response function:

	Mean	Std Dev	Skewness	Kurtosis
response_fn_1	2.870e+02	4.42e+02	9.51e-01	-1.07e+00

95% confidence intervals for each response function:

	LowerCI_Mean	UpperCI_Mean	LowerCI_StdDev	UpperCI_StdDev
response_fn_1	1.99e+02	3.75e+02	3.88e+02	5.13e+02

Simple Correlation Matrix among all inputs and outputs:

	porosm	half_block_m	Kd	porosf	response_fn_1
porosm	1.00e+00				
half_block_m	9.03e-00	1.00e+00			
Kd	-1.12e-00	-6.76e-03	1.00e+00		
Porosf	-2.84e-02	-3.09e-02	-9.51e-02	1.00e+00	
response_fn_1	-2.23e-02	4.89e-02	-8.02e-01	9.96e-02	1.00e+00

Partial Correlation Matrix between input and output:

	response_fn_1
porosm	-5.22e-02
half_block_m	7.47e-02
Kd	-8.02e-01
porosf	4.02e-02

Simple Rank Correlation Matrix among all inputs and outputs:

	porosm	half_block_m	Kd	porosf	response_fn_
porosm	1.00e+00				
half_block_m	7.57e-03	1.00e+00			
Kd	-1.21e-02	-7.69e-03	1.00e+00		
porosf	2.35e-03	7.08e-03	1.46e-02	1.00e+00	
response_fn_1	9.30e-02	-7.11e-02	-7.54e-01	-8.02e-02	1.00e+00

Partial Rank Correlation Matrix between input and output:

	response_fn_1
porosm	1.31e-01
half_block_m	-1.19e-01
Kd	-7.61e-01
Porosf	-1.06e-01

3.3.3.2 Simulations of Pu(IV) transport

The coupled DAKOTA-FEHM codes were also run to simulate Pu(IV) transport from the release point to the transport domain boundary. The same parameter data used for Iodine were used for Pu except for the Kd distribution (Table 3-1). For Pu(IV) the upper bound Kd value is much higher than iodine. Thus, to obtain measurable breakthrough at the boundary the simulation time was increased to 10^6 years. Figures 3-19 to 3-22 show plots of cumulative relative mass against the uncertain input parameters for the

transport of Pu(IV). Figure 3-19 shows a plot of cumulative relative mass vs. Pu(IV) Kd. The plot shows a transition at Kd of about 3.0 mL/g where sorption effectively retards advance of the Pu(IV) mass to the boundary. Table 3-3 shows statistical output of DAKOTA. The Simple Correlation Matrix among the response function (i.e. cumulative relative mass at total time) and Kd shows a value of -0.250 indicating a relatively strong inverse correlation, complementing Figure 3-19. However, the Kd correlation for this case is not as strong as that of Iodine. For most of the range of Pu(IV) Kd values the cumulative relative mass is zero. Figures 3-20 through 3-22 plot cumulative relative mass vs. matrix porosity, fracture porosity and matrix half-block length, respectively. As with Iodine transport these figures do not seem to show clearly defined relationships as was seen with the Kd (Figure 3-19). Table 3-3 shows a simple correlation matrix for the correlation between the cumulative relative mass (the response function) and the input parameters: -0.0363 (matrix porosity), -0.0659 (fracture porosity) and -0.1800 (matrix half-block length). The correlation between relative mass and matrix half-block length is now much stronger than it was for Iodine transport.

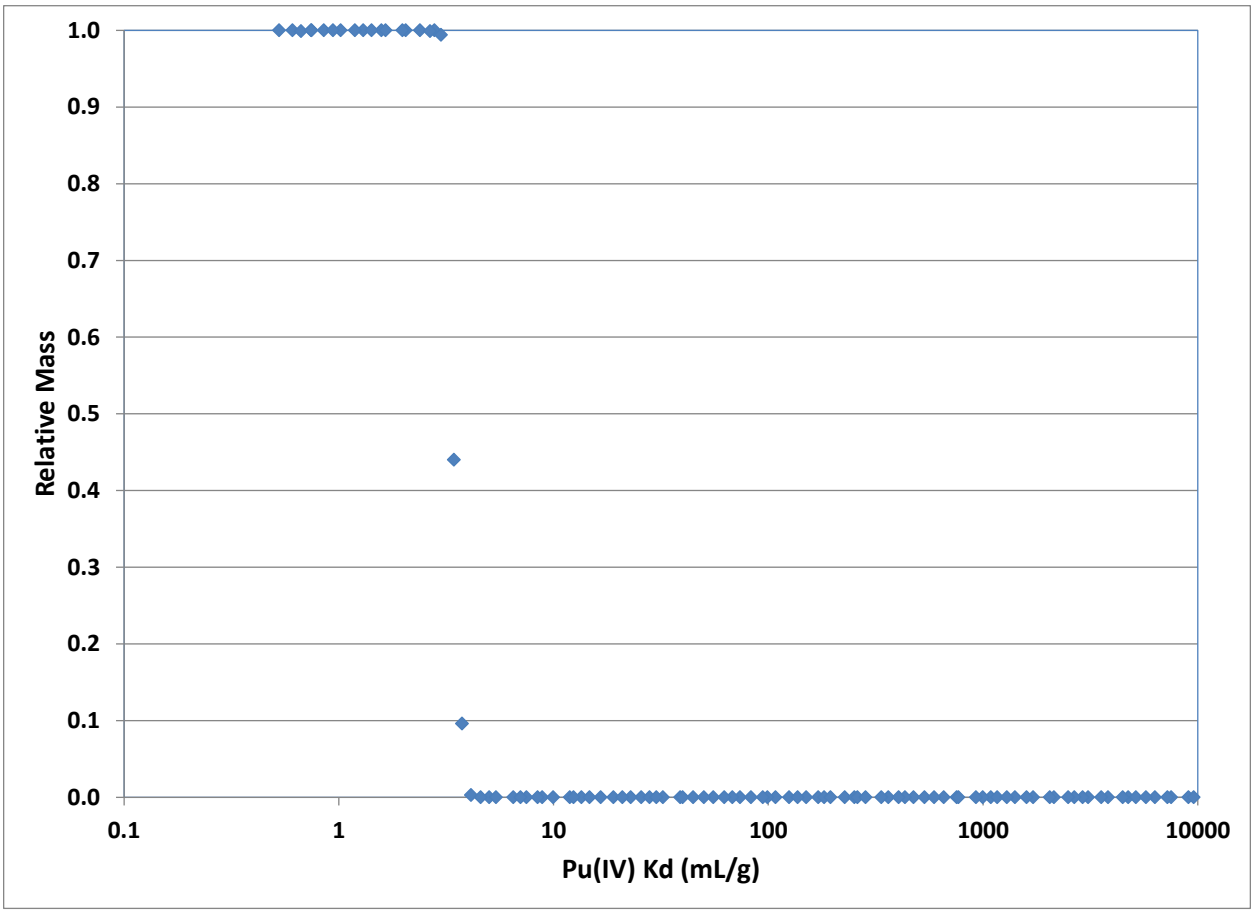

Figure 3-19. Pu(IV) transport simulation: cumulative relative mass at boundary of transport domain at 10^6 years versus sorption (Kd) for the uncertain case (1000 particles placed at the source: x= 3297 m, y = 1715 m, z = -2 m)

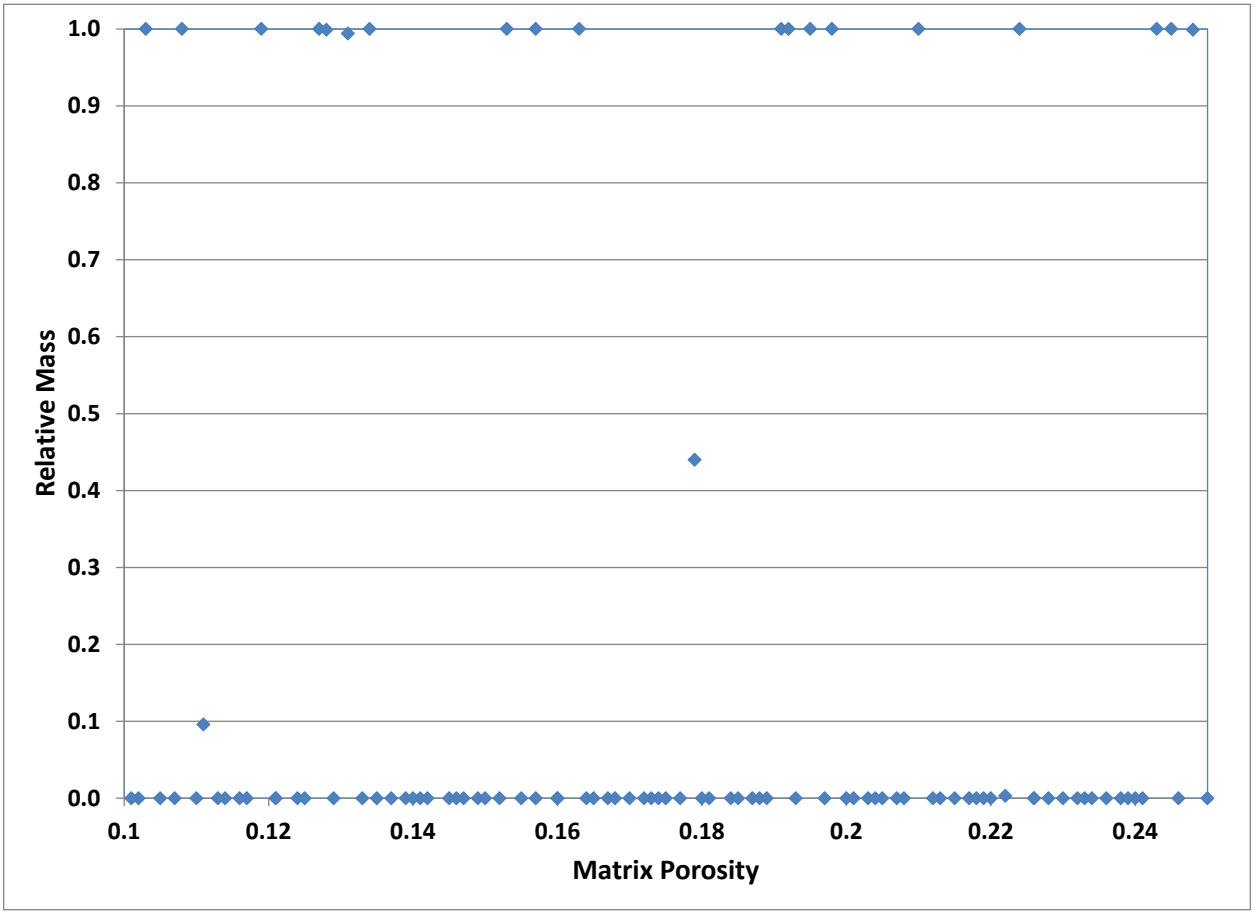

Figure 3-20. Pu(IV) transport simulation: cumulative relative mass at boundary of transport domain at 10^6 years versus matrix porosity for the uncertain case (1000 particles placed at the source: x= 3297 m, y = 1715 m, z = -2 m)

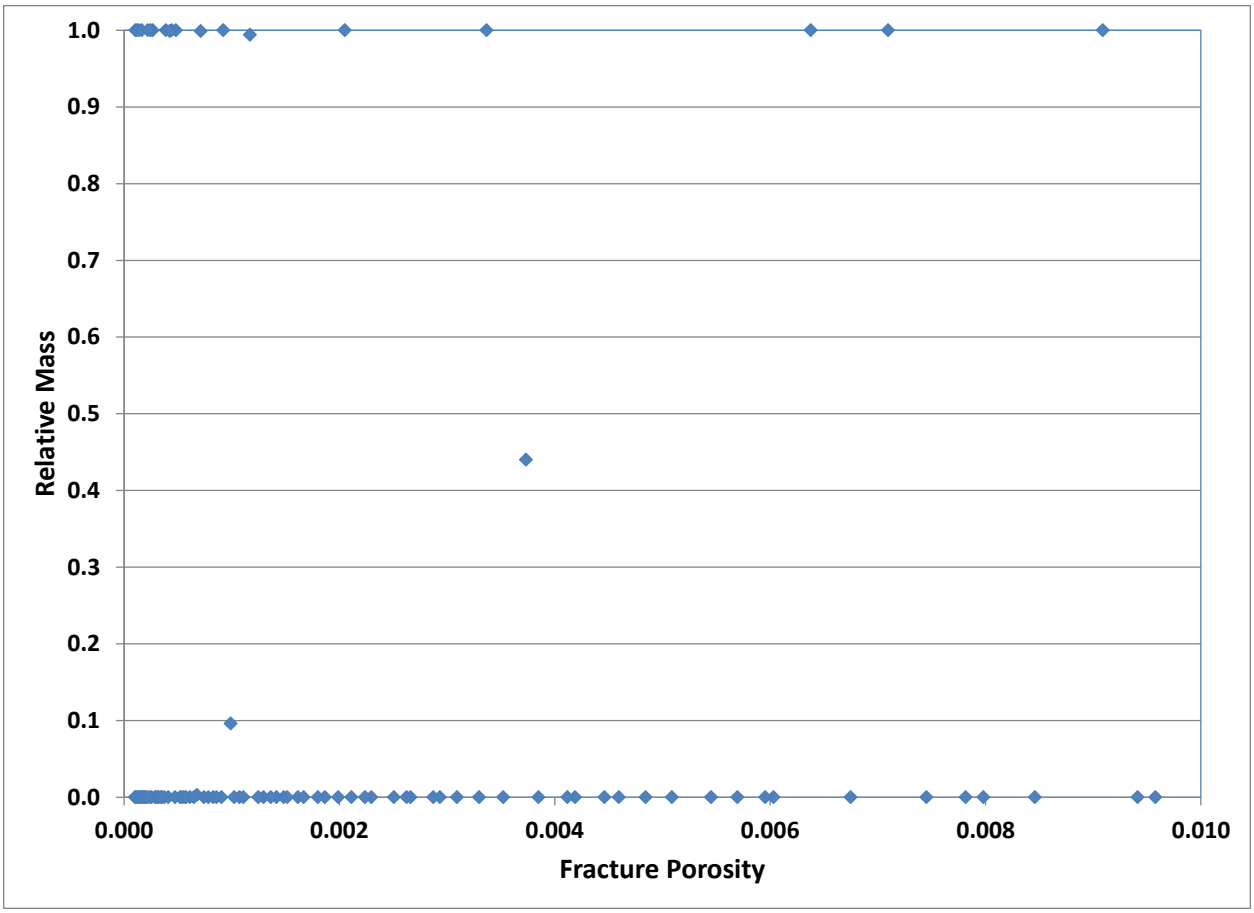

Figure 3-21. Pu(IV) transport simulation: cumulative relative mass at boundary of transport domain at 10^6 years versus fracture porosity for the uncertain case (1000 particles placed at the source: x= 3297 m, y = 1715 m, z = -2 m)

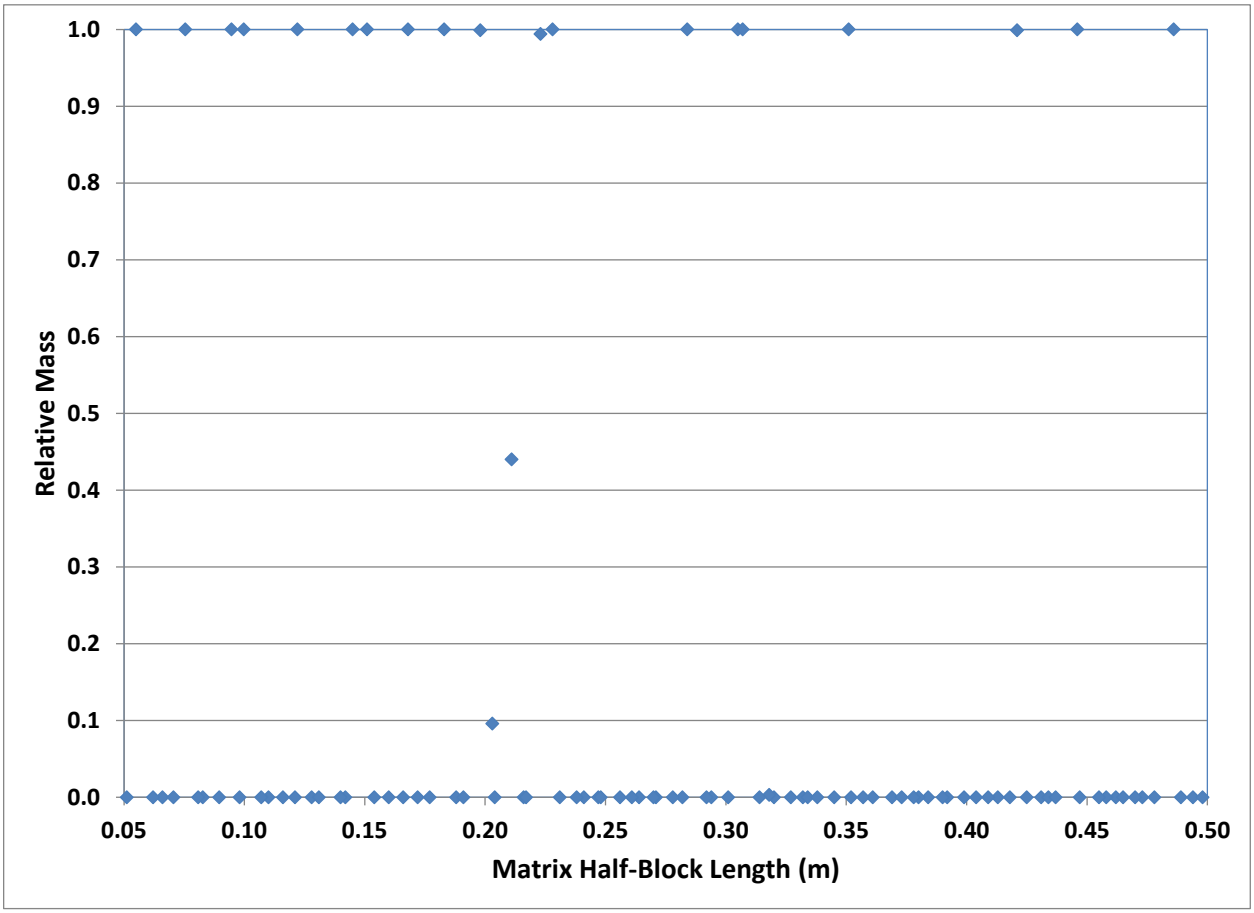

Figure 3-22. Pu(IV) transport simulation: cumulative relative mass at boundary of transport domain at 10^6 years versus matrix half-block length for the uncertain case (1000 particles placed at the source: x= 3297 m, y = 1715 m, z = -2 m)

Table 3-3. DAKOTA output of statistical data for Pu(IV) Transport

Moment-based statistics for each response function:

	Mean	Std Dev	Skewness	Kurtosis
response_fn_1	1.9531000000e+02	3.9404998132e+02	1.5683332130e+00	4.9841492126e-01

95% confidence intervals for each response function:

	LowerCI_Mean	UpperCI_Mean	LowerCI_StdDev	UpperCI_StdDev
response_fn_1	1.17e+02	2.73e+02	3.46e+02	4.58e+02

Simple Correlation Matrix among all inputs and outputs:

	porosm	half_block_m	porosf	Kd	response_fn_1
porosm	1.00e+00				
half_block_m	9.03e-03	1.00e+00			
porosf	-1.35e-02	-4.14e-02	1.00e+00		
Kd	5.20e-03	-2.76e-02	-6.60e-02	1.00e+00	
response_fn_1	-3.63e-02	-1.80e-01	-6.59e-02	-2.50e-01	1.00e+00

Partial Correlation Matrix between input and output:

	response_fn_1
porosm	-3.65e-02
half_block_m	-1.97e-01
Kd	-9.60e-02
porosf	-2.65e-01

Simple Rank Correlation Matrix among all inputs and outputs:

	porosm	half_block_m	porosf	Kd	response_fn_
porosm	1.00e+00				
half_block_m	7.57e-03	1.00e+00			
porosf	-1.21e-02	-7.69e-03	1.00e+00		
Kd	2.35e-03	7.08e-03	1.47e-02	1.00e+00	
response_fn_1	-1.59e-01	-1.04e-01	-5.86e-03	-4.16e-01	1.00e+00

Partial Rank Correlation Matrix between input and output:

	response_fn_1
porosm	-1.74e-01
half_block_m	-1.12e-01
porosf	-2.75e-03
Kd	-4.23e-01

3.3.3.3 Simulations of U(VI) transport

The coupled DAKOTA-FEHM codes were also run to simulate U(VI) transport from the release point to the transport domain boundary. Uranium transport was simulated for 10^5 years. Figures 3.23 to 3.26 show plots of cumulative relative mass against the uncertain input parameters for transport of U(VI). A plot of cumulative relative mass vs. U(VI) Kd is shown in Figure 3-23. The plot shows a transition at Kd similar to that of iodine where sorption effectively retards the advance of radionuclide mass to the boundary. Table 3-4 shows statistical output of DAKOTA. The simple correlation matrix among the response function (i.e. cumulative relative mass at total time) and Kd shows a value of -0.471 indicating a strong inverse correlation, as with iodine and Pu(VI) transport. Figures 3-24 through 3-26 plot cumulative relative mass vs. matrix porosity, fracture porosity and matrix half-block length, respectively. Similar to iodine and Pu(IV) simulation results these figures do not seem to show clearly defined relationships as was seen with Kd. Table 3-4 shows simple correlation matrix with correlations between cumulative relative mass (the response function) and the input parameters: -0.0730 (matrix porosity), -0.0928 (fracture porosity) and -0.1090 (matrix half-block length).

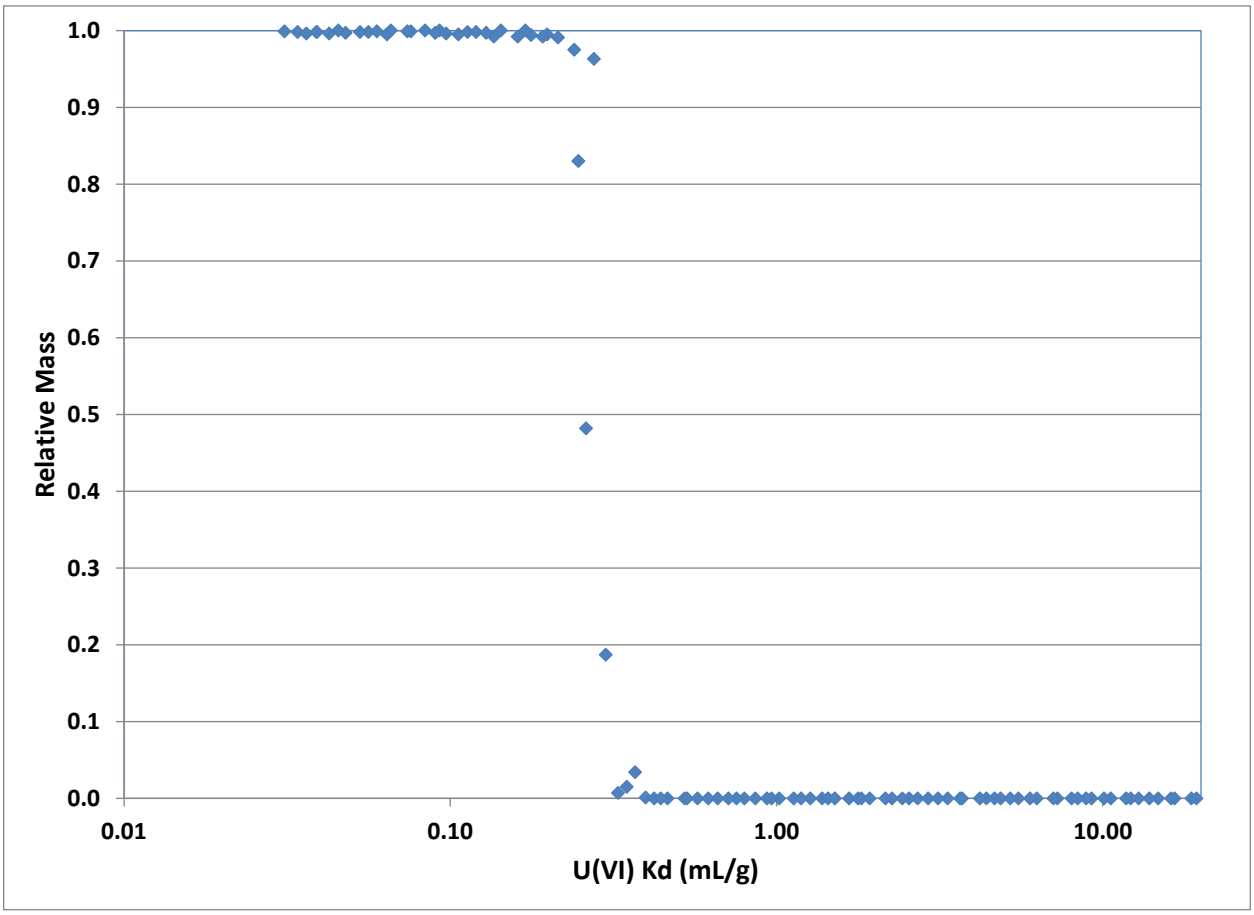

Figure 3-23. U(VI) transport simulation: cumulative relative mass at boundary of transport domain at 10^5 years versus sorption (Kd) for the uncertain case (1000 particles placed at the source: x= 3297 m, y = 1715 m, z = -2 m)

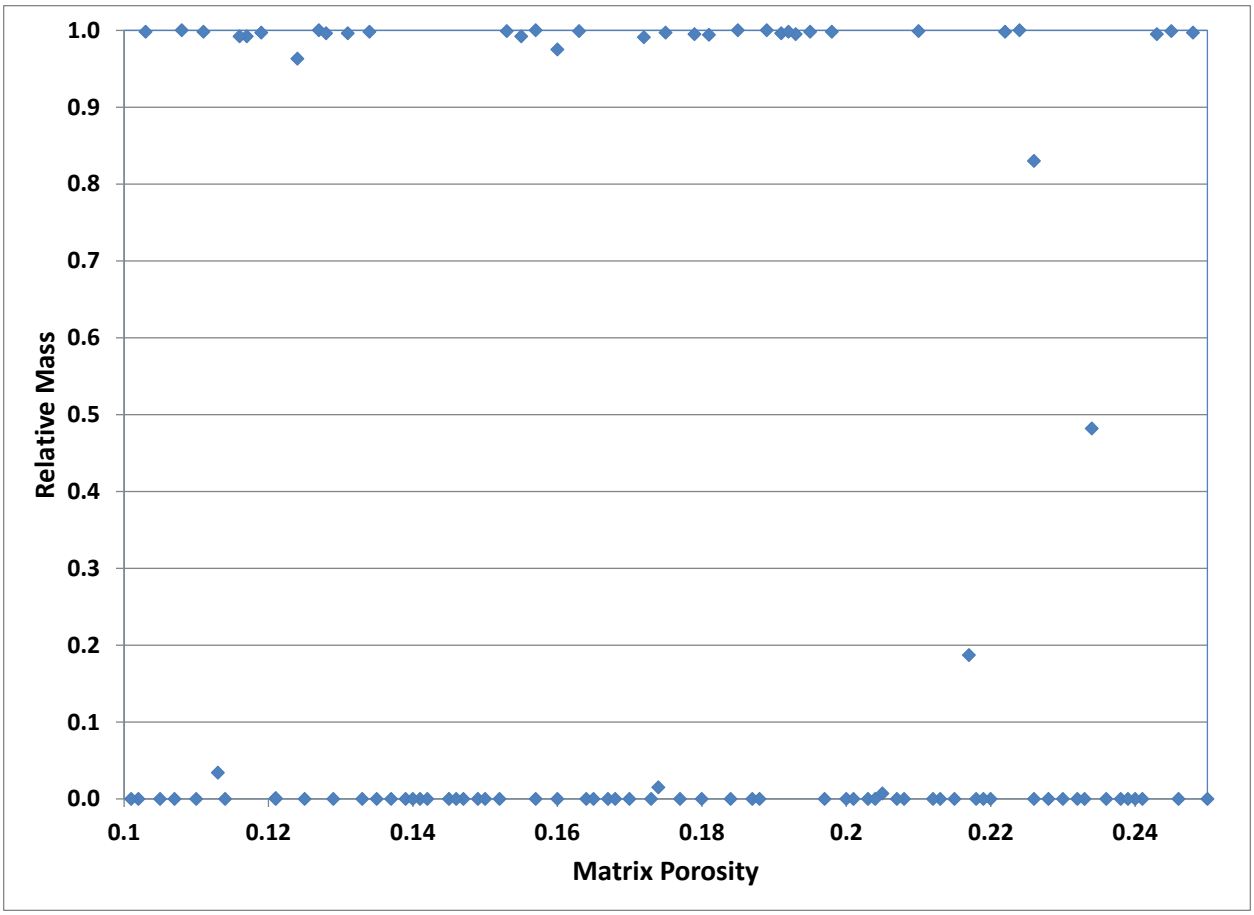

Figure 3-24. U(VI) transport simulation: cumulative relative mass at boundary of transport domain at 10^5 years versus matrix porosity for the uncertain case (1000 particles placed at the source: x= 3297 m, y = 1715 m, z = -2 m)

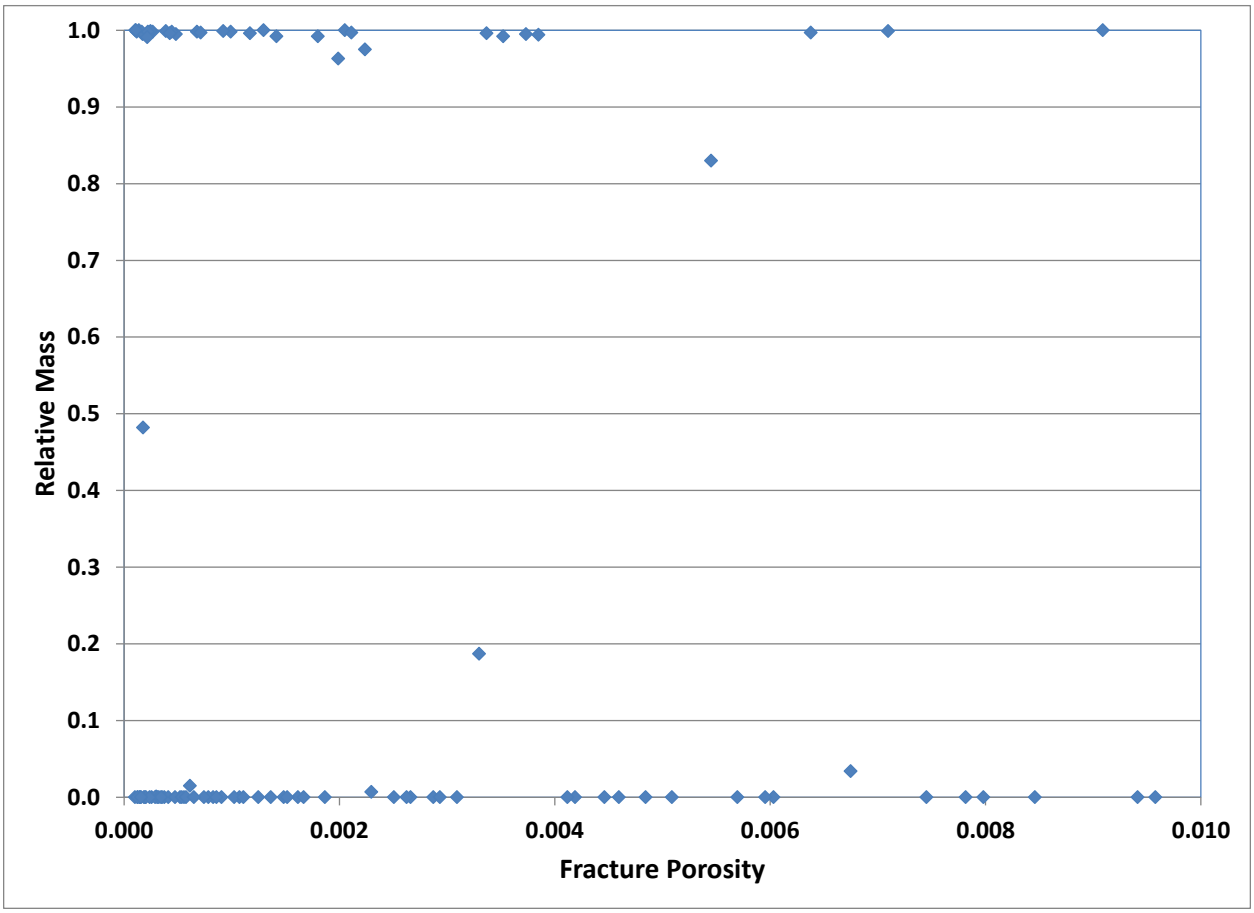

Figure 3-25. U(VI) transport simulation: cumulative relative mass at boundary of transport domain at 10^5 years versus fracture porosity for the uncertain case (1000 particles placed at the source: x= 3297 m, y = 1715 m, z = -2 m)

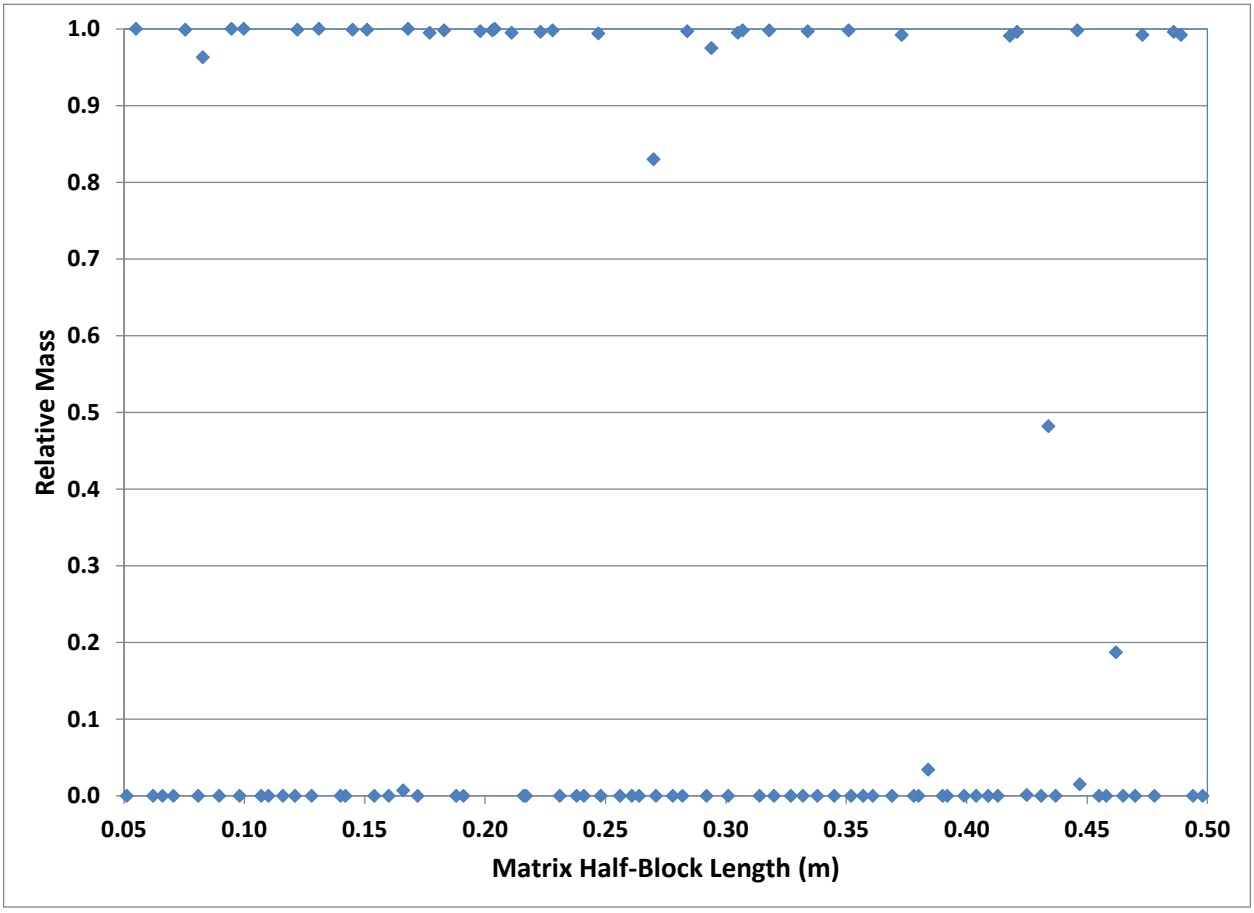

Figure 3-26. U(VI) transport simulation: cumulative relative mass at boundary of transport domain at 10^5 years versus matrix half-block length for the uncertain case (1000 particles placed at the source: x= 3297 m, y = 1715 m, z = -2 m)

Table 3-4. DAKOTA output of statistical data for U(VI) Transport

Moment-based statistics for each response function:

	Mean	Std Dev	Skewness	Kurtosis
response_fn_1	3.44e+02	4.69e+02	6.62e-01	-1.57e+00

95% confidence intervals for each response function:

	LowerCI_Mean	UpperCI_Mean	LowerCI_StdDev	UpperCI_StdDev
response_fn_1	2.51e+02	4.37e+02	4.12e+02	5.45e+02

Simple Correlation Matrix among all inputs and outputs:

	porosm	half_block_m	porosf	Kd	response_fn_1
porosm	1.00e+00				
half_block_m	9.03e-03	1.00e+00			
porosf	-1.35e-02	-4.14e-02	1.000e+00		
Kd	-2.071e-02	-3.15e-02	-5.56e-02	1.00e+00	
response_fn_1	-7.30e-02	-1.09e-01	-9.28e-02	-4.71e-01	1.00e+00

Partial Correlation Matrix between input and output:

	response_fn_1
porosm	-9.66e-02
half_block_m	-1.48e-01
porosf	-1.45e-01
Kd	-4.90e-01

Simple Rank Correlation Matrix among all inputs and outputs:

	porosm	half_block_m	porosf	Kd	response_fn_
porosm	1.00e+00				
half_block_m	7.57e-03	1.00e+00			
porosf	-1.20e-02	-7.69e-03	1.00e+00		
Kd	2.35e-03	7.08e-03	1.47e-02	1.00e+00	
response_fn_1	-1.01e-01	-1.05e-01	-1.31e-01	-7.07e-01	1.00e+00

Partial Rank Correlation Matrix between input and output:

	response_fn_1
porosm	-1.45e-01
half_block_m	-1.46e-01
porosf	-1.77e-01
Kd	-7.18e-01

3.4 Summary

The work documented in this section explores the concept of an enhanced performance assessment system for far-field radionuclide transport. A prototype PA tool was developed by wrapping a multi-phase, multi-component reservoir simulator (FEHM) with an uncertainty quantification and optimization code (DAKOTA). For demonstration, a probabilistic PA analysis was successfully performed for a far-field radionuclide transport in a salt repository, based on transport in the Culebra Dolomite member at WIPP. This is a preliminary work for the development of a new generation of PA tools that can be used for effective modeling of far field radionuclide transport and beyond. The tool demonstration was conducted using real field data (transmissivity fields), the dual-porosity capability of transport code (FEHM), the high performance parallel computing capability of PA driver (DAKOTA), and the embedded LHS sampling and statistical analysis techniques (DAKOTA).

Further work would include optimization of the key parameters in far-field radionuclide transport system as outlined in Figure 3-1. There are a number of additional tools within the DAKOTA framework that could be exercised to evaluate the optimal solution for key parameters. DAKOTA also contains a large number of capabilities which could be exercised for PA analysis.

3.5 References

Adams, B. M., Bohnhoff, W. J., Dalbey, K. R., Eddy, J. P., Eldred, M. S., Gay, D. M., Haskell, K., Hough, P. D., and Swiler, L. P., 2010. DAKOTA, A Multilevel Parallel Object-Oriented Framework for Design Optimization, Parameter Estimation, Uncertainty Quantification, and Sensitivity Analysis, Version 5.0+ User's Manual, SAND2010-2183, Sandia National Laboratories, Albuquerque, NM.

Corbet, T., 1995. Record of FEP Screening Work FEP ID# NS-9 Justification of SECO2D Approximation for PA Transport Calculation. ERMS 230802, Sandia National Laboratories, Carlsbad, NM.

Eldred, M., Giunta, A., van Bloemen Waanders, B., Wojtkiewicz, Jr., S., Hart, W., and Alleva, M., 2002, DAKOTA, A Multilevel Parallel Object-Oriented Framework for Design Optimization, Parameter Estimation, Uncertainty Quantification, and Sensitivity Analysis. Version 3.0 Users Manual, SAND2001-3796, Sandia National Laboratories, Albuquerque, NM.

Hart, D.B., Beauheim, R.L. and McKenna, S.A., 2009. Analysis Report for Task 7 of AP-114: Calibration of Culebra Transmissivity Fields. ERMS 55239, Sandia National Laboratories, Carlsbad, NM.

Helton, J. C., Anderson, D. R., Jow, H.-N., Marietta, M. G., and Basabilvazo G., 2000, Performance assessment in support of the 1996 compliance certification application for the Waste Isolation Pilot Plant, *Risk Analysis*, 19(5): 959-986.

Holt, R.M., 1997. Conceptual Model for Transport Processes in the Culebra Dolomite Member of the Rustler Formation. SAND97-0194, Sandia National Laboratories, Carlsbad, NM.

Kuhlman, K., 2010. Analysis Report for the CRA-2009 PABC Culebra Flow and Transport Calculations, AP-144 Task Number: 1.2.5, Sandia National Laboratories, Carlsbad, NM.

Miller, A. W. and Wang, Y., 2012. Radionuclide Interaction with Clays in Dilute and Heavily Compacted Systems: A Critical Review. *Environ. Sci. Technol*. 2012, p. 46.

SNL 2011. "CUBIT Geometry and Mesh Generation Toolkit." http://cubit.sandia.gov.

Wang, Y., Dewers, T., Hadgu, T., Jove-Colon, C. F., Sun, A. C., and McNeish, J. 2010. Enhanced Performance Assessment System (EPAS) for Carbon Sequestration. SAND2010-6173, Sandia National Laboratories, Albuquerque, NM.

Wang, Y. and Joon H. Lee, 2010, Generic Disposal System Environment Modeling – Fiscal Year 2010 Progress Report. DOE Used Fuel Disposition Campaign.

Zyvoloski, G.A. 2007. *FEHM: A control volume finite element code for simulating subsurface multi-phase multi-fluid heat and mass transfer*. Los Alamos Unclassified Report LA-UR-07-3359. Los Alamos, NM: Los Alamos National Laboratory.

Zyvoloski, G.A., B.A. Robinson, Z.V. Dash, and L.L. Trease 1997. *Summary of the models and methods for the FEHM application A Finite-Element Heat- and Mass-Transfer Code*. LA-13307-MS. Los Alamos, NM: Los Alamos National Laboratory.

4.0 Disposal Systems Material Properties: Thermodynamic Data Collection and Synthesis

4.1 Introduction

As discussed in Section 1.0, key technical data that support model parameterization are an important component of the integrated tool development for the natural system evaluation. Thermodynamic properties of disposal systems materials are one of such data sets that are crucial for both the natural barrier system and the engineered barrier system evaluations. Given their truly site-independent nature, the Used Fuel Disposition Program is specifically interested in developing an integrated high quality thermodynamic database for generic repository studies. This section provides a critical review of the current status of thermodynamic database development.

The work presented in this section is an update of Wolery and Sutton (2011). For the sake of continuity, some review material is retained largely as is. Some other review material has been expanded to support new topics of interest. New information includes revised and extended thermodynamic data for sheet silicates obtained mainly from correlation algorithms. These are mainly focused on smectite clays, which include the montmorillonites and beidellites. A distinction is now made between dehydrated and hydrated smectites. The previous treatment used a smectite model in which hydration corresponding to unit water activity was implicit, and was unable to account for dehydration. The newly developed results do not solve all problems, but serve as a basis for developing a reasonable hydration/dehydration model. A deeper examination has been made of consistency issues associated with taking data from various published sources, including those which might be deemed "authoritative." A very fundamental issue that typically receives little attention involves values for the standard molar entropies of the chemical elements, as these are required to calculate the standard molar Gibbs energy of a chemical substance from the standard molar enthalpy, and vice versa. Data for elemental entropies from six "authoritative" sources have been compared, and unusually large discrepancies have been noted for six elements: Ca, Ce, Pb, S, Sr, and Th. These results suggest that Gibbs energy and enthalpy values for chemical substances taken from some common sources may be inconsistent with preferred elemental entropy values and should be corrected. Preferred values include those available from the NEA Thermodynamic Data series (which started with Grenthe et al., 1992, and is continuing). Some thermodynamic data needing elemental entropy corrections are likely present in the Yucca Mountain Project (YMP) thermodynamic database, which has been inherited by the Used Fuel Disposition Campaign. The SUPCRT92 mineral data (taken from Helgeson et al., 1978; see BSC 2007a) form a core part of the YMP database. It is not well-documented which elemental entropy data were used in deriving the mineral data, and corrections may be appropriate here. Some of the original mineral data from this source may also need to be corrected due to changes in the preferred values for the thermodynamic properties of key aqueous species, notably $SiO_{2(aq)}$, but possibly others as well. A careful examination of Helgeson et al. (1978) indicates that the thermodynamic properties of kaolinite should be corrected. Kaolinite is a key or anchor mineral in the associated dataset, and any change in its properties requires a correction for other aluminosilicate minerals in the dataset, as the data for these is mainly extracted from mineral-mineral phase equilibrium data. Presently there is rising interest in an alternative dataset for aluminosilicates and other minerals, including sulfide minerals (Holland and Powell, 2011). The 2011 version is the latest in a line extending back to 1985. The Holland and Powell dataset is also mainly based on mineral-mineral phase equilibrium data. It is well-regarded for high-temperature (e.g., >300°C) applications where the principal application is to compute mineral-mineral equilibria. However, it also appears to have some issues of concern (e.g.,

how well do the data work in the range 25-300°C?). An attractive path forward would be to resolve the differences between the Helgeson et al. and Holland and Powell datasets. The section also discusses some associated computer files that exemplify the data management aspects associated with thermodynamic data development.

4.2 Uses of Thermodynamic Data in Repository Studies

Thermodynamic data are essential for understanding and evaluating geochemical processes, as by speciation-solubility calculations, reaction-path modeling, or reactive transport simulation. These data are required to evaluate both equilibrium states and the kinetic approach to such states (via the affinity term or its equivalent in commonly used rate laws). These types of calculations and the data needed to carry them out are a central feature of geochemistry in many applications, including water-rock interactions in natural systems at low and high temperatures. Such calculations are also made in engineering studies, for example studies of interactions involving man-made materials such as metal alloys and concrete. They are used in a fairly broad spectrum of repository studies where interactions take place among water, rock, and man-made materials (e.g., usage on YMP and WIPP). Waste form degradation, engineered barrier system performance, and near-field and far-field transport typically incorporate some level of thermodynamic modeling, requiring the relevant supporting data.

Typical applications of thermodynamic modeling involve calculations of aqueous speciation (which is of great importance in the case of most radionuclides), solubilities of minerals and related solids, solubilities of gases, and stability relations among the various possible phases that might be present in a chemical system at a given temperature and pressure. If a phase can have a variable chemical composition, then a common calculational task is to determine that composition. Thermodynamic modeling also encompasses ion exchange and surface complexation processes. Any and all of these processes may be important in a geochemical process or reactive transport calculation.

Such calculations are generally carried out using computer codes. For geochemical modeling calculations, codes such as EQ3/6 and PHREEQC, are commonly used. These codes typically provide “full service” geochemistry, meaning that they use a large body of thermodynamic data, generally from a supporting database file, to sort out the various important reactions from a wide spectrum of possibilities, given specified inputs. Usually codes of this kind are used to construct models of initial aqueous solutions that represent initial conditions for some process, although sometimes these calculations also represent a desired end point. Such a calculation might be used to determine the major chemical species of a dissolved component, the solubility of a mineral or mineral-like solid, or to quantify deviation from equilibrium in the form of saturation indices. Reactive transport codes such as TOUGHREACT and NUFT generally require the user to determine which chemical species and reactions are important, and to provide the requisite set of information including thermodynamic data in an input file. Usually this information is abstracted from the output of a geochemical modeling code and its supporting thermodynamic data file.

The Yucca Mountain Project (YMP) developed two qualified thermodynamic databases to model geochemical processes, including ones involving repository components such as spent fuel. The first of the two (BSC, 2007a) was for systems containing dilute aqueous solutions only, the other (BSC, 2007b) for systems involving concentrated aqueous solutions and incorporating a model for such based on Pitzer’s (1991) equations. A 25°C-only database with similarities to the latter was also developed for the Waste Isolation Pilot Plant (WIPP, cf. Xiong, 2005). The NAGRA/PSI database (Hummel et al., 2002) was developed to support repository studies in Europe. The YMP databases are often used in non-

repository studies, including studies of geothermal systems (e.g., Wolery and Carroll, 2010) and CO_2 sequestration (e.g., Aines et al., 2011).

4.3 Types of Thermodynamic Data

Thermodynamic data of principal concern to geochemical modeling generally appear in one of two forms: standard state Gibbs energies for chemical species or equilibrium constants for reactions. If one has all the necessary standard state Gibbs energies for the chemical species, one can readily calculate the equilibrium constants for an appropriate (independent) set of reactions involving these species.. The reverse is also true, and in some instances Gibbs energies are obtained from solubility data, which equates to measurement of an equilibrium constant. In other instances, Gibbs energies are obtained by calorimetric measurements, which give standard enthalpies and standard entropies, as well as heat capacities. Gibbs energies of mineral species are often derived using mineral-mineral phase equilibrium data (cf. Helgeson et al., 1978; Holland and Powell, 1985, 1990, 1998, 2011; Powell and Holland, 1985, 1988). This approach is powerful in that it preserves the *differences* in Gibbs energies that need to be precisely represented in order to accurately calculate mineral phase assemblages.

Operationally, most database development starts with standard molar Gibbs energies of formation (from the elements in their reference forms) of individual chemical substances. Generally values are obtained for conditions of 25°C and 1 bar pressure. Temperature dependence is dealt with by obtaining values for additional thermodynamic parameters, usually the standard molar entropy of a substance at 25°C and 1 bar pressure and three or four coefficients describing the standard state heat capacity at 1 bar. The pressure dependence to low order requires the standard molar volume at 25°C and 1 bar (for more accurate work, standard molar thermal expansibilities and compressibilities are needed). Typically the standard molar enthalpy of formation is included in database development, but it is not necessary for equilibrium calculations at fixed temperature and pressure. It may be needed if it is necessary to account for chemical production or consumption of heat. Also, it can be used as an alternative to the standard molar entropy in accounting for the temperature dependence of the standard molar Gibbs energy, as that entropy is effectively included in it (as will be discussed below). In some instances, temperature and/or pressure dependence is dealt with using equation of state (EOS) models, which have their own sets of parameters. Once one has the standard molar Gibbs energies of all the relevant species at any temperature and pressure of interest, one can calculate equilibrium constants for appropriate reactions (usually in *log K* format) at the same temperature and pressure. For an explanation of the methodologies used in such calculations, see Helgeson et al. (1978) and Johnson et al. (1992).

In general, the standard molar Gibbs energy of a species at 25°C (reference temperature T_r) and 1 bar pressure (reference pressure P_r) of chemical substance i is the true standard molar Gibbs energy of formation from the chemical elements in their reference forms. However, for other temperatures and pressures, the standard molar Gibbs energy is usually dealt with as the *apparent* standard molar Gibbs energy of formation at the specified temperature and pressure (cf. Helgeson et al., 1978, p. 28), given by:

$$\Delta G^o_{f,i,T,P} = \Delta G^o_{f,i,T_r,P_r} - S^o_{i,T_r,P_r}(T - T_r) + \int_{T_r}^{T} c^o_{p,i,P_r}\, dT - T \int_{T_r}^{T} c^o_{p,i,P_r}\, d\ln T + \int_{P_r}^{P} V^o_{i,T}\, dP \qquad (4\text{-}1)$$

where $\Delta G^o_{f,i,T_r,P_r}$ is the standard molar Gibbs energy of formation at T_r and P_r, S^o_{i,T_r,P_r} is the standard molar entropy at T_r and P_r, c^o_{p,i,P_r} is the standard molar heat capacity at P_r, and $V^o_{i,T}$ is the standard molar volume at temperature T. The standard molar heat capacity is often represented by a temperature function having three or four coefficients. The standard molar volume may be represented as a constant, or by a function

incorporating the thermal expansion and compressibility. Analogous to the apparent standard molar Gibbs energy of formation is the apparent standard molar enthalpy of formation given by:

$$\Delta H^o_{f,i,T,P} = \Delta H^o_{f,i,T_r,P_r} + \int_{T_r}^{T} c^o_{p,i,P_r}\, dT + \int_{P_r}^{P} \left(V^o_{i,T} - T \left[\left(\frac{\partial V^o_i}{\partial T} \right)_P \right]_T \right) dP \qquad (4\text{-}2)$$

where $\Delta H^o_{f,i,T_r,P_r}$ is the standard molar enthalpy of formation at T_r and P_r, and the quantity represented by $\left[\left(\frac{\partial V^o_i}{\partial T} \right)_P \right]_T$ is the partial derivative of the standard molar volume with respect to temperature at pressure P and temperature T (there is some ambiguity in the meaning of the P subscript). These apparent quantity formulations for the standard molar Gibbs energy and enthalpy are preferred because they only require thermodynamic information about the elements in their reference forms at T_r and P_r. Furthermore, standard molar Gibbs energies of reaction and enthalpies of reaction may be calculated from these apparent functions for the relevant chemical species in the usual manner. Most recent works on thermodynamic data use this formalism (e.g., Barin and Platzki, 1995). Some older literature follows other conventions. Also, in some older literature, there may be issues with the appropriate values for the thermodynamic properties of the chemical elements in their reference forms (and the reference forms of may be different may be different for some elements). In any case, the standard molar entropy is treated as the actual standard molar entropy at any temperature and pressure:

$$S^o_{i,T,P} = S^o_{i,T_r,P_r} + \int_{T_r}^{T} c^o_{p,i,P_r}\, d\ln T - T \int_{P_r}^{P} \left[\left(\frac{\partial V^o_i}{\partial T} \right)_P \right]_T dP \qquad (4\text{-}3)$$

The Gibbs energy of the *j*-th reaction *j* at temperature *T* and *P* is given by:

$$\Delta G^o_{r,j,T,P} = \sum_i \nu_{i,j} \Delta G^o_{f,i,T,P}$$

where $\nu_{i,j}$ is the coefficient of the *i*-th species in the reaction. The enthalpy of reaction is given analogously, and the entropy of reaction is also given analogously, but with actual entropies in the summation on the right-hand-side. For geochemical and reactive transport modeling, what is usually employed is some representation of the equilibrium constant (log *K*) as a function of temperature and pressure. The equilibrium constant for the *j*-th reaction is related to the standard molar Gibbs energy of reaction ($\Delta G^o_{r,j,T,P}$) by:

$$\log K_{j,T,P} = -\frac{\Delta G^o_{r,j,T,P}}{2.303\, RT} \qquad (4\text{-}4)$$

where "2.303" is more precisely the base-e logarithm of 10. Often this leads to a situation in which there is a database (of standard molar Gibbs energies and such) behind a *log K*-based database. Some geochemical software does use Gibbs energies and such directly. To preserve general applicability and transparency, thermodynamic data development should cover all key forms of such data, including equilibrium constants, Gibbs energies, enthalpies, entropies, and molar volumes.

For solution phases, including aqueous solutions, standard thermodynamic data are not enough. Thermodynamic models also require data needed to calculate thermodynamic activity coefficients. In the case of dilute aqueous solutions, the familiar Debye-Hückel equation (with some empirical extension) may suffice. Because this model depends on the ionic strength of the solution (in addition to two Debye-Hückel parameters and possibly a third empirical parameter), calculations of activity coefficients are sometimes called "ionic strength corrections." However, this is misleading, as the dependence on aqueous solution composition is in reality more complex. A more sophisticated model for aqueous solutions is

represented by Pitzer's equations (cf. Pitzer, 1991), which contains additional dependency on specific interactions represented by terms containing interaction coefficients. These coefficients represent an additional type of thermodynamic data. Other types of activity coefficient or "solution models" exist for aqueous solutions, solid solutions, and gas mixtures. Equation of state (EOS) models for chemical mixtures incorporate aspects of both standard state thermodynamic data and activity coefficient data.

4.4 Issues with Thermodynamic Data: General

Experimentally, thermodynamic data can be obtained by various means. The most common methods are based on calorimetry, solubility, and phase equilibrium (which technically encompasses solubility). The actual calculation of the data from the direct experimental data may require various corrections, including model-dependent corrections and extrapolations. Original measurements may be re-interpreted to yield somewhat different results, and re-evaluations of older data are not uncommon in the literature. In some instances, thermodynamic data are specific to a given model (e.g., interaction coefficients for Pitzer's equations). Sometimes thermodynamic data are estimated from correlation relations (cf. Helgeson et al., 1978; Tardy and Garrels, 1974) when experimental data are lacking or experimental results are complicated by an inability to separate various controlling factors.

There is always some uncertainty associated with thermodynamic data, regardless of how the data are obtained. In general, estimated uncertainties are not carried in thermodynamic data files intended to support thermodynamic calculations. In part, this is because uncertainties are not always provided by the sources and because when they are provided, they may not result from application of a consistent methodology. However, a larger factor is that it is difficult to carry uncertainties through complex calculations because the input uncertainties would often be correlated. It is nevertheless important to have some notion as to the magnitude of uncertainties in the data at whatever level this is practicable.

A larger issue in the treatment of thermodynamic data is that of consistency. For example, to develop a consistent set of Gibbs energies of formation for various species, it is necessary to have a consistent set of reference forms for the chemical elements and a consistent set of values for the corresponding standard molar entropies at 298.15K and 1 bar (this particular issue will be addressed in more detail later in its own section). In general, consistency problems arise when either: (1) data are combined which depend on other data for which inconsistent values were used, or (2) when a correction is made to some data, but other data whose values depend on those data are not corrected. For example, in the development of the YMP dilute systems database, different values were found to be extant for the standard Gibbs energy of formation of the key aqueous phosphate species (cf. Rard and Wolery, 2007). For the sake of consistency, one set of key values had to be chosen. Then all values depending on these key data needed to be made consistent with the chosen set of key values. Another example discussed in BSC (2007a) concerned the appropriate Gibbs energy for the key species $SiO_{2(aq)}$.

There are basically three types of key or anchor data in the construction of a thermodynamic database. The first, as noted above, consists of values for the standard molar entropies of the chemical elements. For minerals, the best data are usually obtained from mineral-mineral phase equilibrium data, as this approach reduces relative errors in Gibbs energies. This approach requires choosing a set of *key* or *anchor* minerals for which the individual standard molar thermodynamic properties (Gibbs energy, enthalpy, and entropy) are defined, and then using those property values to extract the corresponding individual property values for other minerals. In general, one anchor mineral is required for each chemical component present in the set of minerals for which such phase equilibrium data are to be used (e.g., quartz for SiO_2). For aqueous species, there are key aqueous species for which the individual property values (again the Gibbs energy, enthalpy, and entropy) must be defined. The corresponding data for other aqueous species can then be

extracted from data that more directly represent equilibrium constants. In some instances, thermodynamic properties of a mineral (or an aqueous species) can be extracted from solubility measurement.

Key or anchor data should be of the highest quality. They should be based on experimental results that are transparent and repeatable and carry low uncertainty. This is more easily achieved with some chemical species than others. Equilibrium or completion of reaction may be inhibited by kinetics, compositions may not be stoichiometrically ideal, and order-disorder phenomenon can skew results. Some key data depend on other key data. For example, the data for a key aqueous species will depend on data for the entropies of the relevant chemical elements at 298.15K and 1 bar. This will also be true for key minerals that are not themselves reference forms for chemical elements.

In building a thermodynamic database, it is easy to introduce inconsistencies, because one may not know how certain adopted data were obtained by the sources. There is a particular problem with older tabulations of thermodynamic data (e.g., Wagman et al., 1982) that simply give "recommended data" without identifying the actual sources, let alone the logic leading to the "recommendations." Wagman et al. (1982) give values for the entropies of the chemical elements in their reference forms, but there is no guarantee that there are no inconsistencies with these values in the other data given in their compilation. In more recent times, there has been a shift toward greater transparency in data development, especially in the NEA Thermodynamic Data volumes. Also, the increasing use of computers makes it easier to document data development, check for inconsistencies, and make appropriate corrections.

4.5 Sources of Thermodynamic Data

The development of thermodynamic databases has a long history in geochemistry (e.g., Garrels and Christ, 1965; Helgeson et al., 1969; Helgeson et al., 1978, Johnson et al., 1992; Robie and Hemingway, 1995), paralleled by related and applicable work in the larger scientific community (e.g., Wagman et al., 1982, 1989; Cox et al., 1989; Barin and Platzki, 1995; Binneweis and Milke, 1999). Unfortunately, the National Bureau of Standards (now the National Institutes of Science and Technology) no longer generally addresses thermodynamic data pertaining to aqueous, mineral, and gas species, its last word being the compilation of Wagman et al. (1982) and the errata published in 1989. IUPAC, whose efforts in this area were generally limited to data pertaining to key species only (a small subset), has not done much in this area since the publication of the Cox et al. (1989) report. The standards organizations have been basically inactive regarding thermodynamic data of interest to geochemical and repository studies for over twenty years. For radionuclide elements, much of this void has been filled by the European Nuclear Energy Agency (NEA), which has sponsored a series of review volumes (e.g., Grenthe et al., 1992 [1: uranium]; Silva et al., 1995 [2: americium]; Rard et al., 1999 [3: technetium]; Lemire et al., 2001 [4: neptunium and plutonium]; Guillaumont et al., 2003 [5: update on uranium, neptunium, plutonium americium, and technetium]; Gamsjäger et al., 2005 [6: nickel]; and Olin et al., 2005 [7: selenium]).

Prior to about 1989 (when the Cox et al. report was published), values for such key data as entropies of the elements in their reference forms and Gibbs energies and such for the principal aqueous species were in a fair state of flux, as evidenced by changes in recommended values in various publications (generally in series) by "authoritative" sources including NBS, CODATA, JANAF, and the U.S. Geological Survey [what would be a very long series of appropriate older references will not be included here]. Since then, the situation has been more stable, though there have continued to be remaining issues with the data for a small number of key species. Some examples ($SiO_{2(aq)}$, aqueous phosphate species) are discussed by BSC (2007a). Some additional examples will be noted later in this report.

The YMP dilute systems database is widely used in the geochemistry community for a variety of applications involving rock/water interactions. It builds on the work of Prof. Helgeson and his students (see BSC, 2007a for many applicable references, including ones to the SUPCRT92 code and associated database), and covers a significant range of temperature (25-300°C). The last version (data0.ymp.R5) covers 86 chemical elements, 1219 aqueous species, 1156 minerals and other solid species, and 128 gas species. Many data for actinide species have been adopted from the Nuclear Energy Agency (NEA) series of volumes on actinide thermodynamics (see references given in BSC, 2007a), and the appropriate temperature extrapolations have been applied. The YMP concentrated systems database (data0.ypf.R2) covers a smaller chemical system: 40 chemical elements, 237 aqueous species, 470 minerals and other solids, and 11 gas species. It includes temperature dependence, which for many species extends to 200°C, but for others extends to 250°C, to 110°C, or is restricted to 25°C. It is based on many sources (see BSC, 2007b), but draws in particular from the work of Pabalan and Pitzer (1987) and Greenberg and Møller (1989). In addition to their other characteristics, these databases have a regulatory cachet as qualified products of YMP and have already undergone peer-review and QA review.

A potential new source of data is the "Holland and Powell" database, represented in its most recent form by Holland and Powell (2011). This database series began in 1985 (Holland and Powell, 1985; Powell and Holland, 1985, 1988) and has been subsequently revised and expanded over the years (Holland and Powell, 1990; Holland and Powell, 1998). The Holland and Powell work mainly addresses minerals, rather strongly overlapping the older work by Helgeson et al. (1978). As will be noted later in this report, there are reasons to support revision of the Helgeson et al. (1978) data for minerals. It does not seem advisable, however, to merely supplant the Helgeson et al. data with the latest Holland and Powell data until some potential issues (inconsistency in the key data, extrapolation of high-temperature data to low temperature) are resolved.

4.6 Data Gaps

The purpose of the present task is to improve these databases for use in the Used Fuel Disposition Campaign and maintain some semblance of order that will support qualification in support of the development of future underground high-level nuclear waste disposal. The work is presently supported by THCM, EBS, and Natural Systems, with the THCM support being incorporated into the EBS work package for FY12. The YMP design was based on disposal in volcanic tuff, in a thick vadose zone in which oxidizing conditions were expected to prevail. A 50-year period of tunnel ventilation was planned to limit maximum temperature. Concentrated solutions were not originally expected at Yucca Mountain. Later concerns about dust deliquescence and evaporative concentration led to the development of the YMP concentrated solutions thermodynamic database (see BSC, 2007b). The YMP design scenario was very different from those for planned repositories in other countries, which envision disposal below the water table (generally under reducing conditions) in clay, salt, granite or other hard rock, usually incorporating relatively low maximum temperature in the designs. The Used Fuel Disposition program is investigating potential disposal in mined repositories in these three rock types, plus a deep borehole option (which appears to imply granite or other hard rock). The UFD may consider higher maximum temperatures than are presently being considered in other countries, although at present it is focusing on similar design options.

Although the YMP thermodynamic databases incorporated many data of value to generic geochemistry applications, in some areas development was limited owing to the expected generally oxidizing conditions and limited maximum temperatures associated with the YMP design scenario. Consequently, these databases need some additional development to adequately address the different design scenarios being addressed by the Used Fuel Disposition program. There is a need to address a somewhat wider range of

mineralogy because of the different rock types. There is a need to fill some gaps arising due to the expectation of reducing instead of oxidizing conditions. There is also a need to address some other things that were not addressed because they were not relevant to the YMP design scenario. Finally, in any effort using thermodynamic data, there is the ever-present factor of flaws being discovered in existing data, and the potential impact of new data reported elsewhere. Errors (and the suspicion of errors) generally come to light in the application of the data.

The following areas are now of concern for thermodynamic database development under UFD:

- Data (and mixing models) for complex clays, including illites and smectites, and certain related sheet silicates. Clay minerals play various roles in the geologic disposal of nuclear waste (for an overview of clays from the perspective of the UFD Natural Systems department, see Chapter 4 of *Natural System Evaluation and Tool Development – FY11 Progress Report*: Wang et al., 2011). Specific progress has been made in FY11-12, including the development of estimated properties for dehydrated and end-member hydrated smectites. These data are being used in the development of variable hydration models. New property estimates have been made for other sheet silicates as well. Most of this work is being done on the EBS side of the UFDC. A short summary is given below. For a fuller discussion, see Wolery (2012), milestone report M4FT-12LL0806041.
- Core data for aluminosilicate minerals. These are now taken from SUPCRT92 (see BSC, 2007a), mostly taken from Helgeson et al. 1978). Some consistency issues have been noted. Also, a similar database (Holland and Powell, 2011) could be a potential replacement data source. The issues here are discussed in a separate section later in this report.
- Data for certain zeolites, particularly ones for which the data do not trace to Helgeson et al. (1978). Geothermal systems modeling (Wolery and Carroll, 2010) suggested that the data in question here may not be consistent with proper stable mineral assemblages in the geologic systems of interest.
- Data that continue to come out of the NEA review program (or which have come out but were not incorporated into the YMP databases.
- Other new data from other sources not previously incorporated into the database (e.g., the Fe^{2+} and Fe^{3+} data recommended by Parker and Khodakovskii, 1995, which are likely to be adopted by the NEA).
- Additional data for sulfide minerals (which may be very important in UFD disposal systems but were not important to YMP). The mineral pyrite (nominal composition FeS_2) allows many chemical substitutions and could be a sink for some important radionuclides.
- Isolated errors discovered since the termination of the YMP (example: the Gibbs energy and related calorimetric data for $NaHCO_3$(c) in the YMP concentrated systems database were found to be inaccurate in the course of a CO_2 air capture project).
- Data for ion exchange and surface complexation processes. For surface complexation, one or more specific models need to be chosen (a fair number are extant).

The last YMP dilute systems thermodynamic database (data0.ymp.R5) contains data for various clay compositions. A detailed description of the methods and derivation of the corresponding thermodynamic data is given in the Analysis/Model Report ANL-WIS-GS-000003 Rev. 1 (BSC, 2007a). Correlation algorithms were used to estimate properties for smectites and some related sheet silicates. The development followed that of Tardy and Garrels (1974), except that the final YMP work included updated values for the Gibbs energy data used to regress the values for the silicated oxide components and also (in the case of subsequent calculation of equilibrium constants) updated values for the Gibbs energies of the relevant aqueous species. Data were obtained for idealized clays with implicitly hydrated (to unit water

activity) smectite end-members, including five beidellites, five saponites, five montmorillonites and five nontronites, These data were intended to be used in solid solution models in modeling software. Data were also obtained by the same process for an illite and three celadonites, and some chlorite and chlorite-related sheet silicates, which will not be noted here.

The Tardy and Garrels (1974) approach does not account for the water of hydration present in the smectite interlayer. In reality, a sodium beidellite for example would have a formula represented by $Na_{0.33}Al_2Al_{0.33}Si_{3.67}O_{10}(OH)_2.nH_2O$, where n might potentially be as high as 7. However, a key point is that the amount of interlayer water is variable, depending on temperature, pressure, water activity (or pressure), and which cations are in the interlayer. We are looking at models for variable hydration that can be combined with the Tardy-Garrels approach to achieve more accurate models and data for the smectites. Interesting approaches are suggested by Ransom and Helgeson (1993, 1994ab, 1995), Tardy and Duplay 1992, Viellard (1994ab, 2000), Vidal and Dubacq (2011), and others.

In FY12, we re-estimated the properties for sheet silicates. This time, we made a distinction between dehydrated and hydrated smectites. The estimates for dehydrated smectites are straightforward. For hydrated smectites, the usual estimation procedures appear to be fine for some properties, namely the entropy, heat capacity coefficients, and molar volumes. However, these procedures, which are essentially linear in nature, are not well-suited to describe the Gibbs energy or enthalpy of the hydration process. Thus, Gibbs energies and enthalpies can only be reliably estimated for "fully hydrated" end-members, and hydration-dehydration is treated using a simple non-ideal mixing model involving such end-members and full dehydrated equivalents. The "fully hydrated" end-members are generally fictive, in the sense that their water content may imply a thermodynamic activity for water exceeding unity. Such phases would spontaneously dehydrate. Thus, they would not exist in reality, where the actual "fully-hydrated" form would be limited by unity water activity.

Table 4-1 shows the new estimated data for 23 dehydrated smectite compositions. Table 4-2 shows the data for the corresponding hydrated smectite compositions, for the case of 4.5 moles of H_2O per mole of smectite. Gibbs energies and enthalpies are not included in Table 4-2 because any values would be hydration-model dependent. The data shown along with additional data given in Wolery (2012) provide a foundation for developing specific hydration models.

We intend to improve the existing data/models for complex clays by:

- Explicitly accounting for water in the exchange layers of smectites and vermiculites
- Accounting for a broader spectrum of physical measurements (e.g., basal spacing studies of clay dehydration, swelling pressure data, ion exchange data over a wide range of temperature)
- Including insights from molecular dynamics (MD) modeling regarding dehydration

This work on smectites is expected to continue in FY13.

Table 4-1. Estimated Thermodynamic Data for 23 Dehydrated Smectite Compositions. Data are shown in calorie units (1 cal = 4.184 joule). This table is taken from workbook Clays_TJW_2_Rev1r..

Name	Formula	$\Delta G_f°$ cal/mol	$\Delta H_f°$ cal/mol	S° cal/mol-K	V° cm^3/mol	a cal/mol-K	b x 10^3 cal/mol-K^2	c x 10^{-5} cal-K/mol
H-Beidellite	H0.33Al2Al0.33Si3.67O10(OH)2	-1260140.8	-1351137.7	57.636	126.075	81.438	38.333	17.774
Na-Beidellite	Na0.33Al2Al0.33Si3.67O10(OH)2	-1278599.5	-1368880.0	58.931	127.590	83.277	37.780	18.251
K-Beidellite	K0.33Al2Al0.33Si3.67O10(OH)2	-1281785.7	-1372093.1	59.896	131.052	83.319	38.401	17.919
Ca-Beidellite	Ca0.165Al2Al0.33Si3.67O10(OH)2	-1278541.0	-1368495.6	57.618	126.578	82.191	37.152	18.031
Mg-Beidellite	Mg0.165Al2Al0.33Si3.67O10(OH)2	-1275209.6	-1365228.7	57.050	125.391	81.945	37.260	18.018
H-Saponite	H0.33Mg3Al0.33Si3.67O10(OH)2	-1324331.8	-1409762.5	62.777	135.725	84.486	40.729	13.832
Na-Saponite	Na0.33Mg3Al0.33Si3.67O10(OH)2	-1342790.5	-1427505.2	64.071	137.240	86.325	40.176	14.309
K-Saponite	K0.33Mg3Al0.33Si3.67O10(OH)2	-1345976.7	-1430717.5	65.039	140.702	86.367	40.797	13.977
Ca-Saponite	Ca0.165Mg3Al0.33Si3.67O10(OH)2	-1342732.0	-1427120.5	62.760	136.228	85.239	39.548	14.089
Mg-Saponite	Mg0.165Mg3Al0.33Si3.67O10(OH)2	-1339400.6	-1423853.8	62.190	135.041	84.993	39.656	14.076
H-Nontronite	H0.33Fe2Al0.33Si3.67O10(OH)2	-1055918.4	-1140192.3	66.657	131.753	77.438	54.113	12.944
Na-Nontronite	Na0.33Fe2Al0.33Si3.67O10(OH)2	-1074377.1	-1157936.8	67.945	133.267	79.277	53.560	13.421
K-Nontronite	K0.33Fe2Al0.33Si3.67O10(OH)2	-1077563.2	-1161143.7	68.931	136.730	79.319	54.181	13.089
Ca-Nontronite	Ca0.165Fe2Al0.33Si3.67O10(OH)2	-1074318.6	-1157550.6	66.638	132.256	78.191	52.932	13.201
Mg-Nontronite	Mg0.165Fe2Al0.33Si3.67O10(OH)2	-1070987.1	-1154285.8	66.063	131.068	77.945	53.040	13.188
H-Montmorillonite	H0.33Mg0.33Al1.67Si4O10(OH)2	-1251018.7	-1340729.7	58.968	128.651	79.429	40.683	16.388
Na-Montmorillonite	Na0.33Mg0.33Al1.67Si4O10(OH)2	-1269477.4	-1358472.2	60.263	130.165	81.267	40.130	16.865
K-Montmorillonite	K0.33Mg0.33Al1.67Si4O10(OH)2	-1272663.5	-1361685.0	61.229	133.627	81.310	40.750	16.533
Ca-Montmorillonite	Ca0.165Mg0.33Al1.67Si4O10(OH)2	-1269418.9	-1358087.6	58.951	129.154	80.181	39.501	16.645
Mg-Montmorillonite	Mg0.495Al1.67Si4O10(OH)2	-1266087.4	-1354820.7	58.382	127.966	79.935	39.610	16.632
Low Fe-Mg Smectite	see below	-1261694.8	-1351295.0	65.313	134.706	84.327	41.014	15.634
High Fe-Mg Smectite	see below	-1213458.8	-1303302.8	66.390	131.625	86.685	40.089	15.493
Reykjanes Smectite	see below	-1299800.6	-1390109.9	69.942	138.295	90.231	39.005	15.618

Low Fe-Mg Smectite = Na0.15K0.2Ca0.02(Mg0.9Fe(+++)0.16Fe(++)0.29Al)(Al0.25Si3.75)O10(OH)2
Fe-Mg Smectite = Na0.1K0.2Ca0.025(Mg1.15Fe(+++)0.2Fe(++)0.5Al0.75)(Al0.5Si3.5)O10(OH)2
Reykjanes Smectite = Na0.33K0.03Ca0.66(Mg1.29Fe(+++)0.35Fe(++)0.33Mn0.01Al0.28)(Al0.83Si3.17)O10(OH)2

Table 4-2. Estimated Thermodynamic Data for 23 Smectite Compositions with interlayer hydration number of 4.5. Data are shown in calorie units (1 cal = 4.184 joule). Gibbs energies and enthalpies are not included here, as value would be hydration-model dependent. This table is taken from workbook Clays_TJW_2_Rev1r..

Name	Formula	$\Delta G_f°$ cal/mol	$\Delta H_f°$ cal/mol	S° cal/mol-K	V° cm^3/mol	a cal/mol-K	b x 10^3 cal/mol-K^2	c x 10^{-5} cal-K/mol
H-Beidellite	H0.33Al2Al0.33Si3.67O10(OH)2			116.811	203.565	122.136	93.863	13.368
Na-Beidellite	Na0.33Al2Al0.33Si3.67O10(OH)2			118.106	205.080	123.975	93.310	13.845
K-Beidellite	K0.33Al2Al0.33Si3.67O10(OH)2			119.071	208.542	124.017	93.931	13.513
Ca-Beidellite	Ca0.165Al2Al0.33Si3.67O10(OH)2			116.793	204.068	122.889	92.682	13.626
Mg-Beidellite	Mg0.165Al2Al0.33Si3.67O10(OH)2			116.225	202.881	122.643	92.790	13.612
H-Saponite	H0.33Mg3Al0.33Si3.67O10(OH)2			121.952	213.215	125.184	96.259	9.426
Na-Saponite	Na0.33Mg3Al0.33Si3.67O10(OH)2			123.246	214.730	127.023	95.706	9.903
K-Saponite	K0.33Mg3Al0.33Si3.67O10(OH)2			124.214	218.192	127.065	96.327	9.571
Ca-Saponite	Ca0.165Mg3Al0.33Si3.67O10(OH)2			121.935	213.718	125.937	95.078	9.684
Mg-Saponite	Mg0.165Mg3Al0.33Si3.67O10(OH)2			121.365	212.531	125.691	95.186	9.670
H-Nontronite	H0.33Fe2Al0.33Si3.67O10(OH)2			125.832	209.243	118.136	109.643	8.538
Na-Nontronite	Na0.33Fe2Al0.33Si3.67O10(OH)2			127.120	210.757	119.975	109.090	9.015
K-Nontronite	K0.33Fe2Al0.33Si3.67O10(OH)2			128.106	214.220	120.017	109.711	8.683
Ca-Nontronite	Ca0.165Fe2Al0.33Si3.67O10(OH)2			125.813	209.746	118.889	108.462	8.796
Mg-Nontronite	Mg0.165Fe2Al0.33Si3.67O10(OH)2			125.238	208.558	118.643	108.570	8.782
H-Montmorillonite	H0.33Mg0.33Al1.67Si4O10(OH)2			118.143	206.141	120.127	96.213	11.982
Na-Montmorillonite	Na0.33Mg0.33Al1.67Si4O10(OH)2			119.438	207.655	121.965	95.660	12.459
K-Montmorillonite	K0.33Mg0.33Al1.67Si4O10(OH)2			120.404	211.117	122.008	96.280	12.127
Ca-Montmorillonite	Ca0.165Mg0.33Al1.67Si4O10(OH)2			118.126	206.644	120.879	95.031	12.240
Mg-Montmorillonite	Mg0.495Al1.67Si4O10(OH)2			117.557	205.456	120.633	95.140	12.226
Low Fe-Mg Smectite	see below			124.488	212.196	125.025	96.544	11.228
High Fe-Mg Smectite	see below			125.565	209.115	127.383	95.619	11.088
Reykjanes Smectite	see below			129.117	215.785	130.929	94.535	11.213

Low Fe-Mg Smectite = Na0.15K0.2Ca0.02(Mg0.9Fe(+++)0.16Fe(++)0.29Al)(Al0.25Si3.75)O10(OH)2
Fe-Mg Smectite = Na0.1K0.2Ca0.025(Mg1.15Fe(+++)0.2Fe(++)0.5Al0.75)(Al0.5Si3.5)O10(OH)2
Reykjanes Smectite = Na0.33K0.03Ca0.66(Mg1.29Fe(+++)0.35Fe(++)0.33Mn0.01Al0.28)(Al0.83Si3.17)O10(OH)2

4.7 A Key Data Issue: The Entropies of the Chemical Elements in Their Reference Forms

This section examines data for the entropies of the elements in their reference forms at 298.15K and 1 bar pressure. Data are taken from assorted authoritative sources. They are *key* or *anchor* data for evaluating and synthesizing thermodynamic data for chemical substances, although their role is often taken much for granted. These data are required to calculate the Gibbs energy of a chemical substance (*i*) from its enthalpy or vice versa. The equation relating the two is:

$$\Delta G^o_{f,i} = \Delta H^o_{f,i} - T\Delta S^o_{f,i} \qquad (4\text{-}5)$$

where $\Delta G^o_{f,i}$ is the (standard molar) Gibbs energy of formation, $\Delta H^o_{f,i}$ is the (standard molar) enthalpy of formation, T is the absolute temperature, and $\Delta S^o_{f,i}$ is the (standard molar) entropy of formation. The Gibbs energy and enthalpy of formation are generally tabulated along with the absolute (standard molar) entropy ($S°$), not the entropy of formation. The entropy of formation of a chemical substance is related to the absolute entropy of the substance by:

$$\Delta S^o_{f,i} = S^o_i - \sum_\varepsilon \nu_{\varepsilon,i}\, S^o_\varepsilon \qquad (4\text{-}6)$$

where ε denotes a chemical element, $\nu_{\varepsilon,i}$ is the stoichiometric coefficient of the element in the *i*-th chemical substance, and S^o_ε is the absolute (standard molar) entropy of the element in its reference state. It is noted that the reference state of a chemical element is usually the thermodynamically stable form, though this is not always the case (e.g., white phosphorus instead of red).

Although the above equations generally apply to any temperature and pressure (P), for purposes of tabulating thermodynamic data, they are usually applied in modern practice only at the reference temperature of 298.15K (25°C) and the reference pressure (1 bar or 10^5 Pascals). If they were directly applied for any T and P, the resulting formation properties would then be defined as dependent on T and P. It would be necessary to know (accurately) the entropies of the elements in their reference forms across the range of temperature and pressure. In addition, one would need to account for potential changes in the identity of the reference state itself, due for example to phase changes. In modern practice (e.g., Helgeson et al., 1978; Barin and Platzki, 1995; Chase, 1998) this potential difficulty is avoided by tabulating the Gibbs energy and enthalpy of formation of a chemical substance at the reference T and P and then calculating so-called apparent formation properties at other temperatures and pressures. The actual Gibbs energy of reaction for any T and P can be calculated from the apparent Gibbs energies of formation of the reactants and products at the same T and P.

The entropies of the elements in their reference forms at 298.15K and 1 bar pressure, like all thermodynamic data, have a history of various values that have been reported from original investigations and compiled and recommended by a number of secondary works. Here data are taken from the following fairly recent authoritative secondary (compiled) sources:

NBS 1982 (NBS Tables, Wagman et al., 1982)
CODATA 1989 (CODATA Key Values, Cox et al., 1989)
NEA 1992-2005 (NEA Thermodynamic Data Volumes, Grenthe et al., 1992 through Hummel et al., 2005)
Barin 1995 (Barin and Knacke, 1995)
R & H 1995 (Robie and Hemingway, 1995)

JANAF 1998 (NIST-JANAF Tables, Chase, 1998)

The NBS 1982 tables are outdated, but are included here because of their large scope and influence. There is a 1989 erratum, but it does not affect the data of concern here. The CODATA 1989 values are highly influential, but of limited scope. The NEA volumes adopt CODATA values for elemental reference entropies and supplement them as needed. This series is continuing. NEA data used here are mainly taken from Hummel et al. (2005) , which contains a complete list of earlier volumes postdating Grenthe et al. (1992). Barin 1995 is a volume of considerable scope and is well regarded. There may be a 2004 update, but this has not been confirmed. R & H 1995 is well regarded in the earth sciences community, and is the last contribution in a line of compilations of thermodynamic data produced by the U.S. Geological Survey. JANAF 1998 is influential, but its scope is rather limited. It is the last in a series of JANAF tables, and further represents the last compilation of thermodynamic data for inorganic systems associated with NBS/NIST.

The data are presented in Table 4-3. The number of elements considered is 103, but data are entirely lacking for some. Coverage is mixed for others. NBS 1982 covers 88 elements. CODATA 1989 covers 37. NEA 1992-2005 (subsuming the CODATA data) covers 50. Since the NEA series is continuing, additional data may become available. Barin 1995 covers 89 chemical elements. JANAF 1989 covers 47, while R & H 1995 covers 50. Table 4-4 presents results showing the sensitivity of the calculated Gibbs energy to entropy data when the Gibbs energy is calculated from enthalpy and entropy data. In general, differences in entropy of a few tenths of a J/mol-K are tolerable. For example, an entropy difference of 0.5 J/mol-K leads to a Gibbs energy difference of 149 J/mol. Differences in excess of 1 J/mol-K may be problematic. A 1 J/mol-K leads to a difference of 298 J/mol, and a 2 J/mol-K leads to a difference of 596 J/mol. It must be kept in mind that an entropy difference of 1 J/mol-K for a chemical element usually translates into a larger difference in the entropy of a chemical substance depending on the moles of element per mole of substance. Thus, one would like to see elemental entropies resolved to uncertainties well under 1 J/mol-K. Table 3 shows that a fairly high level of resolution is apparent for most of the chemical elements for which data are available.

In general, NEA data are preferred for new work when available, in part because the NEA subsumes CODATA 1989 and in part for the high level of rigor in review. For elemental reference data not covered by the NEA volumes, Barin 1995 is the next preferred source owing mainly to scope. R & H 1995 and JANAF 1998 do not offer much help from a coverage point of view. Of these two, JANAF 1998 would be preferred owing to its relationship to a standards organization (NIST).

The values tabulated here may be useful in several ways. One is to allow a comparison of recommended values, which may be helpful in identifying elements for which the accuracy or even the basic correctness of the data may be of concern. Elements for which entropy data from these sources show notable discrepancies include Ca, Ce, Pb, S, Sr, and Th. Another potential use is to suggest corrections in instances in which the thermodynamic data for a chemical substance are taken from a source, for which one or more of the relevant elemental entropy data may be considered incorrect. It is important to note that there is no guarantee that the Gibbs energy, enthalpy, and entropy data given by any source are consistent with the elemental entropy data given by the same source. One can, however, easily check for such consistency.

Some other potential sources were excluded here. For example, the handbook of Binnewies and Milke (1999) draws on works published in 1992 or earlier, most of which have been supplanted by later works that are used here. McBride et al. (2001) present data on fifty elements, adopting the less-used convention in which the reference state varies with temperature. It also draws mainly on older works. Earlier works

associated with CODATA, NBS, JANAF, Barin, and the U.S. Geological Survey could be useful in establishing trends or correcting historical data, but were also not considered here.

Table 4-3. Entropies of the Chemical Elements in Their Reference Forms: A Comparison of Data from Assorted Authoritative Sources. Cells with gray backgrounds denote cases of notably discrepant values. This table is taken from workbook Elemental_Entropies_Rev0i.xlsx.

Element	NBS 1982 J/mol-K	CODATA 1989 J/mol-K	NEA 1992- J/mol-K	Barin 1995 J/mol-K	JANAF 1998 J/mol-K	R & H 1995 J/mol-K
Ac	56.5	-----		-----	-----	-----
Ag	42.55	42.55	42.550	42.677	-----	42.55
Al	28.33	28.30	28.300	28.275	28.275	28.30
Am	-----	-----	55.400	54.488	-----	-----
Ar	154.843	154.846	154.846	154.845	154.845	-----
As	35.1	-----	35.100	35.706	-----	35.69
At	-----	-----		-----	-----	-----
Au	47.40	-----		47.497	-----	47.49
B	5.86	5.90	5.900	5.830	5.834	5.83
Ba	62.8	-----	62.420	62.417	62.475	62.42
Be	9.50	9.50	9.500	9.440	9.440	9.50
Bi	56.74	-----	56.740	56.735	-----	56.74
Bk	-----	-----		-----	-----	-----
Br	76.1155	76.105	76.105	76.105	76.103	76.100
C	5.740	5.74	5.740	5.740	5.740	5.74
Ca	41.42	41.59	41.590	41.422	41.588	42.90
Cd	51.76	51.80	51.800	51.798	-----	51.80
Ce	72.0	-----		69.454	-----	72.00
Cf	-----	-----		-----	-----	-----
Cl	111.533	111.5405	111.5405	111.5585	111.5395	111.540
Cm	-----	-----		-----	-----	-----
Co	30.04	-----		30.041	30.067	30.04
Cr	23.77	-----		23.640	23.618	23.62
Cs	85.23	85.23	85.230	85.147	85.147	85.23
Cu	33.150	33.15	33.150	33.164	33.164	33.14
Dy	74.77	-----		74.894	-----	-----
Er	73.18	-----		73.178	-----	-----
Es	-----	-----		-----	-----	-----
Eu	77.78	-----		77.822	-----	-----
F	101.39	101.3955	101.3955	101.3975	101.3945	101.395
Fe	27.28	-----		27.280	27.321	27.09
Fm	-----	-----		-----	-----	-----
Fr	95.4	-----		-----	-----	-----
Ga	40.88	-----		40.828	40.838	-----
Gd	68.07	-----		67.948	-----	-----
Ge	31.09	31.09	31.090	31.087	-----	31.09
H	65.342	65.340	65.340	65.340	65.340	65.340
He	126.150	126.153	126.153	126.148	126.152	-----
Hf	43.56	-----		43.555	43.560	-----
Hg	76.02	75.90	75.900	75.898	76.028	75.90

Ho	75.3	-----		75.019	-----	-----
I	58.0675	58.070	58.070	58.071	58.071	58.070
In	57.82	-----		57.823	-----	-----
Ir	35.48	-----		35.505	-----	-----
K	64.18	64.68	64.680	64.670	64.670	64.67
Kr	164.082	164.085	164.085	164.085	164.084	-----
La	56.9	-----		56.902	-----	-----
Li	29.12	29.12	29.120	29.080	29.085	29.09
Lr	-----	-----		-----	-----	-----
Lu	50.96	-----		50.961	-----	-----
Md	-----	-----		-----	-----	-----
Mg	32.68	32.67	32.670	32.677	32.671	32.67
Mn	32.01	-----		32.008	32.010	32.01
Mo	28.66	-----		28.593	28.605	28.66
N	95.805	95.8045	95.8045	95.8045	95.8045	95.805
Na	51.21	51.30	51.300	51.455	51.455	51.46
Nb	36.40	-----		36.401	36.464	-----
Nd	71.5	-----		71.086	-----	-----
Ne	146.328	146.328	146.328	146.324	146.327	-----
Ni	29.87	-----	29.870	29.874	29.870	29.87
No	-----	-----		-----	-----	-----
Np	-----	-----	50.460	50.459	-----	-----
O	102.569	102.576	102.576	102.5735	102.5735	102.575
Os	32.6	-----		32.635	-----	-----
P	41.09	41.09	41.090	41.070	41.077	41.09
Pa	51.9	-----		51.882	-----	-----
Pb	64.81	64.80	64.800	64.785	64.785	61.80
Pd	37.57	-----		37.823	-----	-----
Pm	-----	-----		-----	-----	-----
Po	-----	-----		-----	-----	-----
Pr	73.2	-----		73.931	-----	-----
Pt	41.63	-----		41.631	-----	41.63
Pu	-----	-----	54.460	51.463	-----	-----
Ra	71	-----		-----	-----	-----
Rb	76.78	76.78	76.780	76.780	76.778	-----
Re	36.86	-----		36.526	-----	-----
Rh	31.51	-----		31.505	-----	-----
Rn	176.21	-----	-----	176.231	176.235	-----
Ru	28.53	-----		28.535	-----	-----
S	31.80	32.054	32.054	32.056	32.056	32.05
Sb	45.69	-----	45.520	45.522	-----	45.52
Sc	34.64	-----		34.644	-----	-----
Se	42.442	-----	42.090	42.258	-----	42.27
Si	18.83	18.81	18.810	18.820	18.820	18.81
Sm	69.58	-----		69.496	-----	-----
Sn	51.55	51.18	51.180	51.195	-----	51.18
Sr	52.3	-----	55.700	55.690	55.694	55.69
Ta	41.51	-----		41.505	41.471	-----
Tb	73.22	-----		73.304	-----	-----
Tc	-----	-----	32.506	33.472	-----	-----
Te	49.71	-----	49.221	49.497	-----	49.71
Th	53.39	51.8	51.800	53.388	-----	51.83

Ti	30.63	30.72	30.720	30.759	30.579	30.76
Tl	64.18	-----		64.183	-----	-----
Tm	74.01	-----		74.015	-----	-----
U	50.21	50.20	50.200	50.292	-----	50.20
V	28.91	-----		28.911	28.936	28.94
W	32.64	-----		32.660	32.660	32.65
Xe	169.683	169.685	169.685	169.683	169.684	-----
Y	44.43	-----		44.434	-----	-----
Yb	59.87	-----		59.831	-----	-----
Zn	41.63	41.63	41.630	41.631	41.717	41.63
Zr	38.99	-----	39.080	38.869	38.869	38.87

Table 4-4. Effect of Entropy Value Difference on Gibbs Energy Calculated from Enthalpy. This table is taken from workbook Elemental_Entropies_Rev0i.xlsx.

δS J/mol-K	TδS J/mol	δS cal/mol-K	TδS cal/mol
0.001	0.29815	0.00024	0.0713
0.005	1.49075	0.00120	0.356
0.01	2.9815	0.00239	0.713
0.05	14.9075	0.0120	3.6
0.1	29.815	0.0239	7.1
0.5	149.075	0.1195	35.6
1	298.15	0.2390	71.3
2	596.3	0.4780	142.5
3	894.45	0.7170	213.8

4.8 A Core Data Issue: Thermodynamic Data for Aluminosilicate Minerals

Aluminosilicate minerals are of great importance to all UFDC disposal scenarios except perhaps disposal in salt. Most of the data for aluminosilicates (and related oxides and certain other minerals) in the thermodynamic database inherited from the Yucca Mountain Project are taken from the SUPCRT92 database created by the late Prof. H.C. Helgeson and his students. For a detailed discussion of SUPCRT92 and its use in the YMP database, see BSC (2007a). The SUPCRT92 database contains information in the form of Gibbs energies and such (e.g., none of the data are in *log K* form). The SUPCRT92 software (Johnson et al., 1992) can be used to generate *log K* values for reactions at various temperatures and pressures.

The mineral part of the SUPCRT92 database was originally based on the work of Helgeson et al. (1978). Examination shows that this part is largely unchanged in its present form. Most of the subsequent attention by Prof. Helgeson, his students, and other associates focused on aqueous species. In the development of the YMP database (see BSC, 2007a for detailed discussion and appropriate references), a notable change was made to the Gibbs energy value for the key aqueous species $SiO_{2(aq)}$. This has the effect of predicting that quartz (SiO_2) is more soluble than was predicted by the older data. At the time, it was recognized that there might be additional consequences of this change. However, a deeper analysis was deferred to future work (which did not take place on the YMP).

A closer look at the Helgeson et al. (1978) paper (supported by discussions with Dr. K.J. Jackson, one of Prof. Helgeson's former students) indicates that in building most of the aluminosilicate data from mineral-mineral phase equilibrium data, kaolinite ($Al_2Si_2O_5(OH)_4$) was used as an anchor mineral for the Al_2O_3 component. Quartz (SiO_2) was used as an anchor mineral for the SiO_2 component. Helgeson et al. do not discuss the anchor mineral concept (as do for example Holland and Powell, 1985). Consequently, their discussion of how the data are developed is not as transparent as it might be. The quartz data are quite solid, derived from excellent and demonstrably repeatable calorimetric measurement. However, Helgeson et al. did not used calorimetric data for the Gibbs energy of kaolinite. Instead, they estimated the Gibbs energy from a solubility (*log K*) approach. The solubility data were taken from a natural system, in which groundwater was assumed to be in equilibrium with kaolinite. This is not an approach that most investigators today (if not then) would prefer. The resulting Gibbs energy for kaolinite was used to derive Gibbs energies for some other aluminosilicates, and so forth in a somewhat complex chain.

At the time of its publication, the Helgeson et al. (1978) paper was almost a model of transparency given the size of its scope. Unfortunately, the details of the kaolinite solubility calculation were not included. The sources of the field geochemical data are given, but there is no information regarding the thermodynamic data that were used as inputs to obtain the result. Such inputs would include the aqueous species considered and the Gibbs energies of H_2O, the aluminum ion (Al^{3+}), and aqueous silica ($SiO_{2(aq)}$, possibly represented as $H_4SiO_{4(aq)}$). The data for H_2O is probably not consequential, as the properties for this were well known at the time. There might be an issue with aluminum species and the Gibbs energy of Al^{3+}. However, there is now definitely an issue with $SiO_{2(aq)}$. Thus, we would propose to go back and apply modern data values for the aqueous components to the original geochemical data in a fresh calculation of the kaolinite Gibbs energy. This result could then be compared with more recent calorimetrically-based values. It would then be a relatively easy step to adjust the remaining Helgeson et al. (1978) aluminosilicate data.

The values of the entropies of the elements in their reference forms, and the sources thereof, used in the Helgeson et al. (1978) work are uncertain. Since this is an older work when such values were in something of a state of flux, possible associated uncertainties should be evaluated.

A potential alternative source of aluminosilicate data is the "Holland and Powell" database, represented in its most recent form by Holland and Powell (2011). This database series began in 1985 (Holland and Powell, 1985; Powell and Holland, 1985, 1988) and has been subsequently revised and expanded over the years (Holland and Powell, 1990; Holland and Powell, 1998). Overall, the body of work is quite impressive in scope and attention to detail. The Holland and Powell work mainly addresses minerals, much overlapping the older work by Helgeson et al. (1978). Like the older work, it addresses minerals other than aluminosilicates (a new part addressing sulfides is notable). In the 1998 version, it introduced data for some aqueous species, using the Anderson et al. (1991) model. This model is in essence an alternative to the Helgeson-Kirkham-Flowers model employed in SUPCRT92.

The Holland and Powell database appears to be highly regarded in the metamorphic petrology community. Its impact outside that community appears to have been limited by two factors: (a) publication in a journal (Journal of Metamorphic Petrology) that is perhaps not widely read outside that community, (b) the power and influence of the aqueous species part of the SUPCRT92 database, and (c) the rather large shadow over the geochemistry community cast by the late Prof. Helgeson.

Like the Helgeson et al. (1978) work, the Holland and Powell database is built mostly on mineral-mineral phase equilibrium data. Also like Helgeson et al., Holland and Powell assume that data needs for entropy, heat capacity, molar volume, thermal expansivity, and compressibility of minerals can largely be

addressed by the use of correlation algorithms. The conceptual underpinnings of both works are very similar. However, the Holland and Powell work is more a creation of the computer age in that the development of the data is run through a computer program, and a least-squares approach is employed in the calculation instead of a straight computation in which "best" input values are used. Given the present scope of the Holland and Powell work, and the fact that its development and revision have continued to the present day, incorporating many data unavailable to Helgeson et al. (1978), replacing the Helgeson et al. mineral data with the corresponding Holland and Powell data becomes an attractive notion.

We know there are some issues with the data from Helgeson et al. (1978). However, there may be some issues with the Holland and Powell database. Its application appears to be mainly in high temperature (>300°C) scenarios, which is also the space in which most of the mineral-mineral phase equilibrium measurements have taken place. It appears that adopting this database would require evaluating how well it does in lower-temperature scenarios (e.g., 25-200°C) that are more applicable to the UFDC. Holland and Powell do not seem to directly indicate their source of data for the entropies of the elements in their reference forms, although it appears from their papers that such data may be taken from Robie and Hemingway (1995) for later versions of the database, and from similar but older U.S. Geological Survey compilations for the earlier versions.

In their original database, Holland and Powell (1985) used corundum (Al_2O_3) as the anchor mineral for the Al_2O_3 component. They explicitly discuss the anchor mineral concept in this and other early papers (e.g., Powell and Holland, 1985). In their 1998 paper (Holland and Powell, 1998), they report abandoning the anchor concept in favor of including individual mineral data for a somewhat larger suite of minerals (letting their overall least-squares approach sort things out). We believe that this is perhaps better described as a *diffuse* anchor concept.

The merit of a least-squares approach over a "best values" approach is that (a) more data can be included and (b) there is more mathematical rigor. However, thermodynamics is often more about consistency than statistical rigor. Consequently, it is important that in using a least-squares approach (or any similar approach involving the use of more than a minimum of inputs) that the residuals be small. Otherwise, all that is guaranteed is a certain minimum of inconsistency. This is another point that needs to be looked at, particularly in the temperature range of interest to the UFDC. Another point is that UFDC needs include accurate solubility prediction. It may be difficult to get this when using a database that appears to have no solubility inputs.

In summary, the UFDC should examine the utility and potential future use of the Holland and Powell database. It does not seem advisable, however, to merely supplant the Helgeson et al. data with it until the issues raised here have been resolved. A path forward would include testing and attempted resolution with the Helgeson et al. data.

Lastly, we note that clays are aluminosilicates, and data for various aluminosilicates (including kaolinite, pyrophyllite, and muscovite) were used to calibrate the FY12 estimations of thermodynamic properties of smectites and some other sheet silicates. Any revision of the data that are input to the estimation process would require a revision of the estimation process and hence revised estimated data for the smectites and other affected sheet silicates.

4.9 Data Management Requirements

The types of thermodynamic data have been discussed previously. We are planning to continue most of the methods and formats used previously for YMP. For the product data files, we will follow the general EQ3/6 format. This consists of a human-readable text file on which log K data are given on a temperature grid. Underlying this will be a SUPCRT92 data file, which is also human-readable, and various types of Excel files that include standard methods for processing thermodynamic data into the desired log K grid form. One of the functions of the Excel files is to carry out the extrapolation of Gibbs energies to higher temperatures and pressures, and to compute the equilibrium constant values for the chosen chemical reactions. Another tool worth noting is the EQPT code from the EQ3/6 package, which is a database file preprocessor that runs many error checks. Basically, all the necessary data management tools run on a Windows PC, although most or all of them can be ported to other operating systems.

An EQ3/6 data file contains the following main elements: a title (descriptive text), a chemical elements block containing elemental symbols and atomic weights, a "superblock" of blocks for aqueous species, a superblock for pure mineral species, a superblock for gas species, a superblock for solid solutions, and a block or superblock of parameters for calculating the activity coefficients of aqueous species. Here a "superblock" is a sequence of data-blocks. An EQ3/6 data-block for an aqueous complex species is illustrated by the following one for $NpO_2(OH)_2^-$ (from the data file data0.ymp.R5):

```
+------------------------------------------------------------------------
NpO2(OH)2-
     sp.type =  aqueous
     [ ]
     charge  =  -1.0
****
     3 element(s):
      2.0000 H              1.0000 Np             4.0000 O
****
     4 species in reaction:
    -1.0000  NpO2(OH)2-                  -2.0000  H+
     1.0000  NpO2+                        2.0000  H2O
*
**** logK grid [0-25-60-100C @1bar; 150-200-250-300C @Psat-H2O]:
        25.5045   23.6147   21.4199   19.4099
        17.4475   15.9411   14.7957   13.9864
*
*    P-T extrapolation method: isocoulombic/isoelectric method
*    Data workup source: AqueousSpecies_j_TJW_1.xls
*    Reference-state data source: 01lem/nea
+------------------------------------------------------------------------
```

The information includes the species name, the electrical charge number, the chemical composition, the associated chemical reaction, the log K grid for that reaction, and information concerning the provenance of the data. A data-block for a mineral species is very similar, but includes a molar volume (V0PrTr) instead of an electrical charge number. The following example is also from data0.ymp.R5.

```
+------------------------------------------------------------------------
Np2O5
     sp.type =  solid
     [ ]
     V0PrTr  =      0.000 cm^3/mol [source:          ]
****
     2 element(s):
      2.0000 Np             5.0000 O
****
     4 species in reaction:
    -1.0000  Np2O5                       -2.0000  H+
     1.0000  H2O                          2.0000  NpO2+
```

```
*
**** logK grid [0-25-60-100C @1bar; 150-200-250-300C @Psat-H2O]:
         4.9214    3.7031    2.1757    0.6695
        -0.9387   -2.3319   -3.5852   -4.7609
*
*    P-T extrapolation method: Mixed Cp integration + SUPCRT calc
*    Data workup source: Minerals_j_PVB_Np.xls
*    Reference-state data source: 01lem/nea
+--------------------------------------------------------------------
```

A data-block for a gas species is very similar. For Pitzer interaction coefficients, a data-block exists for each species pair or triplet. The following example is the data-block for the Na^+-Cl^- pair from data0.ypf.R2.

```
+--------------------------------------------------------------
Na+                       Cl-
  alpha(1) = 2.0
  alpha(2) = 12.0
  beta(0):
    a1 = 7.45618073E-02
    a2 = -4.70789056E+02
    a3 = -1.85114134E+00
    a4 = 1.65564633E-03
  beta(1):
    a1 = 2.75240690E-01
    a2 = -5.21117635E+02
    a3 = -2.88035999E+00
    a4 = 4.71462791E-03
  beta(2):
    a1 = 0
    a2 = 0
    a3 = 0
    a4 = 0
  Cphi:
    a1 = 1.53693372E-03
    a2 = 4.80725476E+01
    a3 = 1.74679979E-01
    a4 = -1.56268596E-04
* Source: refit of 89Gre/Mol [FitPitzerNC_MX_NaCl.xls]
+--------------------------------------------------------------
```

Presently the EQ3/6 format does not include data-blocks for surface complexation model species, but ones analogous to those for aqueous or pure mineral species will be included for future UFD use. The same is true for ion exchange species.

We note that a conversion program was written on YMP to convert data0.ymp.R5 from EQ3/6 to PHREEQC format, and that some other conversion programs may exist or can be written. Thus, it should be possible to provide the data developed under UFD for use in other codes.

For YMP, the thermodynamic databases were documented under the Analysis/Model Report system and kept for download on the Technical Data Management system (TDMS). Generally, for each version of a data file, two data packages (“DTNs”) were prepared, one containing the data file itself, the other containing materials used to construct it (usually SUPCRT92 runs and Excel spreadsheets). In terms of download capability for UFDC, we envision something similar using the Sandia Sharepoint system or some other system to be developed.

Because of the general applicability of these databases in geochemistry and allied fields, it would be highly desirable to make them downloadable to the public on a web page. The advantage of this is that it would allow researchers working in areas like geothermal, underground carbon sequestration, and environmental management to exercise the data and provide useful feedback.

4.10 Data Management Records

The YMP Technical Data Management system (TDMS) had many good features for data management. The principal element was the organization of records into data packages ("DTNs"). The data package itself was organized into a zip file, providing data compression but more importantly a wrapper for the contained files. The data package was identified and named using a Data Tracking Number. Some sort of readme file was generally included. There was also a form involved in submitting a DTN containing such information as the DTN number, a title, a date, the names of the institution and individual submitting the package, some contact information, a list of keywords, and information regarding the use of data from other DTNs. The system then allowed tracking of other DTNs using a given DTN. One could also determine, with some but limited success, the Quality Assurance status of a DTN.

If one had the tracking number for a DTN, or could use the TDMS search facility with success, one could download the associated zip file and obtain the files and information therein. Unfortunately, the search capability was not very good. The problem was that, for subject matter, it was based on the key words predetermined by the DTN submitters, the quality and appropriateness of which was rather variable. For UFDC, an analog to such a system should be based as much as possible on the contents (assuming they are readable) of the data package, using something like the Google search engine. For non-readable files, such as certain types of binary files, a readme file should be included to support search capability and contain most of the information of the sort that YMP included on a DTN submittal form. For readable files, such information might be included in a data file. For example, readme information could be included on a readme worksheet in an Excel workbook.

For thermodynamic data base-related data packages, most of the files were Excel files and text-based data files such as data0.ymp.R5. This would continue for UFDC. One recent example of a file that would represent an appropriate record for thermodynamic database development is the Clays_TJW_2_Rev1r.xlsx workbook used for the clay mineral estimation work described earlier. Another is the Elemental_Entropies_Rev0i.xlsx workbook used to compile and compare values from "authoritative" sources for the entropies of the elements in their reference forms. Examples of data packages containing these files will be uploaded to the Sandia SharePoint site.

4.11 References

Aines. R.D., Wolery, T.J., Bourcier, W.L., Wolfe, T., and Haussmann, C. (2011) Fresh water generation from aquifer-pressured carbon storage: Feasibility of treating saline formation waters. GHGT-10. Energy Procedia 4, 2269-2276.

Anderson, G.M., Castet, S., Schott, J. and Mesmer, R.E. (1991) The density model for estimation of thermodynamic parameters of reactions at high temperatures and pressures. *Geochimica et Cosmochimica Acta, 55*, 1769–1779.

Barin, I. and Platzki, G. (1995) *Thermochemical Data of Pure Substances.* 3rd Edition. Two volumes. New York, New York: VCH Publishers.

Binnewies, M. and Milke, E. (1999) *Thermochemical Data of Elements and Compounds.* New York, New York: Wiley-VCH.

Berman, R.G. (1988) Internally-Consistent Thermodynamic Data for Minerals in the System Na_2O-K_2O-CaO-MgO-FeO-Fe_2O_3-Al_2O_3-SiO_2-TiO_2-CO_2. *Journal of Petrology, 29*, 445-522.

BSC (Bechtel SAIC Company) (2007a) *Qualification of Thermodynamic Data for Geochemical Modeling of Mineral–Water Interactions in Dilute Systems*. ANL-WIS-GS-000003 REV 01. Las Vegas, Nevada: Bechtel SAIC Company. DOC.20070619.0007.

BSC (Bechtel SAIC Company) (2007b) *In-Drift Precipitates/Salts Model*. ANL-EBS-MD-000045 REV 03. Las Vegas, Nevada: Bechtel SAIC Company. DOC.20070306.0037.

Cox, J.D.; Wagman, D.D.; and Medvedev, V.A., eds. (1989) *CODATA Key Values for Thermodynamics.* CODATA Series on Thermodynamic Values. New York, New York: Hemisphere Publishing Company.

Gamsjäger, H.; Bugajski, J.; Gajda, T.; Lemire, R.J.; and Preis, W. (2005) Chemical Thermodynamics of Nickel. Chemical Thermodynamics. Volume 6. New York, New York: Elsevier.

Garrels, R.M., and Christ, C.L. (1965) *Solutions, Minerals, and Equilibria*. Boston, Massachusetts: Jones and Bartlett Publishers

Greenberg, J.P. and Moller, N. (1989) "The Prediction of Mineral Solubilities in Natural Waters: A Chemical Equilibrium Model for the Na-K-Ca-Cl-SO_4-H_2O System to High Concentration from 0 to 250°C." *Geochimica et Cosmochimica Acta* 53, 2503–2518.

Grenthe, I.; Fuger, J.; Konings, R.J.M.; Lemire, R.J.; Muller, A.B.; Nguyen-Trung, C.; and Wanner, H. (1992) Chemical Thermodynamics of Uranium. Chemical Thermodynamics. Volume 1. Amsterdam, The Netherlands: North-Holland Publishing Company.

Guillaumont, R.; Fanghänel, T.; Fuger, J.; Grenthe, I.; Neck, V.; Palmer, D.A.; and Rand, M.H. (2003) Update on the Chemical Thermodynamics of Uranium, Neptunium, Plutonium, Americium and Technetium. Mompean, F.J.; Illemassene, M.; Domenech-Orti, C.; and Ben Said, K., eds. Chemical Thermodynamics. Volume 5. Amsterdam, The Netherlands: Elsevier.

Helgeson, H.C. (1969) Thermodynamics of Hydrothermal Systems at Elevated Temperatures and Pressures. American Journal of Science, 267(6), 729-804.

Helgeson, H.C.; Delany, J.M.; Nesbitt, H.W.; and Bird, D.K. (1978) Summary and Critique of the Thermodynamic Properties of Rock Forming Minerals. *American Journal of Science*, *278-A.* New Haven, Connecticut: Yale University, Kline Geology Laboratory.

Holland, T.J.B. (1989) Dependence of Entropy on Volume for Silicate and Oxide Minerals: A Review and a Predictive Model. *American Mineralogist, 74*, 5-13.

Holland, T.J.B., and Powell, R. (1985) An Internally Consistent Thermodynamic Dataset with Uncertainties and Correlations: 2. Data and Results. *Journal of Metamorphic Geology, 3*, 343-370. [The authors refer to this paper as "DS2".]

Holland, T.J.B., and Powell, R. (1990) An Enlarged and Updated Internally Consistent Thermodynamic Dataset with Uncertainties and Correlations: The System K_2O-Na_2O-CaO-MgO-MnO-FeO-

Fe_2O_3-Al_2O_3-TiO_2-SiO_2-C-H_2-O_2. *Journal of Metamorphic Geology, 8*, 89-124. [The authors (cf. Powell and Holland, 1993) refer to this paper as "DS4".]

Holland, T.J.B., and Powell, R. (1998) An Internally Consistent Thermodynamic Dataset for Phases of Petrological Interest. *Journal of Metamorphic Geology, 16*, 309-343.

Holland, T.J.B., and Powell, R. (2011) An Improved and Extended Consistent Thermodynamic Dataset for Phases of Petrological Interest, Involving a New Equation of State for Solids. *Journal of Metamorphic Geology, 29*, 333-383.

Hummel, W.; Berner, U.; Curti, E.; Pearson, F.J.; and Thoenen, T. (2002) Nagra/PSI Chemical Thermodynamic Data Base 01/01. Parkland, Florida: Universal Publishers.

Johnson, J.W.; Oelkers, E.H.; and Helgeson, H.C. (1992) SUPCRT92: A Software Package for Calculating the Standard Molal Thermodynamic Properties of Minerals, Gases, Aqueous Species, and Reactions from 1 to 5000 Bar and 0 to 1000°C. *Computers & Geosciences, 18*, (7), 899-947. New York, New York: Pergamon Press.

Lemire, R.J., Fuger, J., Nitsche, H., Potter, P., Rand, M.H., Rydberg, J., Spahiu, K., Sullivan, J.C., Ullman, W.J., Vitorge, P., and Wannter, H. (2001) Chemical Thermodynamics of Neptunium and Plutonium. Chemical Thermodynamics. Volume 4. New York, New York: Elsevier.

McBride, B.J., Gordon, S., and Reno, M.A. (2001) Thermodynamic Data for Fifty Reference Elements. NASA Technical Paper 3287/REV1. National Aeronautics and Space Administration.

Olin, A.; Noläng, B.; Öhman, L-O.; Osadchii, E.G.; and Rosén, E. (2005) Chemical Thermodynamics of Selenium. Mompean, F.J.; Perrone, J.; and Illemassène, M., eds. Chemical Thermodynamics. Volume 7. Amsterdam, The Netherlands: Elsevier.

Pabalan, R.T. and Pitzer, K.S. (1987) Thermodynamics of Concentrated Electrolyte Mixtures and the Prediction of Mineral Solubilities to High Temperatures for Mixtures in the System Na-K-Mg-Cl-SO_4-OH-H_2O. *Geochimica et Cosmochimica Acta*, 51(9), 2429-2443

Parker, V.B. and Khodakovskii, I.L. (1995) Thermodynamic Properties of the Aqueous Ions (2+ and 3+) of Iron and the Key Compounds of Iron." *Journal of Physical and Chemical Reference Data, 24*, (5), 1699-1745. Washington, D.C.: American Chemical Society.

Pitzer, K.S. (1991) Ion Interaction Approach: Theory and Data Correlation. Chapter 3 of *Activity Coefficients in Electrolyte Solutions*. 2nd Edition. Pitzer, K.S.,ed. Boca Raton, Florida: CRC Press.

Powell, R., and Holland, T.J.B. (1985a) An Internally Consistent Thermodynamic Dataset with Uncertainties and Correlations: 1. Methods and a Worked Example. *Journal of Metamorphic Geology, 3*, 327-342. [The authors refer to this paper as "DS1".]

Powell, R., and Holland, T.J.B. (1985b) An Internally Consistent Thermodynamic Dataset with Uncertainties and Correlations: 3. Applications to Geobarometry, Worked Examples and a Computer Program. *Journal of Metamorphic Geology, 6*, 173-204. [The authors refer to this paper as "DS3".]

Powell, R., and Holland, T.J.B. (1993a) The Applicability of Least Squares in the Extraction of Thermodynamic Data from Experimentally Bracketed Mineral Equilibria. *American Mineralogist, 78*, 107-112.

Powell, R., and Holland, T.J.B. (1993b) On the Formulation of Simple Mixing Models for Complex Phases. *American Mineralogist, 78*, 1174-1180.

Powell, R., and Holland, T.J.B. (2006) Mineral Activity-Composition Relations and Petrological Calculations Involving Cation Eqipartition on Multisite Minerals: A Logical Inconsistency. *Journal of Metamorphic Geology, 24*, 851-861.

Ransom, B. and Helgeson, H.C. (1993) Compositional End Members and Thermodynamic Components of Illite and Dioctahedral Aluminous Smectite Solid Solutions. *Clays and Clay Minerals* 41(5), 537-550.

Ransom, B. and Helgeson, H.C. (1994a) Estimation of the Standard Molal Heat Capacities, Entropies, and Volumes of 2:1 Clay Minerals. *Geochimica et Cosmochimica Acta,* 58 (21), 4537-4547.

Ransom, B. and Helgeson, H.C. (1994b) A Chemical and Thermodynamic Model o f Aluminous Dioctahedral 2:1 Layer Clay Minerals in Diagenetic Processes: Regular Solution Representation of Interlayer Dehydration in Smectite." *American Journal of Science* 294, 449-484.

Ransom, B. and Helgeson, H.C. (1995) A Chemical and Thermodynamic Model of Aluminous Dioctahedral 2:1 Layer Clay Minerals in Diagenetic Processes: Dehydration of Dioctahedral Aluminous Smectite as a Function of Temperature and Depth in Sedimentary Basins. *American Journal of Science* 295, 245-281.

Rard, J.A., and Wolery, T.J. (2007) The Standard Chemical-Thermodynamic Properties of Phosphorus and Some of its Key Compounds and Aqueous Species: An Evaluation of Differences between the Previous Recommendations of NBS/NIST and CODATA, Journal of Solution Chemistry, v. 36, p. 1585-1599.

Rard, J.A.; Rand, M.H.; Anderegg, G.; and Wanner, H. (1999) Chemical Thermodynamics of Technetium. Sandino, M.C.A., and Östhols, E., eds. Chemical Thermodynamics 3. Amsterdam, The Netherlands: Elsevier.

Robie, R.A., and Hemingway, B.S. (1995) *Thermodynamic Properties of Minerals and Related Substances at 298.15 K and 1 Bar (10^5 Pascals) Pressure and at Higher Temperatures.* Bulletin 2131. Reston, Virginia: U.S. Geological Survey.

Silva, R.J.; Bidoglio, G.; Rand, M.H.; Robouch, P.B.; Wanner, H.; and Puigdomenech, I. (1995) Chemical Thermodynamics of Americium. Chemical Thermodynamics. Volume 2. Amsterdam, The Netherlands: Elsevier.

Tardy, Y., and Garrels, R.M. (1974) A Method of Estimating the Gibbs Energies of Formation of Layer Silicates. *Geochimica et Cosmochimica Acta* 38(7), 1101-1116.

Tardy, Y., and Duplay, J. (1992) A Method of Estimating the Gibbs Free Energies of Formation of Hydrated and Dehydrated Clay Minerals. *Geochimica et Cosmochimica Acta* 56(16), 3007-3029

Vieillard, P. (1994a) Prediction of Enthalpy of Formation Based on Refined Crystal Structures of Multisite Compounds: Part 1. Theories and Examples. *Geochimica et Cosmochimica Acta* 58(19), 4049-4063.

Vieillard, P. (1994b) Prediction of Enthalpy of Formation Based on Refined Crystal Structures of Multisite Compounds: Part 2. Application to Minerals Belonging to the System Li_2O-Na_2O-K_2O-BeO-MgO-CaO-MnO-FeO-Fe_2O_3-Al_2O_3-SiO_2-H_2O. Results and Discussion. *Geochimica et Cosmochimica Acta,* 58(19), 4065-4107.

Vieillard, P. (2000) A New Method for the Prediction of Gibbs Free Energies of Formation of Hydrated Clay Minerals Based on the Electronegativity Scale. *Clay and Clay Minerals,* 48(4), 459-473.

Wagman, D.D.; Evans, W.H.; Parker, V.B.; Schumm, R.H.; Halow, I.; Bailey, S.M.; Churney, K.L.; and Nuttall, R.L. (1982) The NBS Tables of Chemical Thermodynamic Properties, Selected Values for Inorganic and C_1 and C_2 Organic Substances in SI Units. *Journal of Physical and Chemical Reference Data, 11,* (Supplement No. 2), 2-276 - 2-282. Washington, D.C.: American Chemical Society.

Wagman, D.D.; Evans, W.H.; Parker, V.B.; Schumm, R.H.; Halow, I.; Bailey, S.M.; Churney, K.L.; and Nuttall, R.L. (1989) Erratum: The NBS Tables of Chemical Thermodynamic Properties, Selected Values for Inorganic and C_1 and C_2 Organic Substances in SI Units. *Journal of Physical and Chemical Reference Data, 18,* (4), 2-276 - 2-282, 1807-1812. Washington, D.C.: American Chemical Society.

Wang, Y., Simpson, M., Painter, S., Liu, H.-H., and Kersting, A.B. (2011) *Natural System Evaluation and Tool Development – FY11 Progress Report*: Fuel Cycle Research and Development. Document FCRD-USED-2011-000223 (originated from Sandia National Laboratories).

Wolery, T.J., and Sutton, M. (2011) *Generic Natural Systems Evaluation - Thermodynamic Database Development and Data Management*. LLNL-TR-500113, Lawrence Livermore National Laboratory, Livermore, CA. [LLNL input to SNL milestone M41UF034002: *Initiating Natural System Database Design*]

Wolery, T.J., and Carroll, S.A. (2010) CO_2-Rock Interactions in EGS-CO_2: New Zealand TVZ Geothermal Systems as a Natural Analog. GRC Transactions 34, 729-736.

Wolery, T.J. (2012) *FY12 Thermodynamic Properties Report: Thermodynamic Database Development, With Emphasis On Complex Clay Minerals*. LLNL-TR-554331, Lawrence Livermore National Laboratory, Livermore, CA. [milestone M4FT-12LL0806041]

Xiong, Y.-L. (2005) Release of FMT-050405.CHEMDAT. E-mail to J.F. Kanney and J.J. Long, April 5, 2005. Carlsbad, NM: Sandia National Laboratories. ERMS 539304.

5.0 Compilation of Key Technical Data for the Evaluation of Generic Disposal Environments

5.1 Introduction

As mentioned in Section 1.0, the Used Fuel Disposition (UFD) Program is currently considering four generic waste disposal environments: granite, shale/clay, salt, and deep borehole in crystalline rocks. Development of a representative set of material properties for each generic disposal environment is an important part of the UFD natural system evaluation effort, because these data will provide needed constraints on the physical and chemical conditions for the on-going or planned UFD laboratory and field tests. Since the salt repository environment has now been considered in a separate work package, we here focus ourselves exclusively on granite and clay disposal environments. Note that the data obtained for the granite environment may also applicable to the deep borehole disposal option.

In FY11, we developed an integration plan for UFD data management, especially for the technical data that will be collected and used to support UFD generic repository studies (Wang, 2011). As an initial step of the implementation of this plan, in FY12, we have set up a SharePoint site for temporally archiving the technical data to be collected. The data documented in the previous section and this section are among the first batches of data that will be uploaded to the SharePoint site and will be used as example data for developing an appropriate data model for the development of an integrated UFD technical database. This database will include key technical data to support natural barrier system evaluation and programmatic decisions. Furthermore, the data collected in this section will provide a technical basis for constraining model input parameters for a total system performance assessment of a generic repository.

5.2 Data for THMC Modeling of the Near Field of a Clay Repository

Modeling of thermal-hydrological-mechanical-chemical (THMC) processes requires extensive parameter inputs to support process relationships for thermal, hydrological, mechanical, and chemical processes, as well as some additional parameters to support process coupling. The parameters needed depend in part on the process models to be used. Therefore, a discussion of the models that are expected to be used is in order.

Data are provided for two argillaceous formations that have been intensively investigated for nuclear waste disposal: the Opalinus Clay at Mont Terri, Switzerland and the Boom Clay at Mol, Belgium. The Opalinus Clay is an indurated, stiff clay whereas the Boom Clay is a soft, plastic clay formation. Note that a range of values is presented where available but for some parameters only a best estimate or average value is available. Many of the parameters are also functions of thermodynamic conditions (e.g., temperature, pressures, composition) however these functional dependencies are not quantified in this report. Instead, the parameters are mainly reported at ambient conditions for the underground laboratories, or in some cases at generic standard conditions. In addition, rock and fluid parameters will generally be spatially variable, which is not addressed in this report. Spatial variability may require representing these parameters as a function of position.

5.2.1 Hydrologic Model

Hydrologic parameters for the Opalinus Clay and Boom Clay are given in Tables 5-1 through 5-3. The near-field, where THMC processes are most critical, also must consider the fact that an argillaceous host rock may have a fracture network within the disturbed rock zone (DRZ). Whether a dual-continuum approach or a discrete fracture network approach is used, hydrological properties are needed for the fractures and for the rock (matrix). The near-field rock will also likely be unsaturated for some time period following repository closure. Therefore, unsaturated flow parameters are also needed. The parameters in Table 5-2 are specifically for a dual-continuum approach. This is used now because specific parameters for a discrete fracture approach are still in development. The choice mainly impacts fracture geometry parameterization, which for a discrete fracture model would have additional parameters. Fracture geometry in the continuum model is defined by the fracture porosity and interface area per unit volume. A non-Newtonian flow parameter, as described in Liu et al. (2011), is also included in Table 5-1 however this parameter has not been evaluated for flow data from the Opalinus Clay or Boom Clay. Because hydrologic parameters can be, and generally are, spatially variable, the database needs to be able to accommodate spatial dependence of the parameters. For the Opalinus clay, bedding planes result in anisotropic behavior represented by parameterization parallel and perpendicular to bedding, such as hydraulic conductivity in Table 5-1. This anisotropy is less pronounced for the Boom Clay (Bertrand, et al., 2009, section 4.3.1).

Note that only limited fracture data is currently available for the Opalinus Clay and the Boom Clay and these data pertain to the DRZ around repository excavations. There are indications from the geologic record that natural fractures and flow processes through natural fracture pathways in argillaceous rock is possible (Cosgrove 2001; Arnould 2006). However, this information also indicates that fractures and associated flow processes are transient and that any record of fractures or flow through fractures can be difficult to identify. Hydrological parameters for two-phase flow in fractures are not available for the Opalinus Clay and Boom Clay. These parameters include the same parameter types as given in Table 5-2 for rock plus the active fracture parameter that quantifies preferential flow effects in fracture networks (Liu et al., 1998).

Table 5-1. Hydrologic: Single-phase properties for rock matrix

Property	Opalinus Clay	Boom Clay
Total porosity (HTO) (-)	0.14 – 0.247[1]	0.30 – 0.40[2]
Geochemical porosity (Cl^-, I^-) (-)	0.08 – 0.10[1]	0.12 – 0.25[3]
Grain density (kg-m^{-3})	2700 – 2770[1]	2600 – 2670[4]
Hydraulic conductivity parallel to bedding (m-s^{-1})	2e – 13[1]	2e-12 – 5e-12[2]
Hydraulic conductivity perpendicular to bedding (m-s^{-1})	4e – 14[1]	
Specific Storativity (m^{-1})	1e-7 – 1e-4[1]	7e-5 – 2e-4[8]
Non-Newtonian (non-Darcy) flow parameter[5]	NA	NA
Dispersivity (m)	0.12 – 0.2[6]	0.004[7]

1. Bossart (2012, Pages 4-17 and 4-19); 2. Shaw (2010, Table 1) 3. ONDRAF/NIRAS (2001, Section 11.3.8.2.3) and Aertsens et al. (2003, p. 433); 4. Shaw (2010, Table 1) and Aertsens et al. (2003, p. 432); 5. Liu et al. (2011, Section 2.2); 6. Zheng et al. (2007, p. 369) and De Windt et al. (2004, Table 1); 7. Martens et al. (2008, Table 4); 8. Based on Bernier and Neerdael (1996) value of 0.95 m^2/yr hydraulic diffusivity, with specific storativity computed from hydraulic conductivity divided by hydraulic diffusivity.
NA = not available

Table 5-2. Hydrologic: Two-phase properties for rock matrix

Property	Opalinus Clay	Boom Clay
rock van Genuchten pore size distribution index, m (-)	0.33 – 0.5[2]	0.3[1]
rock van Genuchten capillary strength α (Pa^{-1})	4.8e-8 – 2.0e-7[2]	2.9e-7[1]
rock residual aqueous saturation (-)	0 – 50%[2]	20%[3]
rock residual gas saturation (-)	0 – 5%[2]	17.4%[3]
aqueous-gas interfacial tension (Pa-m) (at natural temperature – see Table 4)	0.074[4]	0.073[4]
aqueous-gas-mineral contact angle (°)	NA	NA

1. Shaw et al. (2010); 2. Johnson (2004, p. 44); 3. Dymitrowska et al. (2009, p. 20, Table 3); 4. Batchelor (1967, Appendix1)
NA = not available

Table 5-3. Hydrologic: Single-phase properties for fractures

Property	Opalinus Clay	Boom Clay
DRZ fracture porosity (porosity of fracture domain) (-)	NA	NA
DRZ fracture grain density ($kg\text{-}m^{-3}$)	NA	NA
DRZ fracture conductivity maximum ($m\text{-}s^{-1}$)	2e-8 – 2e-5[1]	2e-11 – 5e-11[2]
DRZ fracture interface area per unit volume (m^{-1})	NA	NA
Dispersivity (m)	NA	NA

1. Bossart (2004, p. 437); 2. Yu et al. (2011, p. 31 – indicates one order of magnitude damage, which has been applied to matrix conductivity values from Table 1)
NA = not available

Tables 5-4 and 5-5 provide physical fluid property parameters relevant to natural conditions for the Opalinus Clay and Boom Clay. The database needs to be able to accommodate temperature and, in some cases, pressure and compositional dependence of these parameters.

Table 5-4. Aqueous Phase: Physical Properties and Conditions

Property	Opalinus Clay	Boom Clay
natural temperature (°C)	13 – 15[1]	16[2]
viscosity (Pa-s) (at natural temperature)	1.14e-3 – 1.20e-3[3]	1.11e-3[3]
density ($kg\text{-}m^{-3}$) (at natural temperature and TDS level – see Table 10)	1013[4]	1000[4]
dielectric constant (relative permittivity) (-)(at natural temperature)	78[5]	82[5]

1. Degueldre et al. (2003, Table 4); 2. DeCraen et al. (2004, Table 1-1); 3. Batchelor (1967, Appendix1) ; 4.Fischer et al. (1979, Appendix 1) ; 5. Klein and Swift (1977, Figure 3)

Table 5-5. Gas phase – Moist Air (100% relative humidity): Physical Properties

Property	Opalinus Clay	Boom Clay
viscosity (Pa-s) (at natural temperature – see Table 4 – and atmospheric pressure)	1.8e-5[1]	1.8e-5[1]
density (kg-m^{-3}) (at natural temperature – see Table 4 – and atmospheric pressure)	1.2[1]	1.2[1]

1. Tsilingiris (2008, Figures 1 and 2)

5.2.2 Mechanical Model

Mechanical models for THMC processes in clay host rock are currently based on elasticity theory for rock, supplemented with coupling terms to account for water saturation and aqueous compositional effects on swelling clays. Parameter values for the Opalinus Clay and the Boom Clay are provided in Tables 5-6 through 5-9. The elasticity theory has also been expanded upon for a dual-domain situation, as described in Liu et al., (2010; 2011), in which there is a "hard part" that only experiences small deformations and a "soft part" that can experience large deformations. Conceptually, the "hard part" and "soft part" roughly correspond to the rock matrix and fractures, respectively. The parameters for the mechanical model and for coupling with hydrological conditions are given in Table 5-8. Because rock mechanical parameters can be, and generally are, spatially variable, the database needs to be able to accommodate spatial dependence of the parameters. For the Opalinus clay, bedding planes result in anisotropic mechanical properties represented by parameterization parallel and perpendicular to bedding. This anisotropy is not as pronounced for the Boom Clay.

Table 5-6. Mechanical: Elastic properties

Property	Opalinus Clay	Boom Clay
Young's modulus – perpendicular to bedding (MPa)	2100 – 3500[1]	300 – 400[2]
Young's modulus – parallel to bedding (MPa)	6300 – 8100[1]	
Poisson's ratio – perpendicular to bedding	0.28 – 0.38[1]	0.125 – 0.45[2]
Poisson's ratio – parallel to bedding	0.16 – 0.32[1]	
Shear Modulus (MPa)	800 – 1600[1]	40[3]
Uniaxial tensile strength perpendicular to bedding (MPa)	1[1]	0.1[3**]
Uniaxial tensile strength parallel to bedding (MPa)	2[1]	
Uniaxial compressive strength perpendicular to bedding (MPa)	23.1 – 28.1[1]	2.2[3**]
Uniaxial compressive strength parallel to bedding (MPa)	4.0 – 17.0[1]	
Young's modulus soft part (MPa)	0.6 – 3.6[4]	NA
Young's modulus hard part (MPa)	2080 – 3345[4]	NA
Volume fraction soft part (-)*	0.00036 – 0.0048[4]	NA
Volume fraction hard part (-)*	0.9952 – 0.99964[4]	NA

1. Bossart (2012, p. 4-4); 2. Shaw (2010, Table 1); 3. Dehandshutter et al. (2005, Table 1); 4. Liu et al. (2011, Table 2-1);
NA = not available

*Note: volume fractions of hard and soft parts add to 1.

** Marked as questionable by Dehandshutter et al. (2005, Table 1).

Table 5-7. Mechanical: Plasticity

Property	Opalinus Clay	Boom Clay
Plastic limit (%)	21 – 25[1]	22 – 28[2]
Liquid limit (%)	33 – 43[1]	59 – 83[2]

1. Martin and Lanyon (2003, Table 1); 2. Shaw (2010, Table 1)

Table 5-8. Mechanical: Mohr-Coulomb-Griffith Failure and Moisture Coupling Properties

Property	Opalinus Clay	Boom Clay
Cohesive strength (MPa)	2.2 – 5.5[1]	0.175 – 0.300[2]
Friction angle (°)	24 – 26[1]	18[2]
Yield stress (MPa)	20 – 22[5]	NA
Swelling pressure (MPa)*	5.5[4]	0.6[3]
Swelling strain (axial, %)*	7.5[4]	5 – 10[3]
Swelling strain (radial, %)*	2[4]	NA
Swelling strain (volumetric, %)*	11.5[4]	NA
Swelling pressure perpendicular to bedding (MPa)**	1.2[1]	NA
Swelling pressure parallel to bedding (MPa)**	0.5[1]	NA
Swelling strain perpendicular to bedding (%)**	5 – 9[1]	NA
Swelling strain parallel to bedding (%)**	0.5 – 2.0[1]	NA

1. Bossart (2012, p. 4-21 to 4-23); 2. Dehandshutter et al. (2005, Table 1); 3. Bernier et al. (1997, Figures 14 and 15). 4. Zhang et al. (2010, p. 48-49); 5. Horseman et al. (2005, Figure 20)
NA = not available

*Note that the swelling tests reported by Bernier et al. (1997) for the Boom Clay were conducted by controlling relative humidity, which ranged over a complete wetting-drying cycle. Since water was introduced as a vapor, it would also be free of dissolved constituents. Therefore, the swelling data for the Boom Clay represent swelling caused by altering water composition and water content. The swelling data reported by Zhang et al. (2010) for the Opalinus Clay also were measured through controlling capillary pressure through relative humidity and are comparable with those reported by Bernier et al. (1997) for the Boom Clay.

** Note that the swelling tests for the Opalinus Clay reported by Bossart (2012, page 4-23) are conducted using IRSM standard methods. Undisturbed samples that have their native water content are used for the test (Madsen, 1999, page 294). These samples are immersed in distilled water to determine the swelling pressure for confined conditions or swelling strain if unconfined. Because undisturbed samples should be saturated, this test provides information on the effects of changing aqueous composition on swelling stress and strain. It is not clear from the presentation, however, whether swelling strain represents volumetric, axial, or radial strain.

Table 5-9. Mechanical: In-Situ Conditions

Property	Opalinus Clay	Boom Clay
Maximum stress (MPa)	6 – 7[1]	4.5[2]
Maximum stress direction (trend, plunge)(°)	210, 70[1]	vertical
Intermediate stress (MPa)	4 – 5[1]	1.4 – 4.1[2]
Intermediate stress direction (trend, plunge)(°)	320, 10[1]	horizontal
Minimum stress (MPa)	0.6 – 2[1]	1.4 – 4.1[2]
Minimum stress direction (trend, plunge)(°)	50, 15[1]	horizontal
Pore pressure (MPa)	1 – 2[1]	2.2[2]
Overconsolidation ratio (OCR) (-)	2.5 – 4.8[5,6]	1 – 2.4[3,4]

1. Martin and Lanyon (2003, p. 1085 and 1087); 2. Bernier et al. (2007, p. 230); 3. Mertens et al. (2003, p. 310) - The minimum OCR for the Boom Clay is an apparent OCR based on the current overburden being the same as the maximum; 4. Shaw (2010, Table 3). 5. Lemy et al. (2006, p. 3) 6. The maximum OCR for the Opalinus Clay is an apparent OCR based on a current overburden of 280 m and a maximum overburden of 1350 m (Bossart, 2012, p. 4-11).

5.2.3 Chemical Model

The current chemical model involves aqueous complexation, cation exchange, and mineral precipitation/dissolution. Other site-specific information includes aqueous chemical composition, specific surface areas, and diffusion and sorption parameters. The parameters for chemical processes are given in Tables 5-10 through 5-17.

Table 5-10. Aqueous: Chemical Composition

Property	Opalinus Clay	Boom Clay
pH (–log[H^+])	7.3 – 7.96[1]	8.5[2]
Eh (mV)	-227[1]	-274[2]
Ionic strength (mol-L^{-1})	0.350[1]	0.016[2]
Mineralization TDS (total dissolved solids) (mg-L^{-1})	18,296[1]	935[3]
Alkalinity (mEq-L^{-1})	0.749 –2.5[1]	15.12[2]
Total organic carbon (TOC) (mg-L^{-1} as carbon)	14[1]	150[4]
Total inorganic carbon (TIC) (mg-L^{-1} as carbon)	8.5[1]	181.3[2]
pCO_2 (log bars)	-3.58 to -2.69[1]	-2.62[2]
Ca (mg-L^{-1})	609.0[1]	2.0[2]
Li (mg-L^{-1})	0.4[1]	NA
Na (mg-L^{-1})	5640[1]	359[2]
Mg (mg-L^{-1})	415.0[1]	1.6[2]
K (mg-L^{-1})	43.4[1]	7.2[2]
Fe (mg-L^{-1})	0.14[1]	0.2[2]
Al (mg-L^{-1})	0.013[1]	0.6e-3[2]
Si (mg-L^{-1})	1.61[1]	3.4[2]
NH_4 (mg-L^{-1})	10.2[1]	NA
Ba (mg-L^{-1})	0.019[1]	NA
B (mg-L^{-1})	1.61[1]	NA

Mn (mg-L^{-1})	0.346[1]	NA
Sr (mg-L^{-1})	35.00[1]	NA
Cl (mg-L^{-1})	10,170[1]	26[2]
SO_4 (mg-L^{-1})	1,320[1]	2.2[2]
Br (mg-L^{-1})	35.0[1]	0.6[4]
HCO_3 (mg-L^{-1})	NA	878.9[2]
I (mg-L^{-1})	2.2[1]	NA
NO_3 (mg-L^{-1})	10.0[1]	NA
NO_2 (mg-L^{-1})	2.0[1]	NA
F (mg-L^{-1})	0.75[1]	3[4]

1. Bossart (2012, p. 4-14 to 4-16); 2. Li et al. (2007, Table 4.2); 3. DeCraen (2006, p. 7); 4. DeCraen et al. (2006, Table 3)
NA = not available

A database of thermodynamic parameters that include equilibrium constants, molecular weights of aqueous species and minerals, parameters for calculating activity coefficients, molar volumes of minerals is required. A standard database for chemical equilibria is the EQ3/6V7.2b database. This information is too voluminous to present here, so the general citation to Wolery (1992) is used. This information is site-specific to the extent that the speciation, compositions, and thermodynamic conditions that are applicable to the Opalinus Clay and Boom Clay are adequately represented.

Table 5-11. Chemical Reaction: Chemical Equilibrium Parameters

Property	Opalinus Clay	Boom Clay
Equilibrium constants (dimensions are reaction dependent)	Wolery (1992)	Wolery (1992)

Chemical kinetic parameters for a model of the Opalinus Clay are given in Liu et al. (2011, Table 4-7) and is reproduced here in Table 5-12. Similar parameters should also apply to the Boom Clay, but specific information for this formation is not available.

Table 5-12. Chemical Reaction: Chemical Kinetic Parameters for Opalinus Clay, (Liu et al., 2011, table 4-7)

Mineral	A (cm^2-g^{-1})	Parameters for Kinetic Rate Law							
		Neutral Mechanism		Acid Mechanism			Base Mechanism		
		k_{25} (mol-$m^{-2}s^{-1}$)	E_a (KJ-mol^{-1})	k_{25} (mol-$m^{-2}s^{-1}$)	E_a (KJ-mol^{-1})	$n(H^+)$	k_{25} (mol-$m^{-2}s^{-1}$)	E_a (KJ-mol^{-1})	$n(H^+)$
***Primary*:**									
Calcite	Assumed at equilibrium								
Quartz	9.8	1.023×10^{-14}	87.7						
K-feldspar	9.8	3.89×10^{-13}	38	8.71×10^{-11}	51.7	0.5	6.31×10^{-12}	94.1	-0.823
Kaolinite	1.95×10^{5}	6.91×10^{-14}	22.2	4.89×10^{-12}	65.9	0.777	8.91×10^{-18}	17.9	-0.472
Illite	6.68×10^{5}	1.66×10^{-13}	35	1.05×10^{-11}	23.6	0.34	3.02×10^{-17}	58.9	-0.4
Chlorite	9.8	3.02×10^{-13}	88	7.76×10^{-12}	88	0.5			
Dolomite	12.9	2.52×10^{-12}	62.76	2.34×10^{-7}	43.54	1			
Ankerite	9.8	1.26×10^{-9}	62.76	6.46×10^{-4}	36.1	0.5			
Smectite-Na	5.64×10^{5}	1.66×10^{-13}	35	1.05×10^{-11}	23.6	0.34	3.02×10^{-17}	58.9	-0.4
Na-montmorillonite	5.64×10^{5}	1.66×10^{-13}	35	1.05×10^{-11}	23.6	0.34	3.02×10^{-17}	58.9	-0.4

Note: k_{25} = kinetic rate parameter at 25° C, E_a = activation energy, $n(H^+)$ = power term (Xu et al., 2006, Table 8)

Additional parameters are needed if transport processes involving dissolved species are to be included in the model. These parameters relate to diffusion and dispersion phenomena and to sorption interactions between aqueous species and mineral surfaces. The database needs to be able to accommodate spatial dependence of these parameters.

Table 5-13. Aqueous: Diffusion Coefficient

Property	Opalinus Clay	Boom Clay
H(HTO) (m^2-s^{-1}) parallel to bedding	4e-11 – 1e-10[1]	1.1e-10 – 5.5e-10[2]
H(HTO) (m^2-s^{-1}) perpendicular to bedding	1e-11 – 2e-11[1]	
H(HTO) accessible porosity (%)	15 – 17[1]	34 – 40[2]
I^- (m^2-s^{-1}) parallel to bedding	8.0e-12 – 3.0e-11[1]	9.1e-11 – 5.2e-10[2]
I^- (m^2-s^{-1}) perpendicular to bedding	2.4e-12 – 4.2e-12 [1]	
I^- accessible porosity (%)	5 – 15[1]	14 – 18[2]
Cl^- (m^2-s^{-1}) parallel to bedding	1.8e-11 – 6.8e-11[1]	NA
Cl^- (m^2-s^{-1}) perpendicular to bedding	4.8e-12[1]	NA
Cl^- accessible porosity (%)	6 – 12[1]	NA
Br^- (m^2-s^{-1}) parallel to bedding	1.7e-11 – 4.5e-11[1]	NA
Br^- accessible porosity (%)	10 – 15[1]	NA
Cs^+ (m^2-s^{-1}) parallel to bedding	2.6e-10 – 2.7e-10[1]	NA
Cs^+ accessible porosity (%)	17 – 18[1]	NA
$^{22}Na^+$ (m^2-s^{-1}) parallel to bedding	7.2e-11[1]	NA
$^{22}Na^+$ accessible porosity (%)	17 – 18[1]	NA
$^{85}Sr^{2+}$(m^2-s^{-1}) parallel to bedding	6.5e-11 – 7.0e-11[1]	NA
$^{85}Sr^{2+}$ accessible porosity (%)	15 – 17[1]	NA
$^{60}Co^{2+}$ (m^2-s^{-1}) parallel to bedding	6.0e-11[1]	NA
$^{60}Co^{2+}$ accessible porosity (%)	15[1]	NA
$^{6}Li^+$ (m^2-s^{-1}) parallel to bedding	7.0e-11[1]	NA
$^{6}Li^+$ accessible porosity (%)	16[1]	NA
SeO_4^{2-} (m^2-s^{-1})	NA	1.5e-11 – 7.3e-11[3]
SeO_4^{2-} accessible porosity (%)	NA	5 – 18[3]
HSe^- (m^2-s^{-1})	NA	8e-11 – 1.7e-10[3]
HSe^- accessible porosity (%)	NA	12 – 18[3]

1. Bossart (2012, p. 4-19 to 4-20); 2. Aertsens et al. (2004, p. 37); 3. De Cannière et al. (2010, Table 5.3-1)
NA = not available

Table 5-14. Mineralogical: Composition

Property	Opalinus Clay	Boom Clay
Total clay (% total dry weight)	28 – 93[1]	30 – 60[2]
Illite (% total dry weight)	15.0 – 30.0[1]	10 – 45[2]
Chlorite (% total dry weight)	3.0 – 18.0[1]	0 – 5[2]
Kaolinite (% total dry weight)	15.0 – 37.0[1]	5 – 20[2]
Illite/smectite ML (% total dry weight)	5.0 – 20.0[1]	10 – 30[2]
Chlorite/smectite ML (% total dry weight)	NA	0 – 5[2]
Quartz (% total dry weight)	10.0 – 32.0[1]	15 – 60[2]
Feldspars – K (% total dry weight)	0.0 – 6.0[1]	1 – 10[2]
Feldspars – albite (% total dry weight)	0.0 – 2.0[1]	1 – 10[2]
Calcite (% total dry weight)	4.0 – 22.0[1]	1 – 5[2]
Dolomite/ankerite (% total dry weight)	0.0 – 1.0[1]	present[2]
Siderite (% total dry weight)	0.0 – 6.0[1]	present[2]
Pyrite (% total dry weight)	0.0 – 3.0[1]	1 – 5[2]
Gypsum (% total dry weight)	0.0 – 0.5[1]	NA
Organic Carbon (% total dry weight)	0.4 – 1.2[1]	1 – 5[2]

1. Bossart (2012, p. 4-12); 2. DeCraen et al. (2004, Table 1-2)
NA = not available

Table 5-15. Mineralogical: Cation Exchange Capacity (CEC)

Property	Opalinus Clay	Boom Clay
Total CEC (mEq/100 g rock)	9.44 – 13.35[1]	24.00[2]
Exchangeable Na (mEq/100 g rock)	3.61 – 6.37[1]	8.7[2]
Exchangeable K (mEq/100 g rock)	0.58 – 0.92[1]	2.3[2]
Exchangeable Ca (mEq/100 g rock)	2.25 – 3.58[1]	3.8[2]
Exchangeable Mg (mEq/100 g rock)	1.55 – 2.38[1]	3.7[2]
Exchangeable Sr (mEq/100 g rock)	0.10 – 0.36[1]	NA
Selectivity – log(Na/K)	0.7 – 0.84[3]	1.2[2]
Selectivity – log(Na/Mg)	0.0 – 2.0[3]	0.32[2]
Selectivity – log(Na/Ca)	4.0 to 22.0[3]	0.18[2]
Selectivity – log(Na/Sr)	0.0 – 1.0[3]	NA

1. Bossart (2012, p. 4-13); 2. Lolivier et al. (1998, Table II); 3. Pearson et al. (2010, Table 4)
NA = not available

Table 5-16. Mineralogical: Sorption Coefficients

Property	Opalinus Clay *	Boom Clay**
H(HTO) (m^3-kg^{-1})	0 - 0[1]	NA
C(inorg.) (m^3-kg^{-1})	0.0016 - 0.0016[1]	NA
C(org.) (m^3-kg^{-1})	0 - 0[1]	NA
Cl(-I) (m^3-kg^{-1})	0 - 0[1]	NA
Ca(II) (m^3-kg^{-1})	0.0002 - 0.0066[1]	NA
Co(II) (m^3-kg^{-1})	0.033 - 7.4[1]	NA
Ni(II) (m^3-kg^{-1})	0.080 - 10.8[1]	NA
Se(-II) (m^3-kg^{-1})	0 - 0[1]	NA
Sr(II) (m^3-kg^{-1})	0.0002 - 0.0066[1]	NA
Zr(IV) (m^3-kg^{-1})	0.56 - 214.0[1]	NA
Nb(V) (m^3-kg^{-1})	0.22 - 72.8[1]	NA
Mo(VI) (m^3-kg^{-1})	0.0011 - 0.257[1]	NA
Tc(IV) (m^3-kg^{-1})	8.79 - 349.0[1]	52.2 - 65.7[2]
Ru(III/IV) (m^3-kg^{-1})	0.33 - 75[1]	NA
Pd(II) (m^3-kg^{-1})	0.33 - 75[1]	NA
Ag(I) (m^3-kg^{-1})	0 - 0[1]	NA
Cd(II) (m^3-kg^{-1})	0.011 - 2.95[1]	NA
Sn(IV) (m^3-kg^{-1})	7.86 - 1540[1]	NA
Sb(III) (m^3-kg^{-1})	0.22 - 143.0[1]	NA
I(-I) (m^3-kg^{-1})	0 - 0.0005[1]	NA
Cs(I) (m^3-kg^{-1})	0.092 - 3.3[1]	NA
Ce(III) (m^3-kg^{-1})	9.49 - 377.0[1]	NA
Pm(III) (m^3-kg^{-1})	9.49 - 377.0[1]	NA
Sm(III) (m^3-kg^{-1})	9.49 - 377.0[1]	NA
Eu(III) (m^3-kg^{-1})	13.3 - 269.0[1]	0.32 - 12.6[2]
Ho(III) (m^3-kg^{-1})	9.49 - 377.0[1]	NA
Hf(IV) (m^3-kg^{-1})	0.55 - 213.6[1]	NA
Pb(II) (m^3-kg^{-1})	0.057 - 128.0[1]	NA
Po(IV) (m^3-kg^{-1})	0.013 - 2.52[1]	NA
Ra(II) (m^3-kg^{-1})	0.0001 - 0.0046[1]	NA
Ac(III) (m^3-kg^{-1})	2.07 - 139.0[1]	NA
Th(IV) (m^3-kg^{-1})	12.3 - 249.0[1]	0.69 - 21.8[2]
Pa(IV) (m^3-kg^{-1})	0.5 - 50[1]	NA
U(IV) (m^3-kg^{-1})	3.25 - 129.0[1]	NA
Np(IV) (m^3-kg^{-1})	8.79 - 349.0[1]	6.42 - 75.5[2]
Pu(III) (m^3-kg^{-1})	2.76 - 185.0[1]	12.8 - 37.0[2]
Am(III) (m^3-kg^{-1})	2.93 - 98.6[1]	0.86 - 21.8[2]
Cm(III) (m^3-kg^{-1})	2.07 - 139.0[1]	4.87 - 13.4[2]
Pa(V) (m^3-kg^{-1})	NA	0.84 - 233.2[2]
Pu(IV) (m^3-kg^{-1})	NA	176.9 - 387.0[2]

1. Bradbury and Baeyens (2003, Tables 7 and 9); 2. Maes et al. (2011, p. 1597)
NA = not available

* Bradbury and Baeyens (2003), Table 7 mean values divided or multiplied by the uncertainty factors in Bradbury and Baeyens (2003) Table 9
**Values computed from retardation factors using conversion given in Maes et al. (2011) Table 4 note a).

Gouy-Chapman theory is used to represent clay swelling effects that result from aqueous compositional changes (Liu et al., 2011, Section 4). This theory requires density of solid and aqueous phases (Tables 1 and 4), porosity (Table 1), volume fraction of swelling clay minerals (Table 14), exchangeable cations (Table 15), cation exchange capacity (Table 15), aqueous chemical composition (Table 10), the initial half-widths between swelling and non-swelling mineral platelets (Table 17), specific surface area (Table 17), and some general scientific parameters such as elementary electric charge and Boltzmann's constant (Table 18), and the dielectric constant of pore fluid (Table 4).

Table 5-17. Mineralogical: Additional Parameters for the Gouy-Chapman Model

Property	Opalinus Clay	Boom Clay
nondimensional midplane potential - nondimensional distance function parameter, *a* (for pure smectite)	1.81 – 3.54[1]	1.81 – 3.54[1]
nondimensional midplane potential - nondimensional distance function parameter, *b* (for pure smectite)	-4.13 to -3.17[1]	-4.13 to -3.17[1]
Basal half-spacing for swelling clay (A)	20 – 40[1]	20 – 40[1]
Basal half-spacing for non-swelling clay (A)	10[1]	10[1]
Specific surface area (m^2-g^{-1})	24 – 37 (BET); 112 – 147 (adsorption)[2]	44 (BET); 200 – 250 (adsorption)[3]

1. Liu et al. (2011, Table 4-2 and p. 91); 2. Bossart (2012, p. 4-17); 3. Mazurek et al. (2003, p. 160)

5.2.4 Thermal Model

The thermal model uses Fourier's theory for conductive heat transfer as well as convective heat transfer. This theory requires thermal conductivity for saturated and dry conditions, the dry bulk rock specific heat, and aqueous specific heat. Porosity and density of the rock and fractures, as well as the aqueous density are also needed for the thermal model, but these have already been discussed for the hydrological model. Thermal-mechanical coupling requires parameters for the thermal expansion of the rock and aqueous phase. Thermal properties are given in Table 5-18. The database needs to be able to accommodate spatial dependence of these parameters.

Table 5-18. Thermal: Conductive/Convective Heat Transfer and Thermal-Mechanical

Property	Opalinus Clay	Boom Clay
bulk rock thermal conductivity parallel to bedding (W-m^{-1}-°C^{-1})	1.7 – 2.1[1,2]	1.35 – 1.7[3]
bulk rock thermal conductivity perpendicular to bedding (W-m^{-1}-°C^{-1})	0.8 – 1.2[1,2]	
bulk rock specific heat (J-kg^{-1}-°C^{-1})	860 – 920[1,2]	1402[4]
bulk rock thermal expansion coefficient (°C^{-1})	1.5e-6 – 1.5e-5[1,2]	1e-5 – 5e-5[3]
aqueous specific heat (J-kg^{-1}-°C^{-1}) (at natural temperature – see Table 4)	4186 – 4188[5]	4185[5]
aqueous thermal conductivity (W-m^{-1}-°C^{-1}) (at natural temperature – see Table 4)	0.59[5]	0.59[5]
aqueous thermal expansion coefficient (°C^{-1}) (at natural temperature – see Table 4)	1.3e-4 – 1.5e-4[5]	1.6e-4[5]
moist air specific heat (J-kg^{-1}-°C^{-1}) (at natural temperature – see Table 4)	1.0e3[6]	1.0e3[6]
moist air thermal conductivity (W-m^{-1}-°C^{-1}) (at natural temperature – see Table 4)	2.5e-2[6]	2.5e-2[6]
thermal expansion coefficient (°C^{-1}) (dry air at 15° C)	3.48e-3[5]	3.48e-3[5]

1. Bossart (2012, p. 4-18); 2. Jobmann and Polster (2007, Table 2); 3. Li et al. (2007, Table 4.4); 4. Li et al. (2007, Tables 4.3 and 4.4 – volumetric heat capacity divided by bulk density) ; 5. Batchelor (1967, Appendix1); 6. Tsilingiris (2008, Figures 3 and 4)

5.2.5 Non-Environment-Specific Parameters

Other parameters used for modeling of THMC processes are not environment-specific. These parameters are summarized in table 5-19.

Table 5-19. Non-Environment-Specific Parameters

Property	Value
gravitational acceleration ($m\text{-}s^{-2}$)	9.80[1]
molecular weight (kg)	molecule dependent
Boltzmann's constant ($J\text{-}°C^{-1}$)	1.38e-23[1]
elementary electric charge (coulombs (C))	1.60e-19[1]
permittivity of free space ($C^2\text{-}N^{-1}\text{-}m^{-2}$)	8.85e-12[1]

1. Reynolds and Perkins (1977, Table A4 and p. 9)

5.3 Data for Modeling Granite Far Field Flow and Transport

Crystalline rock is generally considered a favorable medium that could provide the required safeguard for long-term storage of nuclear wastes. It may be located in very old, stable tectonic settings. Geochemistry is often reducing (or can be sited for this), which lowers radionuclide solubilities and increases their sorption relative to oxidizing environments. Heterogeneity in geochemical/mineralogic properties tends to be lower than in many other settings. It is very amenable to retrievability (will remain open for very long periods of time). On the other hand, the hardness of crystalline rock and low matrix porosity and permeability leads to fracture flow, which tends to be more rapid and less predictable than flow in other environments. Fracture flow in low porosity environment results in less matrix diffusion and less surface area available for sorption. Also, it tends to have less sorptive mineralogies than many other rock types. More reliance is generally needed on engineered barriers for crystalline rock environment because of these hydrogeologic features. It is expensive to mine, but generally safe and stable. Assessing the physical, chemical and hydrological properties of crystalline rock is an important step in the investigation process to identify and select a site with favorable media. Table 5-20 compiles some key granite far field parameters from different sources.

Table 5-20. Sorption Coefficient – SKB1

Element	Chemical form/redox state	Non-saline	Uncertainty interval	Saline	Uncertainty interval
		Kd (m^3/kg)		Kd (m^3/kg)	
C	HCO_3^-	0.001	(0.0005-0.002)	0.001	(0.0005-0.002)
Cl	Cl^-	0	-	0	-
Co	Co(II)	0.1	(0.05-0.5)	0.02	(0.01-0.1)
Ni	Ni(II)	0.1	(0.05-0.5)	0.02	(0.01-0.1)
Se	Se(-II, IV,VI)	0.001	(0.0005-0.005)	0.001	(0.0005-0.005)
Kr	inert gas	0	-	0	-
Sr	Sr(II)	0.01	(0.005-0.05)	0.0002	(0.0001-0.001)
Zr	Zr(IV)	1	(0.5-3)	1	(0.5-3)
Nb	Nb(V)	1	(0.5-3)	1	(0.5-3)
Tc	Tc(IV)	1	(0.3-3)	1	(0.3-3)
Tc	Tc(VII)	0		0	
Pd	Pd(II)	0.1	(0.01-0.5)	0.01	(0.001-0.05)
Ag	Ag(I)	0.5	(0.1-1)	0.05	(0.01-0.1)
Cd	Cd(II)	0.1	(0.05-0.5)	0.02	(0.01-0.1)
Sn	Sn(IV)	0.001	(0-0.01)	0.001	(0-0.01)
I	I-	0	-	0	-
Cs	Cs(I)	0.5	(0.1-1)	0.05	(0.01-0.1)
Sm	Sm(III)	2	(1-5)	2	(1-5)
Eu	Eu(III)	2	(1-5)	2	(1-5)
Ho	Ho(III)	2	(1-5)	2	(1-5)
Ra	Ra(II)	0.1	(0.05-0.5)	0.02	(0.01-0.1)
Ac	Ac(III)	3	(1-5)	3	(1-5)
Th	Th(IV)	5	(1-10)	5	(1-10)
Pa	Pa(IV,V)	1	(0.5-5)	1	(0.5-5)
U	U(IV)	5	(1-10)	5	(1-10)
U	U(VI)	0.01	(0.005-0.02)	0.005	(0.001-0.01)
Np	Np(IV)	5	(1-10)	5	(1-10)
Np	Np(V)	0.01	(0.005-0.05)	0.005	(0.001-0.01)
Pu	Pu(III,IV)	5	(1-10)	5	(1-10)
Am	Am(III)	3	(1-5)	3	(1-5)
Cm	Cm(III)	3	(1-5)	3	(1-5)

Data sources: Carbol and Engkvist (1997, SKB technical report R-97-13, table 12-1)
The non-saline and the saline groundwaters are represented by the type of water found at the Gideå and Äspö study site, respectively. The restrictions for the non-saline water are: pH≥7, [Cl-] < 500 mg/l and Eh< -200 mV. The restrictions for the saline water are: pH≥7, 500 mg/l < [Cl-] < 6500 mg/l and Eh< -200 mV.

Table 5-21. Sorption Coefficient – SKB2

Radionuclide (Redox State)	Best estimate Kd (m3/kg)	$log_{10}K_d$ – μ	$log_{10}K_d$ – σ	Lower K_d limit (m3/kg)	Upper K_d limit (m3/kg)
Ac(III)	1.48·10–2	–1.83	0.72	5.74·10–4	3.83·10–1
Ag(I)	3.49·10–4	–3.46	0.51	3.46·10–5	3.52·10–3
Am(III)	1.48·10–2	–1.83	0.72	5.74·10–4	3.83·10–1
C, HCO3 –	0	–	–	0	0
C, CH4	0	–	–	0	0
C, -CO2H	0	–	–	0	0
Cd(II)	1.10·10–3	–2.96	0.65	5.97·10–5	2.04·10–2
Cl(-I)	0	–	–	0	0
Cm(III)	1.48·10–2	–1.83	0.72	5.74·10–4	3.83·10–1
Cs(I)	3.49·10–4	–3.46	0.51	3.46·10–5	3.52·10–3
Eu(III)	1.48·10–2	–1.83	0.72	5.74·10–4	3.83·10–1
H(I)	0	–	–	0	0
Ho(III)	1.48·10–2	–1.83	0.72	5.74·10–4	3.83·10–1
I(-I)	0	–	–	0	0
Mo(VI)	0	–	–	0	0
Nb(V)	1.98·10–2	–1.70	0.64	1.11·10–3	3.53·10–1
Ni(II)	1.10·10–3	–2.96	0.65	5.97·10–5	2.04·10–2
Np(IV)	**5.29·10–2**	**–1.28**	**0.65**	**2.84·10–3**	**9.84·10–1**
Np(V)	4.13·10–4	–3.38	0.74	1.48·10–5	1.15·10–2
Pa(IV)	5.92·10–2	–1.23	0.48	6.76·10–3	5.18·10–1
Pa(V)	**5.92·10–2**	**–1.23**	**0.48**	**6.76·10–3**	**5.18·10–1**
Pb(II)	2.52·10–2	–1.60	0.56	2.05·10–3	3.10·10–1
Pd(II)	5.20·10–2	–1.28	0.83	1.22·10–3	2.21
Pu(III)	**1.48·10–2**	**–1.83**	**0.72**	**5.74·10–4**	**3.83·10–1**
Pu(IV)	5.29·10–2	–1.28	0.65	2.84·10–3	9.84·10–1
Pu(V)	9.14·10–3	–2.04	0.6	6.19·10–4	1.35·10–1
Pu(VI)	9.14·10–3	–2.04	0.6	6.19·10–4	1.35·10–1
Ra(II)	2.42·10–4	–3.62	0.41	3.87·10–5	1.51·10–3
S(-II)	0	–	–	0	0
Se(-II)	**2.95·10–4**	**–3.53**	**0.55**	**2.50·10–5**	**3.48·10–3**
Se(IV)	2.95·10–4	–3.53	0.55	2.50·10–5	3.48·10–3
Se(VI)	2.95·10–4	–3.53	0.55	2.50·10–5	3.48·10–3
Sm(III)	1.48·10–2	–1.83	0.72	5.74·10–4	3.83·10–1
Sn(IV)	1.59·10–1	–0.80	0.28	4.51·10–2	5.58·10–1
Sr(II)	3.42·10–6	–5.47	0.99	3.84·10–8	3.05·10–4
Tc(IV)	**5.29·10–2**	**–1.28**	**0.65**	**2.84·10–3**	**9.84·10–1**
Tc(VII)	0	–	–	0	0
Th(IV)	5.29·10–2	–1.28	0.65	2.84·10–3	9.84·10–1
U(IV)	**5.29·10–2**	**–1.28**	**0.65**	**2.84·10–3**	**9.84·10–1**
U(VI)	**1.06·10–4**	**–3.97**	**0.66**	**5.53·10–6**	**2.05·10–3**
Zr(IV)	2.13·10–2	–1.67	0.35	4.48·10–3	1.02·10–1

Data sources: SKB technical report TR-10-50, Table 2-4. K_d values for use in SR-Site simulations of the Forsmark site. The predominant species for redox sensitive elements are highlighted in bold text. Values are given for the best estimate (median), parameters for the lognormal distribution (μ and σ), as well as lower and upper limits corresponding to the 2.5% and 97.5% percentiles, respectively.

Table 5-22. Sorption Coefficient – JAEA

Species	Data (range) (unit: cc/g)	Geometric mean (cc/g)	Geometric STDV (dimensionless)	Mean of log10(data) data unit (m^3/kg)	STDV of log10(data)
Am	220 - 190000	9096.03	4.306	0.959	0.634
Pu	0.2 - 401000	1736.9	13.957	0.24	1.145
Np	0.65 - 2720	31.61	5.667	-1.5	0.753
U	0 - 280000	16.04	9.215	-1.795	0.965
Tc	0.1 - 200000	15.5	56.54	-1.81	1.752
Sn	173 - 2940	688.4	2.754	-0.162	0.44
Cs	1 - 131000	135.76	7.991	-0.867	0.903
I	0.5 – 1.9	0.89	1.43	-3.052	0.155
Se	0 - 18	2.63	3.114	-2.579	0.493
Th	501 - 10000	1245.51	2.322	0.095	0.366
Pa	2.4 – 7.3	4.14	1.558	-2.383	0.193
Ra	30.1 - 3800	504.84	4.302	-0.297	0.634
Pb	1600 - 4400	2653.3	1.658	0.424	0.22
Sr	1 - 880	20.87	3.785	-1.68	0.578
Sb	450 - 519	483.27	1.074	-0.316	0.031
Zr	2.6 - 3160000	839.02	12.746	-0.076	1.105
Nb	7 - 142000	465.596	4.996	-0.332	0.699
Ac	83 - 40000	6687.15	8.17	0.825	0.912
Pd	142 - 82800	2256.63	5.301	0.353	0.724

Note: Data with de-ionized and other water chemistry that are obviously not relevant are not included except for Ac and Pd. For these two species no other data are available.
Data sources: Japan JAEA database: http://migrationdb.jaea.go.jp/english.html

Table 5-23. Sorption Coefficient – SNL

Element	Kd (m^3/kg
C, Cl, I	0
Se	0.0005
Pd, Sn	0.001
Sr	0.005
Nb	0.02
Am, Cm, Ac	0.04
Pa, Tc, Cs	0.05
Sb	0.1
U	0.1
Np, Th, Ra, Zr	0.2
Pu	0.5
Pb	1

Data sources: Mariner et al. (2011), table 2-3.

Table 5-24. Solubility – SNL

Element	Solubility	Units
Actinium (Ac)	6.00E-06	mol/L
Americium (Am)	6.00E-06	mol/L
Carbon (C)	1.00E+50	mol/L
Curium (Cm)	6.00E-06	mol/L
Cesium (Cs)	1.00E+50	mol/L
Iodine (I)	1.00E+50	mol/L
Niobium (Nb)	4.00E-05	mol/L
Neptunium (Np)	1.00E-09	mol/L
Protactinium (Pa)	1.00E-09	mol/L
Lead (Pb)	1.00E+50	mol/L
Paladium (Pd)	3.00E-06	mol/L
Plutonium (Pu)	2.00E-07	mol/L
Radium (Ra)	1.00E-06	mol/L
Antimony (Sb)	1.00E-07	mol/L
Selenium (Se)	4.00E-08	mol/L
Tin (Sn)	3.00E-08	mol/L
Strontium (Sr)	1.00E+50	mol/L
Technetium (Tc)	3.00E-08	mol/L
Thorium (Th)	4.00E-07	mol/L
Uranium (U)	4.00E-10	mol/L
Zirconium (Zr)	2.00E-08	mol/L

Note: no limit represented by 1E+50 mol/L
Data sources: Mariner et al. (2011), table 2-5 (pH 7.5, T = 25 deg C).
C, Cs, I, Sr, and Pb assumed infinitely soluble.

Table 5-25. Solubility – SKB

Element	Solubility	Unit
Ac-227	$1.00 \cdot 10^{17}$	mol/L
Ag-108m	$1.10 \cdot 10^{-5}$	mol/L
Am-241	$2.50 \cdot 10^{-6}$	mol/L
Am-242m	$2.50 \cdot 10^{-6}$	mol/L
Am-243	$2.50 \cdot 10^{-6}$	mol/L
C-14	$1.00 \cdot 10^{17}$	mol/L
Cd-113m	$1.00 \cdot 10^{17}$	mol/L
Cl-36	$1.00 \cdot 10^{17}$	mol/L
Cm-245	$2.60 \cdot 10^{-6}$	mol/L
Cm-246	$2.60 \cdot 10^{-6}$	mol/L
Cs-135	$1.00 \cdot 10^{17}$	mol/L
Cs-137	$1.00 \cdot 10^{17}$	mol/L
Eu-152	$1.00 \cdot 10^{17}$	mol/L
H-3	$1.00 \cdot 10^{17}$	mol/L
Ho-166m	$4.10 \cdot 10^{-6}$	mol/L
I-129	$1.00 \cdot 10^{17}$	mol/L
Mo-93	$1.00 \cdot 10^{17}$	mol/L
Nb-93m	$4.90 \cdot 10^{-5}$	mol/L
Nb-94	$4.90 \cdot 10^{-5}$	mol/L
Ni-59	$3.00 \cdot 10^{-4}$	mol/L
Ni-63	$3.00 \cdot 10^{-4}$	mol/L
Np-237	$1.00 \cdot 10^{-9}$	mol/L
Pa-231	$3.30 \cdot 10^{-7}$	mol/L
Pb-210	$1.70 \cdot 10^{-6}$	mol/L
Pd-107	$3.90 \cdot 10^{-6}$	mol/L
Pu-238	$4.80 \cdot 10^{-6}$	mol/L
Pu-239	$4.80 \cdot 10^{-6}$	mol/L
Pu-240	$4.80 \cdot 10^{-6}$	mol/L
Pu-242	$4.80 \cdot 10^{-6}$	mol/L
Ra-226	$9.10 \cdot 10^{-7}$	mol/L
Se-79	$6.70 \cdot 10^{-9}$	mol/L
Sm-151	$1.10 \cdot 10^{-7}$	mol/L
Sn-121m	$9.00 \cdot 10^{-8}$	mol/L
Sn-126	$9.00 \cdot 10^{-8}$	mol/L
Sr-90	$3.70 \cdot 10^{-3}$	mol/L
Tc-99	$3.80 \cdot 10^{-9}$	mol/L
Th-229	$2.60 \cdot 10^{-9}$	mol/L
Th-230	$2.60 \cdot 10^{-9}$	mol/L
Th-232	$2.60 \cdot 10^{-9}$	mol/L
U-233	$9.50 \cdot 10^{-10}$	mol/L
U-234	$9.50 \cdot 10^{-10}$	mol/L
U-235	$9.50 \cdot 10^{-10}$	mol/L
U-236	$9.50 \cdot 10^{-10}$	mol/L
U-238	$9.50 \cdot 10^{-10}$	mol/L
Zr-93	$1.80 \cdot 10^{-8}$	mol/L

Data sources: SKB technical report TR-10-50, Table 3-4, for temperate condition.
Note: $1.x10^{17}$ represents unlimited solubility.

Table 5-26. Diffusivity - JAEA

Species	De : effective diffusivity (range) (unit: m^2/s)	Dp : pore diffusivity (range) (unit: m^2/s)	Mean (Dp)	Standard Deviation (Dp)
Am				
Pu	$1.28e^{-13}$ – $2.76e^{-13}$	$2.61e^{-11}$ – $5.63e^{-11}$	4.10E-11	1.07E-11
Np	$2.10e^{-13}$ – $5.41e^{-13}$	$2.80e^{-11}$ – $1.10e^{-10}$	6.99E-11	2.75E-11
U	$2.20e^{-14}$ – $4.40e^{-14}$	$3.14e^{-12}$ – $6.29e^{-12}$	5.14E-12	1.42E-12
Tc	$4.20e^{-14}$– $4.20e^{-14}$	$4.20e^{-12}$ – $4.20e^{-12}$	4.20E-12	0
Sn				
Cs	$5.04e^{-13}$– $1.80e^{-11}$	$1.03e^{-10}$– $3.75e^{-10}$	2.11E-10	1.05E-10
I	$3.90e^{-13}$– $2.60e^{-12}$	$7.96e^{-11}$– $3.38e^{-10}$	1.57E-10	6.02E-10
Se	$1.90e^{-12}$– $5.30e^{-12}$	$8.26e^{-11}$– $9.46e^{-11}$	8.93E-11	5.00E-12
Th				
Pa				
Ra				
Pb				
Sr	$2.00e^{-13}$– $1.60e^{-12}$	$2.86e^{-11}$– $4.00e^{-10}$	6.65E-11	9.66E-11
Sb				
Zr				
Nb				
Ac				
Pd				

Note: Dp (pore diffusivity) (Dp = De/porosity) is generally used in dual-porosity model as matrix diffusion coefficient. Data with de-ionized water are not included. Blank line means no data available.
Data sources: Japan JAEA database: http://migrationdb.jaea.go.jp/english.html

Table 5-27. Various Far Field Parameters

SKB technical report TR-10-52, table 6-91

Parameter Description	Value	mean	Stdv	Units	Distribution Type	Index
Bulk Density	2700			kg/m3		1
Porosity	0.0018			[]		2
permeasbility	10^{-20} to 10^{-19}			m^2		3
Longitude dispersivity	50			m		4
Equivalent flow rate	$4.2x10^{-6}$ to $1.2x10^{-4}$			m^3/yr		5
Colloid concentrations	10			mg/l		6
Colloid concentrations (with dilute glacial melt water)	10			g/l		7
Hydraulic conductivity (for depth 200 to 400 m)	$3x10^{-9}$ to $1x10^{-7}$			m/s		8
Hydraulic conductivity (for depth > 400 m)	10^{-13} to 10^{-10}			m/s		9
Fracture zone mean fracture aperture	$5x10^{-4}$			m		10
Fracture aperture	10^{-5} to $3x10^{-3}$			m		11
Fractutre spacing	0.25 to 15			m		12
Fracture length	1.5 to 76			m		13
Heat conductivity	2.77 to 3.34			$W m^{-1} K^{-1}$		14
Heat capacity	2.17 to 2.24			$MJ\ m^{-3} K^{-1}$		15
	Best estimate	**$Log_{10}D_e$ (m^2/s)**	**$Log_{10}D_e$ (m^2/s)**			
Effective diffusivity (cations, non-charged solutes)	$2.1x10^{-14}$	-13.7	0.25	m^2/s	Log-normal	16
Effective diffusivity (anions)	$6.6x10^{-15}$	-14.2	0.25	m^2/s	Log-normal	17

Data sources:

1. SKB technical report TR-10-52, Table 3-2
2. SKB technical report TR-10-52, Table 3-2
3. Sandia report SAND2011-6203, p75-76
4. SKB technical report TR-10-52, Table 6-85
5. SKB technical report TR-10-50, Table 3-5
6. SKB technical report TR-10-50
7. SKB technical report TR-10-50
8. SKB technical report TR-10-52, Table 6-78
9. Sandia report SAND2011-6203, Table 1-3
10. Posiva 2010. Models and Data Report 2010. POSIVA 2010-01. Posiva Oy, Olkiluoto, Finland.
11. Kalinina et al. Paper "Analysis of the Effect of Hterogeneity on Heat Extraction in an EGS Represented with the Continuum Fracture Model", data from granite sites in US, Czech Republic, France, Spain, Portugal, Sweden, Egypt and Japan.
12. Kalinina et al. Paper "Analysis of the Effect of Hterogeneity on Heat Extraction in an EGS Represented with the Continuum Fracture Model", data from granite sites in US, Czech Republic, France, Spain, Portugal, Sweden, Egypt and Japan.
13. Kalinina et al. Paper "Analysis of the Effect of Hterogeneity on Heat Extraction in an EGS Represented with the Continuum Fracture Model", data from granite sites in US, Czech Republic, France, Spain, Portugal, Sweden, Egypt and Japan.
14. based on values at Forsmark and Laxemar (SKB 2006, Table 9-4)
15. based on values at Forsmark and Laxemar (SKB 2006, Table 9-4)
16. SKB technical report TR-10-52, Table 6-91
17. SKB technical report TR-10-52, Table 6-91

Table 5-28. Global Transport Parameter

	Median	5 percentilce	95 percentile	Unit
Hydrodynamic Transport Resistance Parameter (F)	4.00E+06	3.00E+05	1.00E+08	yr/m
Travel time	150	30	1000	yr

Note: 500 m travel distance. Should be scaled to other values.

Data sources: SKB technical report TR-10-52, Figure 6-67; Painter, S., Cvetkovic, V., Mancillas, J., Pensado, O. (2008): Time domain particle tracking methods for simulating transport with retention and first-order transformation. Water Resources Research 43(9), W01406; SKB. 2010. Radionuclide transport report for the safety assessment SR-Site. SKB Technical Report TR-10-50. Swedish Nuclear Fuel and Waste Management Co.

The parameters hydrodynamic transport resistance and global travel time are integrated quantities of a flowpath/streamline. Within some models of radionuclide transport (e.g. Painter et al., 2008 and SKB, 2010), these two parameters are the only flow related parameters controlling radionuclide transport. The transport resistance parameter is the flow-rate normalized flow-wetted surface area of a streamtube of infinitesimal cross-section. It is denoted beta in Painter et al. (2010) and F in SKB (2010). The global travel time is the travel time of a non-dispersing, non-sorbing, non-diffusing tracer moving with the groundwater flow.

Table 5-29. Groundwater Composition

Parameter	Olkiluoto, Finland	Olkiluoto, Finland	Olkiluoto, Finland	Laxemar, Sweden	Forsmark, Sweden	Pinawa, Canada	East Bull Lake, Canada
Borehole	OL-KR20	OL-KR10	OL-KR12	KLX03	KFM02A	WN-4	EBL-2
Depth (m)	360	487	708	380	512	513	538
TDS (g L^{-1})	10.5	22.1	49.5	2.8	9.3	7.5	2.3
Ionic strength (eq L^{-1})	0.22	0.48	1.18	0.05	0.19	0.16	0.05
pH	7.4	8	8.2	7.9	7.2	8.1	7.4
Na (mol L^{-1})	0.11	0.21	0.36	0.03	0.09	0.07	0.03
Ca (mol L^{-1})	0.03	0.09	0.25	0.01	0.02	0.03	0.01
K (mol L^{-1})	2.8E-04	3.6E-04	4.9E-04	1.4E-04	9.0E-04	5.3E-04	5.4E-05
Mg (mol L^{-1})	2.6E-03	1.6E-03	1.5E-03	4.4E-04	9.3E-03	1.1E-03	7.0E-05
Sr (mol L^{-1})	1.6E-04	3.7E-04	1.1E-03	nr	nr	nr	3.3E-05
Mn (mol L^{-1})	5.8E-06	7.3E-06	9.3E-06	nr	nr	nr	nr
Cl (mol L^{-1})	0.18	0.38	0.86	0.04	0.15	0.11	0.04
SO4 (mol L^{-1})	2.1E-04	1.0E-05	5.0E-05	1.3E-03	5.2E-03	6.6E-03	1.4E-04
CO3 (mol L^{-1})	5.5E-04	1.1E-04	4.0E-05	3.1E-03	2.2E-03	3.5E-03	5.0E-04
SiO2 (mol L^{-1})	3.6E-04	2.8E-04	2.1E-04	nr	nr	nr	5.4E-05
Fe (mol L^{-1})	2.5E-06	2.0E-06	3.8E-07	8.0E-06	3.3E-05	nr	nr
S(-II) (mol L^{-1})	5.6E-06	<3.1 E-7	1.3E-06	3.0E-07	0.0E+00	nr	nr
Reference	Posiva (2010), Table 6-6	Posiva (2010), Table 6-6	Posiva (2010), Table 6-6	SKB (2006d), p. 382	SKB (2006d), p. 382	Gascoyne et al. (1987), Table 3	Gascoyne et al. (1987), Table 3

Note: nr =not reported

Data sources: Mariner et al. (2011), table 2-1 Sample groundwater composition in granite at depths from 360 to 708 m.

Table 5-30. Groundwater chemistry information for granite in Japan

Analyte	**Unit**	**Results (range)**
Temperature	0C	17.5 - 25
pH		8.1 – 9.2
Eh	mv	0 - -280
Conductivity	ms/m	32.7 - 525
Na+	mg/L	58.7 – 393.5
K+	mg/L	0.2 – 9.4
Ca2+	mg/L	5.9 – 638.6
Ma2+	mg/L	<0.1 – 0.4
Si	mg/L	5.5 – 8.6
DIC*	mg/L	0 – 12.3
SO32-	mg/L	<0.4 – 9.5
Cl-	mg/L	37.5 – 1645.4
F-	mg/L	1.7 – 12.0
Br-	mg/L	<0.1 – 2.9

*DIC=Dissolved Inorganic Carbon=HCO3- + CO32-

Data sources: T. Iwatsuki et al., Applied Geochemistry 20 (2005) 2283-2302.

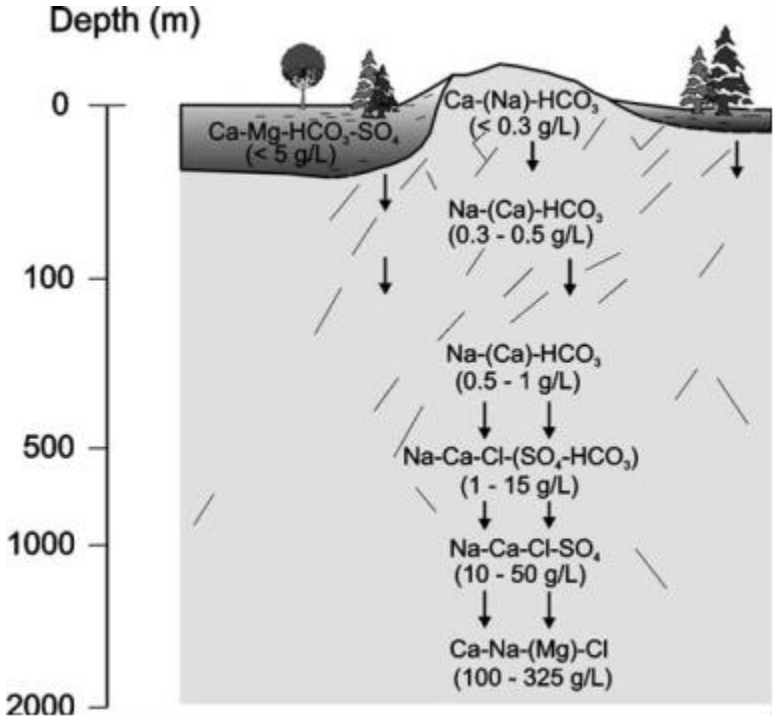

Figure 5-1. Major ion chemistry of Canadian granite water (values are total dissolved solids) (Gascoyne, 2004)

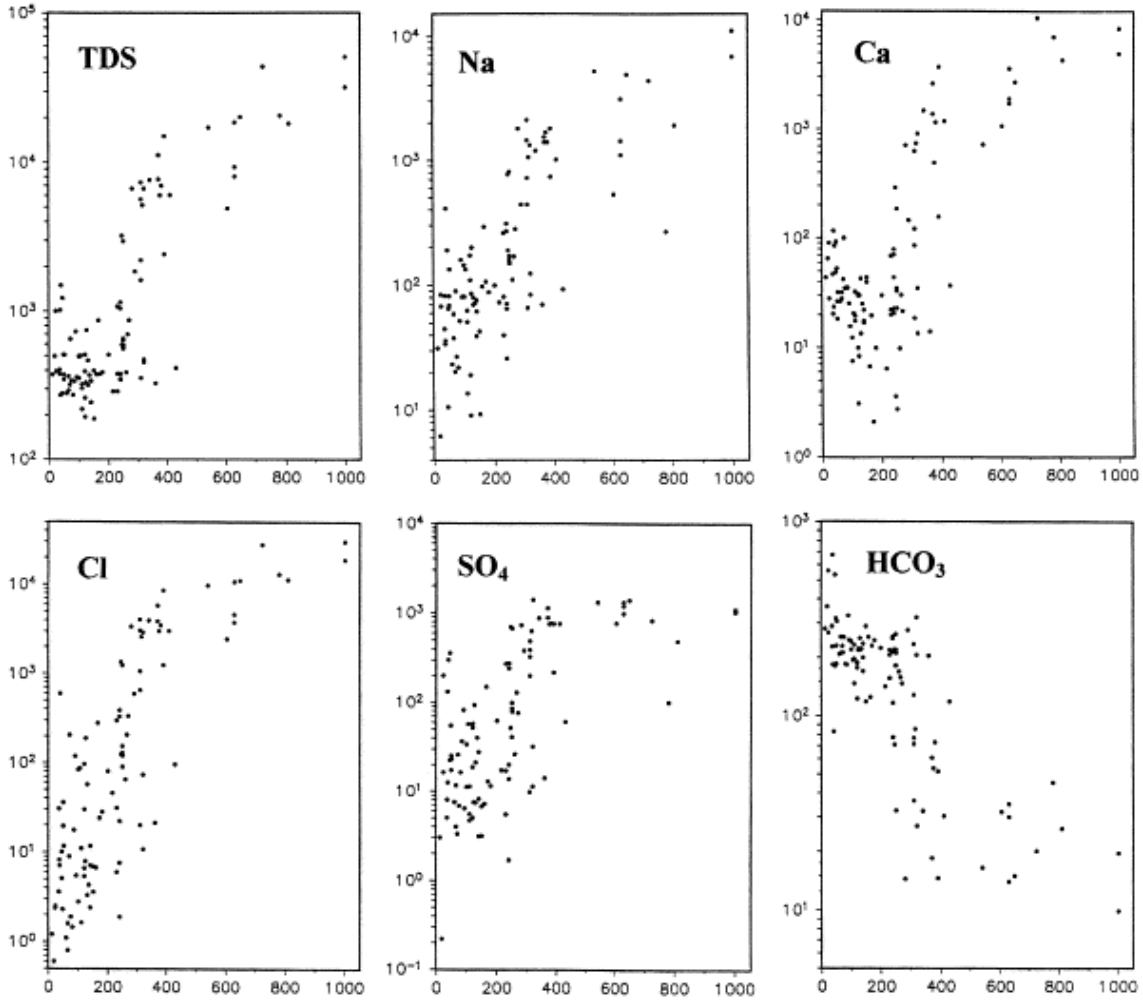

Figure 5-2. Major ions of Canadian granite water as a function of depth below surface in meters (mg/L) (Gascoyne, 2004). pH values (7 to 9) with no obvious trend with depth, while Eh values (-200 to 300) with tendency toward lower (more reducing) values with increasing depth.

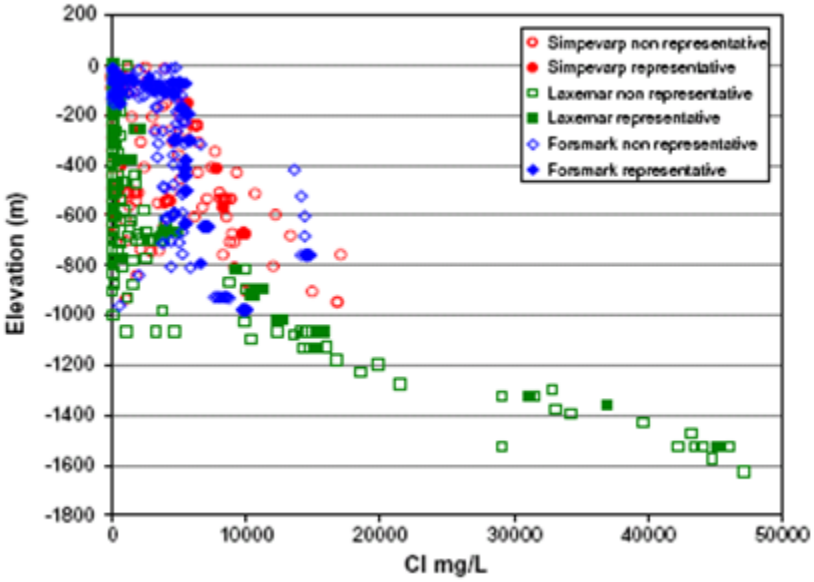

Figure 5-3. Chloride distribution with depth for Swedish granite sites (Laaksoharju et al., 2008): Laxemar (green), Simpevarp (red), Forsmark (blue). Open symbols represent samples considered unsuitable. Elevation indicated above sea level. Note: Chloride charge is balanced almost entirely by Na^{+} and Ca^{2+} (the sum of the concentrations of these two ions should be approximately $4/7^{ths}$ that of Cl^{-} in mg/L).

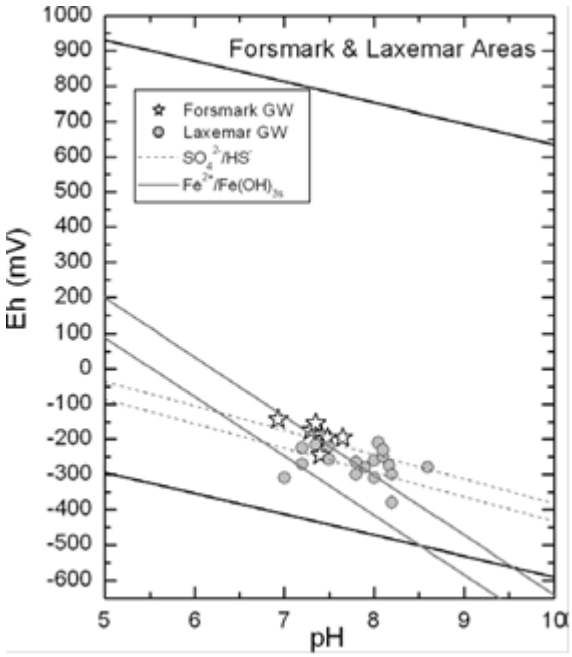

Figure 5-4. Eh and pH ranges at Swedish sites (Eh generally decreases with depth) (Laaksoharju et al., 2008).

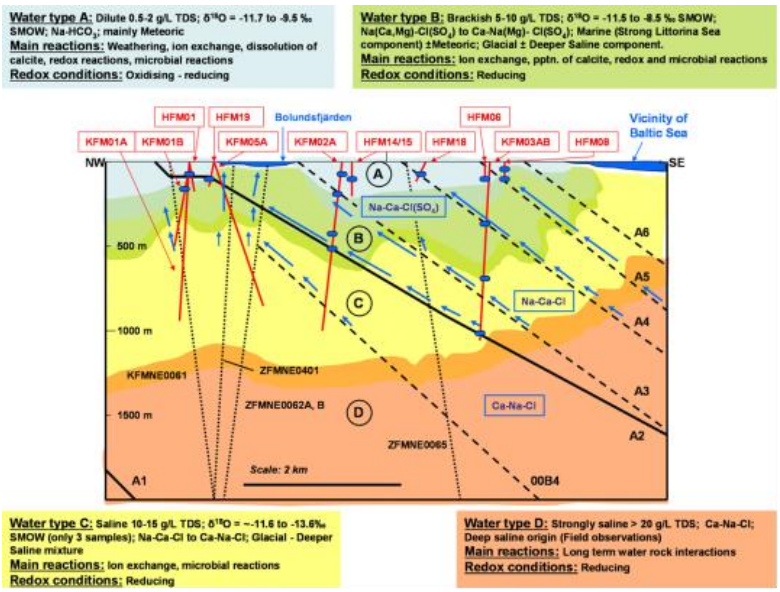

Forsmark site.

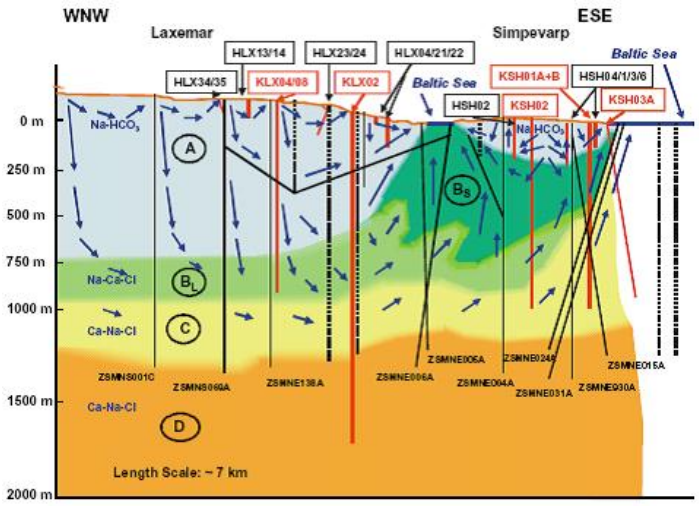

Laxemar/Simpevarp site

Figure 5-4. Types and distributions of groundwater at two Swedish granite sites (Laaksoharju et al., 2008). A - fresh groundwater (<2000 mg/L Cl; 0.5–3.5 g/L TDS), mainly meteoric and Na–HCO3 in type, and marginally oxidizing close to the surface, otherwise reducing. B_L - brackish groundwater (2000–10,000 mg/L Cl; 3.5–18.5 g/L TDS), meteoric, mainly Na–Ca–Cl in type, glacial/deep saline components, and reducing; B_S - brackish groundwater (2000–10,000 mg/L Cl, 3.5–18.5 g/L TDS). meteoric, mainly Na–Ca–Cl in type but some Na–Ca(Mg)–Cl(Br) types, glacial/deep saline components, and reducing; C - saline (10,000–20,000 mg/L Cl; 18.5–30 g/L TDS), dominantly Ca–Na–Cl in type at Laxemar but Na–Ca–Cl changing to Ca–Na–Cl only at the highest salinity levels at the Simpevarp site, and reducing; and D - highly saline (>20,000 mg/L Cl; to a maximum of ~70 g/L TDS), dominantly Ca–Na–Cl, and reducing.

Table 5-31. Groundwater chemistry of Switzerland Grimsel test site (~1730 m above sea level) (Schafer and Iijima, 2007). Low ionic strength water (~0.001 M, ~50 mg/L TDS), dominated by NaHCO3 (secondary ions are Ca^{2+} and Cl^-) with Eh = -200 ± 50 mV and pH = 9.5 ± 0.2.

Parameter	Value	Unit
pH	9.6	
Eh	-170	mV
Ionic Strength	0.0017	M
Na	0.56	mM
K	0.006	mM
Mg	0.00058	mM
Ca	0.14	mM
Al	12.7	ppb
SO_4^{2-}	0.052	mM
F^-	0.31	mM
Cl^-	0.15	mM
HCO_3^-	0.283	mM

Table 5-31. Formation Properties

Location	Reference	Lithologic Classification	Porosity (%)	Bulk Hydraulic Conductivity (m s-1)	Young's Modulus (GPa)	Poisson's Ratio	Compressive Strength (MPa)
Barre Granite, Vermont	Krech et al. (1974)	Granodiorite	0.51	$< 10^{-10}$	46	0.23	197
St. Cloud Granodiorite, Minnesota	Krech et al. (1974)	Granodiorite	0.08	$< 10^{-10}$	71	0.25	282
Westerly Granite, Rhode Island	Krech et al. (1974)	Granodiorite	0.35	$< 10^{-10}$	50	0.21	233
Sherman Granite, Wyoming	Touloukian et al. (1981)	Granite	0.002	9.8×10^{-13}			
Granite, Wyoming	Touloukian et al. (1981)	Granite					142, 129
Fremont Canyon	Touloukian et al. (1981)	Granite			45	0.1	
California	Touloukian et al. (1981)	Granodiorite					116
Stone Mountain Granite, Georgia	Touloukian et al. (1981); Hoek & Brown (1980)	Granite	0.3				116
Hardhat Granite	Touloukian et al. (1981)	Granite		4×10^{-14}			
Atikokan, Ontario	Gascoyne et al. (1987)	Granite		$10^{-12} – 10^{-5}$ (<400 m) $10^{-13} – 10^{-10}$ (>400 m)			
Olkiluoto, Finland	Posiva (2010)[a]	Pegmatitic granite	0.01 – 0.2	10^{-7} (near surface) 10^{-11} (at depth)	65	0.29	108
Laxemar, Sweden	SKB (2006b), Table A-42; SKB (2006d)	Granite to Granodiorite	0.14	$10^{-10} – 10^{-5}$ (<200 m) $10^{-11} – 10^{-6}$ (>200 m)			165-210
Forsmark, Sweden	SKB (2006b), Table A-42	Granite to Granodiorite	0.09		76	0.24	

[a]Approximate range of flow porosities, which are 1/10th the approximate diffusion porosities (Posiva, 2010, tables C-3, C-4, and C-5); Mariner et al. (2011).

5.4 References

Aertsens, M., Put, M., and Dierckx, A. (2003) An Analytical Model for the Interpretation of Pulse Injection Experiments Performed for Testing the Spatial Variability of Clay Formations, Journal of Contaminant Hydrology 61 (2003) 423– 436.

Aertsens, M., Wemaere, I., Wouters, L. (2004) Spatial variability of Transport Parameters in the Boom Clay, Applied Clay Science, 26, 37– 45.

Arnould, M. (2006) Discontinuity Networks in Mudstones: A Geological Approach - Implications for Radioactive Wastes Isolation in Deep Geological Formations in Belgium, France, Switzerland, Bull Eng Geol Environ (2006) 65:413–422.

Batchelor, G.K. (1967) An Introduction to Fluid Dynamics, Cambridge University Press.

Bernier, F., Li, X.-L., And Bastiaens, W. (2007) Twenty-Five Years' Geotechnical Observation and Testing in the Tertiary Boom Clay Formation, Géotechnique, 57, No. 2, 229–237.

Bernier, F., Volckaert, G., Alonso, E., Villar, M. (1997) Suction-Controlled Experiments on Boom Clay, Engineering Geology, 47, 325-338.

Bernier, F., and B. Neerdael. (1996) Overview of In-Situ Thermomechanical Experiments in Clay: Concept, Results and Interpretation, Engineering Geology, 41, 51-64.

Bertrand, F., L. Laloui, C. Laurent. (2009) Thermo-Hydro-Mechanical Simulation of ATLAS In Situ Large Scale Test in Boom Clay, Computers and Geotechnics, 36, 626–640.

Bossart, P. (2012) Characteristics of the Opalinus Clay at Mont Terri. http://www.mont-terri.ch/internet/mont-terri/en/home/geology/key_characteristics.parsys.49924.DownloadFile.tmp/characteristicsofopa.pdf

Bossart, P., Trick, T., Meier P.M., Mayord, J.-C. (2004) Structural and Hydrogeological Characterisation of the Excavation-Disturbed zone in the Opalinus Clay (Mont Terri Project, Switzerland), Applied Clay Science, 26, 429– 448.

Bradbury, M., and Baeyens, B. (2003) Far Field Sorption Data Bases for Performance Assessment of a High-Level Radioactive Waste Repository in an Undisturbed Opalinus Clay Host Rock, Nuclear Energy and Safety Research Department Laboratory for Waste Management, PSI Bericht Nr. 03-08, Nagra NTB 02-19, http://les.web.psi.ch/publications/Liste03.html

Carbol, P. and Engkvist, I. (1997) Compilation of radionuclide sorption coefficients for performance assessment, *SKB rapport R-97-13*.

Cosgrove, J.W. (2001) Hydraulic Fracturing During the Formation and Deformation of a Basin: A Factor in the Dewatering of Low-Permeability Sediments, AAPG Bulletin, v. 85, no. 4, pp. 737–748.

De Cannière, P., Maes, A., Williams, S., Bruggeman, C., Beauwens, T., Maes, N., and Cowper, M. (2010) Behaviour of Selenium in Boom Clay, External Report, SCK•CEN-ER-120, 10/PDC/P-9. http://publications.sckcen.be/dspace/bitstream/10038/7079/1/er_120.pdf

De Craen, M. (2006) The Boom Clay Geochemistry: Natural Evidence, Mat. Res. Soc. Symp. Proc. Vol. 932 © 2006 Materials Research Society.

De Craen, M., Wemaere, I., Labat, S., and Van Geet, M. (2006) Geochemical analyses of Boom Clay Pore Water and Underlying Aquifers in the Essen-1 Borehole, External Report of the Belgian Nuclear Research Centre, SCK•CEN-ER-19, 06/MDC/P-47. http://publications.sckcen.be/dspace/bitstream/10038/430/1/er_19.pdf

De Craen, M., Wang, L., Van Geet M., and Moors, H. (2004) Geochemistry of Boom Clay Pore Water at the Mol Site, Scientific Report, SCK•CEN-BLG-990, 04/MDC/P-48. http://www.google.com/url?sa=t&rct=j&q=&esrc=s&frm=1&source=web&cd=3&ved=0CDkQFjAC&url=http%3A%2F%2Fwww.sckcen.be%2Ffr%2Fcontent%2Fdownload%2F16123%2F217784%2Fversion%2F1%2Ffile%2FGeochemistry%2Bof%2BBoom%2BClay%2Bpore%2B-%2BStatus%2B2004.pdf&ei=Db-ET9f4DImPiALfsvD1BA&usg=AFQjCNHOtkH7XpWt0uWNceqVyWex0po6nQ

Degueldre, C., Andreas Scholtis, A., Laube, A.,Turrero, M.J., and Thomas, B. (2003) Study of the Pore Water Chemistry through an Argillaceous Formation: A Paleohydrochemical Approach, Applied Geochemistry, 18, 55–73.

Dehandschutter, B., Vandycke, S., Sintubin, M., Vandenberghe, N., Wouters, L. (2005) Brittle Fractures and Ductile Shear Bands in Argillaceous Sediments: Inferences from Oligocene Boom Clay (Belgium), Journal of Structural Geology 27 (2005) 1095–1112.

De Windt, L., Pellegrini, D., and van der Lee, J. (2004) Reactive Transport Modelling of a Spent Fuel Repository in a Stiff Clay Formation Considering Excavation Damaged Zones, Radiochim. Acta 92, 841–848.

Dymitrowska, M., Genty, A., Lukin, D., Navarro, D., Weetjens, E. (2009) PAMINA-Performance Assessment Methodologies in Application to Guide Development of the Safety Case – PA Approach to Gas Migration, Deliverable D-N^{o} :3.2.1, European Commission under the Euratom Research and Training Programme on Nuclear Energy within the Sixth Framework Programme (2002-2006). http://www.ip-pamina.eu/downloads/pamina3.2.1.pdf

Fischer, H.B., List, E.J., Koh, R.C.Y., Imberger, J., Brooks, N.H. (1979) Mixing in Inland and Coastal Waters, Academic Press.

Gascoyne, M. (2004) Hydrogeochemistry, groundwater ages and sources of salts in a granitic batholith on the Canadian Shield, Southeastern Manitoba, *Applied Geochemistry*, 19, 519-560.

Horseman, S.T., Harrington, J.F., Birchall, D.J., Noy, D.J., and Cuss, R.J. (2005) Consolidation and Rebound Properties of Opalinus Clay: A Long-Term, Fully-Drained Test, Environmental Protection Programme Commissioned Report CR/05/128N, Technical Report CR/05/128, British Geological Survey. http://nora.nerc.ac.uk/11314/1/CR05128N.pdf

Iwatsuki, T., Furue, R., Mie, H., Ioka, S. and Mizuno, T. (2005) Hydrochemical baseline condition of groundwater at the Mizunami underground research laboratory (MIU), *Applied Geochemistry*, 20, 2283-2302.

JAEA (Japan Atomic Energy Agency) Diffusion and sorption coefficient database. Japan Atomic Energy Agency. http://migrationdb.jaea.go.jp/english.html.

Jobmann, M., and Polster, M. (2007) The Response of Opalinus Clay Due to Heating: A Combined Analysis of In Situ Measurements, Laboratory Investigations and Numerical Calculations, Physics and Chemistry of the Earth, 32, 929–936.

Johnson, L., Marschall, P., Zuidema, P., Gribi, P. (2004) Effect of Post-Disposal Gas Generation in a Repository for Spent Fuel, High-Level Waste, and Long-Lived Intermediate-Level Waste Sited in Opalinus Clay, Nagra Technical Report 04-06. http://www.nagra.ch/documents/database/dokumente/$default/Default%20Folder/Publikationen/NTBs%202001-2010/e_ntb04-06.pdf

Kalinina, E., McKenna, S.A., Hadgu, T. and Lowry, T. (2012) Analysis of the Effect of Heterogeneity on heat extraction in an EGS represented with the continuum fracture model, *Proceedings of 37th Stanford Geothermal Reservoir Engineering Workshop*, January 30 – February 1, 2012, Stanford, California.

Klein, L.A., Swift, C.T. (1977) An Improved Model for the Dielectric Constant of Sea Water at Microwave Frequencies, IEEE Transactions on Antennas and Propagation.

Laaksoharju, M., Smellie, J., Tullborg, E., Gimeno, M., Molinero, J., Gurban, I. and Hallbeck, L. (2008) Hydrogeochemical evaluation and modelling performed within the Swedish site investigation programme, *Applied Geochemistry*, 23, 1761-1795.

Lemy, F., Yong, S., And Schulz, T. (2006) A Case Study of Monitoring Tunnel Wall Displacement using Laser Scanning Technology, IAEG2006 Paper number 482, The Geological Society of London 2006.

Li, X., Bernier, F., Vietor, T., Lebon, P. (2007) TIMODAZ (Contract Number: FI6W-CT-036449), DELIVERABLE (N°: 2), European Commission Community Research. http://www.google.com/url?sa=t&rct=j&q=&esrc=s&frm=1&source=web&cd=1&sqi=2&ved=0CCAQFjAA&url=http%3A%2F%2Fwww.timodaz.eu%2Fdeliverables.aspx%3Fdwnld%3DTIMODAZD2formatECfinal.doc%26itemid%3Dbc9c5d91-17e1-4cec-929c-2c8a49ff777f%26id%3DWP2&ei=07qET5CqMaqhiAL3weD1BA&usg=AFQjCNFC7W7Q6Gi5m7sIPcdMx8YGkoEoYQ

Lolivier, Ph., Lemmens, K., And Van Iseghem, P. Geochemical Modelling of the Interaction of HLW Glass with Boom Clay Media, Mat. Res. Soc. Symp. Proc. Vol. 506 © 1998 Materials Research Society.

Liu, H.H, Li, L., Zheng, L., Houseworth, J. and Rutqvist, J. (2011) Investigations of Near-Field Thermal-Hydrologic-Mechanical-Chemical Models for Radioactive Waste Disposal in Clay/Shale Rock, Lawrence Berkeley National Laboratory report, LBNL-4872E

Liu H. H., Rutqvist J., Zheng L., Sonnenthal E., Houseworth J. and Birkholzer J. (2010) Modeling coupled process in clay formation for radioactive waste disposal. Lawrence Berkeley National Laboratory report, LBNL-3900E.

Liu, H.H.; Doughty, C.; and Bodvarsson, G.S. (1998) "An Active Fracture Model for Unsaturated Flow and Transport in Fractured Rocks." *Water Resources Research, 34,* (10), 2633-2646. Washington, D.C.: American Geophysical Union.

Madsen, F.T. (1999) International Society for Rock Mechanics Commission on Swelling Rocks and Commission on Testing Methods - Suggested Methods for Laboratory Testing of Swelling Rocks, International Journal of Rock Mechanics and Mining Sciences, 36, 291-306.

Maes, N., Bruggeman, C., Govaerts, J., Martens, E., Salah, S., Van Gompel, M. (2011) A Consistent Phenomenological Model for Natural Organic Matter Linked Migration of Tc(IV), Cm(III), Np(IV), Pu(III/IV) and Pa(V) in the Boom Clay, Physics and Chemistry of the Earth, 36, 1590–1599.

Mariner, P.E., Lee, J.H., Hardin, E.L., Hansen, F.D., Freeze, G.A., Lord, A.S., Goldstein, B. and Price, R.H. (2011) Granite disposal of U.S. high-level radioactive waste, *Sandia Report SAND2011-6203*, Sandia National Laboratories, Albuquerque, NM.

Martens, E., Wang, L., and Jacques, D. (2008) Modelling of Cation Concentrations in Outflow of $NaNO_3$ Percolation Experiments through Boom Clay Cores, External Report SCK•CEN-ER-85, 08/EMa/P-54. http://publications.sckcen.be/dspace/bitstream/10038/1038/1/er_85.pdf

Martin, C.D., Lanyon, G.W. (2003) Measurement of In-Situ Stress in Weak Rocks at Mont Terri Rock Laboratory, Switzerland, International Journal of Rock Mechanics & Mining Sciences 40 (2003) 1077–1088.

Mazurek, M., Pearson, F.J., Volckaert, G., and Bock, H. (2003) Features, Events and Processes Evaluation Catalogue for Argillaceous Media, OECD, Nuclear Energy Agency Organisation for Economic Co-Operation and Development. http://www.oecd-nea.org/rwm/reports/2003/nea4437-FEP.pdf

Mertens, J., Vandenberghe, N., Wouters, L., Sintubin, M. (2003) The Origin and Development of Joints in the Boom Clay Formation (Rupelian) in Belgium, From: VAN RENSBERGEN, P., HILLIS, R.R., MALTMAN, A.J. & MORLEY, C.K. (eds) 2003. Subsurface Sediment Mobilization. Geological Society, London, Special Publications, 216, 309-321. 0305-8719/031515 © The Geological Society of London

ONDRAF/NIRAS (2001) Chapter 11: Long-term safety assessment, from Safety Assessment and Feasibility Interim Report 2 Belgian agency for radioactive waste and enriched fissile materials NIROND 2001–06E. http://www.nirond.be/engels/PDF/Part02-Text02-Chap11-13.pdf

Painter, S., Cvetkovic, V., Mancillas, J. and Pensado, O. (2008) Time domain particle tracking methods for simulating transport with retention and first-order transformation, *Water Resources Research*, 43(9), W01406.

Pearson, F.J., Tournassat, C.,Gaucher, E. (2010) Biogeochemical Processes in a Clay Formation In-Situ Experiment: Part E - Equilibrium Controls on Chemistry of Pore Water from the Opalinus Clay, Mont Terri Underground Research Laboratory, Switzerland, Applied Geochemistry, 26, 990-1008.

Posiva (2010) Models and Data Report 2010, *POSIVA 2010-01*, Posiva Oy, Olkiluoto, Finland.

Reynolds, W.C., and Perkins, H.C. (1977) Engineering Thermodynamics, McGraw-Hill Book Company.

Schafer, T. and K. Iijima (2007) CFM Phase I – Status report of the laboratory programme, *Nagra Report NAB 07-41*, National Cooperative for the Disposal of Radioactive Waste, Wettingen, Switzerland.

Shaw, R. (2010) Review of Boom Clay and Opalinus Clay parameters, FORGE Report D4.6 – VER 1.0. Euratom 7th Framework Programme Project. http://www.bgs.ac.uk/forge/docs/reports/D4.6.pdf

SKB (2006) Long-term safety for KBS-3 repositories at Forsmark and Laxemar — A first evaluation, *Technical Report TR-06-09*, Swedish Nuclear Fuel and Waste Management Co.

SKB (2010a) Radionuclide transport report for the safety assessment SR-Site, *Technical Report TR-10-50*, Swedish Nuclear Fuel and Waste Management Co.

SKB (2010b) Data report for the safety assessment SR-Site, *Technical Report TR-10-52*, Swedish Nuclear Fuel and Waste Management Co.

Tsilingiris, P.T. (2008) Thermophysical and Transport Properties of Humid Air at Temperature Range between 0 and 100°C, Energy Conversion and Management, 49, 1098–1110.

Wang, Y. (2011) Integrated Plan for Used Fuel Disposition (UFD) Data Management. U.S. Department of Energy Used Fuel Disposition Campaign. FCRD-USED-2011-000386.

Wolery, T.J., 1992. EQ3/6: Software Package for Geochemical Modeling of Aqueous Systems: Package Overview and Installation Guide (version 7.0). Lawrence Livermore National Laboratory Report UCRL-MA-110662 PT I, Livermore, CA.

Xu, T., Sonnenthal, E., Spycher, N., and Pruess, K. (2006) TOUGHREACT—A Simulation Program for Non-Isothermal Multiphase Reactive Geochemical Transport in Variably Saturated Geologic Media: Applications to Geothermal Injectivity and CO_2 Geological Sequestration, Computers & Geosciences, 32, 145–165.

Yu, L., Weetjens, E., Vietor, T. (2011) Integration of TIMODAZ Results within the Safety Case and Recommendations for Repository Design, SCK•CEN-ER-188 11/Lyu/P-64. http://publications.sckcen.be/dspace/bitstream/10038/7598/1/er_188.pdf

Zhang, C.L., Wieczorek, K., and Xie, M.L. (2010) Swelling Experiments on Mudstones, Journal of Rock Mechanics and Geotechnical Engineering, 2 (1): 44–51.

Zheng, L., Samper, J., Montenegro, L., and Mayor, J.C. (2007) Flow and Reactive Transport Model of a Ventilation Experiment in Opalinus Clay, Estudios de la Zona No Saturada del Suelo Vol. VIII. J.V. Giráldez Cervera y F.J. Jiménez Hornero.

6.0 Summary and Future Work

The work documented in this report is aimed to develop an integrated modeling framework that can be used for systematically analyzing the performance of a natural barrier system and identifying key factors that control the performance of the system. This framework is designed as an integrated tool for prioritization and programmatic decisions of UFDC natural system R&D activities, and it includes three key components: (1) detailed process models (with appropriate levels of fidelity) for flow field and radionuclide transport, (2) a probabilistic performance assessment capability, and (3) an associated technical database supporting model calculation. The integrated tool development for natural system evaluation adopts a phased approach. This report documents the results of phase I activities, which is focused on identifying relevant tools and performing preliminary demonstrations. The FY12 accomplishments are summarized as follows:

- Two separate modeling frameworks were explored using different combinations of process simulators and performance assessment drivers: (1) PFLOTRAN + PEST and (2) FEHM + DAKOTA. Their preliminary application to flow and radionuclide transport in fractured granite and dolomite media was demonstrated using Monte-Carlo simulations. The potential application of a "plug-and-play" concept, common data format, and high performance computing techniques were explored.
- Calibration-constrained uncertainty analyses were performed for a flow field in a hypothetical fractured granite medium using PFLOTRAN and PEST.
- The modeling framework developed was demonstrated to be able to use real field data (transmissivity fields), the dual-porosity capability of transport code (FEHM), the high performance parallel computing capability of PA driver (DAKOTA), and the embedded LHS sampling and statistical analysis techniques (DAKOTA).
- A comprehensive review of thermodynamic data relevant to nuclear waste disposal was performed. The related data gaps were identified, especially for layered aluminosilicates.
- A comprehensive literature survey and data compilation were performed for modeling the near-field thermal-hydrological-mechanical-chemical evolution of a clay repository and for modeling flow and radionuclide transport in a fractured granite medium. These data will be used to develop an appropriate data model for UFDC data management.

Future work will include:

- Move the integrated tool development from phase I into phase II by merging the existing two separate modeling frameworks into a single integrated framework.
- Develop the capability to incorporate an advanced flow-transport model for fractured geologic media, such as a discrete fracture network (DFN) flow model, into the framework.
- Continue to explore and demonstrate the capability of model parameter estimation and uncertainty analyses using the established framework.
- Continue data collection and synthesis to establish a comprehensive technical database for natural system evaluation.